INVESTIGATION OF THE OZONE FORMATION POTENTIALS OF SELECTED BRANCHED ALKANES AND MINERAL SPIRITS SAMPLES

Report to
Safety-Kleen Corporation

by

William P. L. Carter, Dongmin Luo, and Irina L. Malkina

July 11, 2002

College of Engineering
Center for Environmental Research and Technology
University of California
Riverside, California 92521

00-AP-RT82-001-FR

ABSTRACT

As the second phase of our study of the atmospheric ozone formation potentials of mineral spirits, which consist primarily of mixtures of C_8 - C_{15} alkanes, a series of environmental chamber experiments and computer model simulations were carried out to assess the atmospheric ozone formation potentials of the selected representative branched alkanes, and an updated modeling analyses of previous experiments on representative mineral spirits samples was carried out. The experiments consisted of determining the effects on NO oxidation, ozone formation and OH radical levels when adding 2-methyl nonane, 2,6-dimethyl octane, or 3,4-diethyl hexane to varying simulated model photochemical smog systems. The OH radical rate constants for these compounds were measured to be 1.28×10^{-11}, 1.29×10^{-11}, and 7.96×10^{-12} cm^3 $molec^{-1}$ s^{-1}, respectively, using a relative rate method. These branched alkanes were found to be inhibitors of radical levels, and rates of NO oxidation and O_3 formation in experiments that are sensitive to radical effects, but to a somewhat lesser extent than observed for normal alkanes and alkyl cyclohexanes in the same molecular weight range. The results were used to determine whether the current SAPRC-99 atmospheric chemical mechanism could accurately simulate the effects of these compounds on ozone formation and other manifestations of photochemical smog. The SAPRC-99 mechanism gave satisfactory simulations of the data for 2-methyl nonane, but tended to slightly underpredict the inhibiting characteristics of the more branched alkanes. The current mechanism also gave very good simulations of the results the previous experiments with actual mineral spirits samples, in contrast with the poor performance of the earlier mechanism used when modeling the results of these experiments when they were first reported. The current mechanism also performed significantly better in simulating the results of the branched alkane experiments. The reasons for the improved performance of the updated mechanism are discussed. The current mechanism was then used to calculate ozone impacts of the representative alkanes and mineral spirits samples in various urban photochemical smog scenarios. The impacts of the all-alkane mineral spirits samples on peak ozone yields were variable, but generally were 20-30% those of an equal mass of VOC emissions from all sources. The ozone impacts of the mineral spirits sample with 8% aromatics and alkenes were about 2-3 times those of the all-alkane samples. The relative impacts on maximum 8-hour average ozone levels were generally less than their relative impacts on peak ozone levels, especially in scenarios with relatively low NO_x conditions.

ACKNOWLEDGEMENTS

The authors acknowledge Mr. Dennis Fitz for assistance in administering this program, Mr. Kurt Bumiller for assistance in carrying out the environmental chamber experiments, Dr. Roger Atkinson for helpful discussions, and Ms. Anne O'Donnell of the Safety-Kleen Corp. providing useful mineral spirits analysis data and for helpful discussions.

This work on the branched alkanes and the previous work on the mineral spirits samples was funded primarily by Safety-Kleen Corporation. The College of Engineering Center for Environmental Research and Technology at the University of California at Riverside provided funding to cover the portions of the cost of this project that Safety-Kleen was unable to pay due to bankruptcy. The environmental chamber work on the normal and cyclic alkanes that is discussed in this work was obtained under funding from the Aluminum Association. The development of SAPRC-99 mechanism that is discussed in this report was funded by the California Air Resources Board. However, the opinions and conclusions expressed in this report are entirely those of the primary author, Dr. William P. L. Carter. Mention of trade names or commercial products does not constitute endorsement or recommendation for use.

This report reflects work carried out through August of 2000.

TABLE OF CONTENTS

LIST OF TABLES

LIST OF FIGURES

INTRODUCTION

Mineral spirits are petroleum distillate fractions that are widely used as solvents for cleaning and other applications. Normal use of these products often results in their emissions into the atmosphere, where they can react with oxides of nitrogen (NO_x) and sunlight to form photochemical ozone, a serious air quality problem in many urban areas. Methods to reliably quantify their reactivities towards ozone formation in the lower atmosphere are of interest to producers and users of those solvents, as well as to local and state air quality control agencies. Estimates of the ozone formation reactivities of such solvents require quantitative information on the types of chemical constituents they contain, and an ability to predictively model the effects of the reactions of these constituents on atmospheric ozone. Although their composition vary, mineral spirits typically consist of mixtures of normal, branched and cyclic alkanes in the C_9 - C_{15} range, with some samples also containing varying amounts of aromatics and alkenes (Carter et al 1997a). The large number of isomers they contain means it is not possible to unambiguously identify all of the individual species present, though it is possible to derive the compositions in terms of the classes of chemical species currently used in detailed atmospheric photochemical mechanisms (Carter et al, 1997a). However, even if all the components of the mineral spirits mixtures were completely characterized, the estimates of their atmospheric reactivities would be no more reliable than the chemical mechanisms for their constituents.

The only way to determine the reliability of the predictions of a model of the atmospheric ozone impacts of a particular compound or mixture is to determine if their ozone impacts under various controlled conditions in environmental chamber experiments are consistent with model predictions. We had previously carried out such experimental and modeling studies for n-octane (Carter et al, 1993, 1995a, 1997b) and $C_{\geq 12}$ normal alkanes (Carter et al, 1996), and showed that the results are reasonably consistent with model predictions, though some adjustments to the estimated mechanisms were necessary. However, under funding from Safety-Kleen Corporation, we conducted such experiments with selected mineral spirits mixtures and found that the model significantly overpredicted their ozone impacts (Carter et al., 1997a). These mixtures consist of ~70-95% branched and cyclic alkanes, which the model predicted are about twice as reactive as n-alkanes with the same carbon numbers. However, the chamber data were simulated much better by the model if it was assumed that the branched and cyclic alkanes had about the same mechanisms and ozone impacts as the normal alkanes. Either the analysis of these mineral spirits samples were seriously in error, or the model for the $C_{\geq 8}$ branched and cyclic alkanes, at least those in those particular mineral spirits samples, was not correct. However, it was considered to be unlikely that problems with the mineral spirits analysis are the reasons for this discrepancy (Carter et al, 1997a).

It was clear that additional work was needed on the chemical mechanisms used to estimate the atmospheric ozone impacts of the mineral spirits, particularly the branched and cyclic alkane constituents. At the time the study of Carter et al (1997a) was carried out, there were no data to evaluate mechanisms for $C_{\geq 9}$ branched or cyclic alkanes, and the mechanisms used to represent these constituents were based on various estimates and extrapolations. Since that time, experiments on the representative cycloalkanes

hexyl cyclohexane and octyl cyclohexane were carried out under funding from the Aluminum Association (Carter et al, 2000a), but data on representative $C_{\geq 9}$ branched alkanes were still needed. In addition, laboratory data were needed to reduce uncertainties concerning the atmospheric reactions of the higher alkanes, particularly the yields of organic nitrates from the reactions of $C_{>8}$ peroxy radicals with NO.

To address these needs, the Safety-Kleen Corporation contracted with the College of Engineering Center for Environmental Research and Technology (CE-CERT) of the University of California at Riverside (UCR) to carry out an experimental and modeling study of the atmospheric reactions of representative branched alkane mineral spirits constituents, and to update the atmospheric ozone impact estimates for the representative mineral spirits samples. The representative branched alkanes studied were 2-methyl nonane, 2,6-dimethyl octane, and 3,4-diethyl hexane; these were chosen to represent various degrees of branching that are possible for the C_{10} alkane isomers. In addition, primarily under funding from the California Air Resources Board, new data was obtained concerning the atmospheric reaction mechanisms for the higher alkanes (Arey et al, 2000, Atkinson et al, 2000), and the chemical mechanism used for predicting the ozone impacts of all volatile organic compounds (VOCs) underwent a comprehensive update to take these and other data into account (Carter, 2000). This report documents the results of the experiments on the representative branched alkanes, and updates the modeling and ozone reactivity analysis of the mineral spirits samples based on the results of these recent studies.

EXPERIMENTAL AND DATA ANALYSIS METHODS

Environmental Chamber Experiments

Overall Experimental Approach

Most of the environmental chamber experiments for this program consisted of measurements of "incremental reactivities" of the three branched alkane isomers under various conditions. These involve two types of irradiations of model photochemical smog mixtures. The first is a "base case" experiment where a mixture of reactive organic gases (ROGs) representing those present in polluted atmospheres (the "ROG surrogate") is irradiated in the presence of oxides of nitrogen (NO_x) in air. The second is the "test" experiment that consists of repeating the base case irradiation except that the VOC whose reactivity is being assessed is added. The differences between the results of these experiments provide a measure of the atmospheric impact of the test compound, and the difference relative to the amount added is a measure of its reactivity. To provide data concerning the reactivities of the test compound under varying atmospheric conditions, three types of base case experiments were carried out:

Mini-Surrogate Experiments. This base case employed a simplified ROG surrogate and relatively low ROG/NO_x ratios. Low ROG/NO_x ratios represent "maximum incremental reactivity" (MIR) conditions, which are most sensitive to VOC effects. This is useful because it provides a sensitive test for the model, and also because it is most important that the model correctly predict a VOC's reactivity under conditions where the atmosphere is most sensitive to the VOCs. The ROG mini-surrogate mixture employed consisted of ethene, n-hexane, and m-xylene. This surrogate was employed in our previous studies (Carter et al, 1993; 1995a-c, 1997b, 2000b), and was found to provide a more sensitive test of the mechanism than the more complex surrogates that more closely represent atmospheric conditions (Carter et al, 1995b). This high sensitivity to mechanistic differences makes the mini-surrogate experiments useful for mechanism evaluation. The experiments with 2-methyl-nonane used the same mini-surrogate composition as used in our previous studies, and the average initial reactant concentrations of these experiments were (in ppm): NO: 0.27, NO_2: 0.09, n-hexane: 0.46, ethene: 0.83, and m-xylene: 0.13. In the experiments with 2,6-dimethyl octane and 3,4-diethyl hexane, a "modified mini-surrogate" was employed where the m-xylene was replaced with 0.2 ppm of toluene and 0.05 ppm of 1,3,5-trimethyl benzene. This modification was employed in an attempt to improve the precision of the integrated OH radical measurements, as discussed later.

High NO_x Full Surrogate Experiments. This base case employed a more complex ROG surrogate under somewhat higher, though still relatively low, ROG/NO_x conditions. While less sensitive to the some aspects of the mechanism employed, experiments with a more representative ROG surrogate are needed to evaluate the mechanism under conditions that more closely resemble the atmosphere. The ROG surrogate employed was the same as the 8-component "lumped molecule" surrogate as employed in our previous study (Carter et al. 1995b), and consists of n-butane, n-octane, ethene, propene, trans-2-butene, toluene, m-xylene, and formaldehyde. Calculations have indicated that use of this 8-component mixture

will give essentially the same results in incremental reactivity experiments as actual ambient mixtures (Carter et al. 1995b). The average initial reactant concentrations of these experiments were (in ppm): NO: 0.25, NO_2: 0.04, n-butane: 0.37, n-octane: 0.10, ethene: 0.06, propene: 0.06, trans-2-butene: 0.06, toluene: 0.09 and m-xylene: 0.09.

Low NO_x Full Surrogate Experiments. This base case employing the same 8-component "lumped molecule" surrogate as the full surrogate experiments described above, except that lower NO_x levels (higher ROG/NO_x ratios) were employed to represent NO_x-limited conditions. Such experiments are necessary to assess the ability of the model to properly simulate reactivities under conditions where NO_x is low. The initial ROG and NO_x reactant concentrations were comparable to those employed in our previous studies (Carter et al. 1995b, 1997b, 2000b). The average initial NO and NO_2 were 0.06 and 0.03 ppm, respectively, and the initial concentrations of the 8 ROG surrogate components were the same as in the high NO_x full surrogate experiments.

An appropriate set of control and characterization experiments necessary for assuring data quality and characterizing the conditions of the runs for mechanism evaluation were also carried out. These are discussed where relevant in the results or modeling methods sections (see also Carter et al, 1995c, 2000b).

Environmental Chamber

All experiments for this program were carried out using the CE-CERT "Dividable Teflon Chamber" (DTC) with a blacklight light source. This consists of two ~6000-liter 2-mil heat-sealed FEP Teflon reaction bags located adjacent to each other and fitted inside an 8' x 8' x 8' framework, and which uses two diametrically opposed banks of 32 Sylvania 40-W BL black lights as the light source. The lighting system in the DTC was found to provide so much intensity that only half the lights were used for irradiation. Four air blowers that are located in the bottom of the chamber were used to help cool the chamber as well as mix the contents of the chamber. The CE-CERT DTC is very similar to the SAPRC DTC which is described in detail elsewhere (Carter et al, 1995b,c). This is the same chamber as used in our previous studies of normal (Carter et al, 1996) and cyclic (Carter et al, 2000a) alkanes and mineral spirits samples (Carter et al, 1997a)

The blacklight light source has the advantage of being relatively inexpensive to operate and provides a reasonably good simulation of natural sunlight in the region of the spectrum that is important in affecting most photolysis reactions of importance for non-aromatic VOCs (Carter et al, 1995c,d). This is therefore appropriate for studies of reactivities of compounds, such as these alkanes, which are not photoreactive or believed to form significant yields of photoreactive products whose action spectra are not well characterized.

The DTC is designed to allow simultaneous irradiations of experiments with and without added test reactants under the same reaction conditions. Since the chambers are actually two adjacent FEP Teflon reaction bags, two mixtures can be simultaneously irradiated using the same light source and with the same temperature control system. These two reaction bags are referred to as the two "sides" of the

chambers (Side A and Side B) in the subsequent discussion. The sides are interconnected with two ports, each with a box fan, which rapidly exchange their contents to assure that base case reactants have equal concentrations in both sides. In addition, a fan is located in each of the reaction bags to rapidly mix the reactants within each chamber. The ports connecting the two reactors can then be closed to allow separate injections on each side, and separate monitoring of each side.

Experimental Procedures

The reaction bags were flushed with dry air produced by an AADCO air purification system for 14 hours (6pm-8am) on the nights before experiments. The continuous monitors were connected prior to reactant injection and the data system began logging data from the continuous monitoring systems. The reactants were injected as described below (see also Carter et al, 1993, 1995c). The common reactants were injected in both sides simultaneously using a three-way (one inlet and two outlets connected to side A and B respectively) bulb of 2 liters in the injection line and were well mixed before the chamber was divided. The contents of each side were blown into the other using two box fans located between them. Mixing fans were used to mix the reactants in the chamber during the injection period, but these were turned off prior to the irradiation. The sides were then separated by closing the ports that connected them, after turning all the fans off to allow their pressures to equalize. After that, reactants for specific sides (the test compound in the case of reactivity experiments) were injected and mixed. After the run, the contents of the chamber were emptied by allowing the bags to collapse, and then the chamber was flushed with purified air. The contents of the reactors were vented into a fume hood.

The procedures for injecting the various types of reactants were as follows. The NO and NO_2 were prepared for injection using a high vacuum rack. Known pressures of NO, measured with MKS Baratron capacitance manometers, were expanded into Pyrex bulbs with known volumes, which were then filled with nitrogen (for NO) or oxygen (for NO_2). The contents of the bulbs were then flushed into the chamber with nitrogen. The gaseous reactants were prepared for injection either using a high vacuum rack or a gas-tight syringes whose amounts were calculated to achieve the desired concentrations in the chamber. Sufficiently volatile liquid reactants (which included all the liquid reactant compounds used in this study) were injected using a micro syringe into a 1-liter Pyrex bulb equipped with stopcocks on each end and a port for the injection of the liquid. Then one end of the bulb was attached to the injection port of the chamber and the other to a nitrogen source. The stopcocks were then opened, and the contents of the bulb were flushed into the chamber with a combination of nitrogen and heat gun for approximately 5 minutes.

Formaldehyde was prepared in a vacuum rack system by heating paraformaldehyde in an evacuated bulb until the pressure corresponded to the desired amount of formaldehyde. The bulb was then closed and detached from the vacuum system and its contents were flushed into the chamber with dry air through the injection port.

Kinetic Experiments

In addition to the environmental chamber experiments for mechanism evaluation, a limited number of experiments were carried out to determine the rate constant for the reactions of OH radicals with the branched alkanes studied for this project, using a relative rate technique. Experiments were carried out using either a ~200-liter "pillow bag" constructed of 2 mil FEP Teflon film and placed inside an enclosure to permit blacklight irradiation, or in one of the DTC reactors discussed above. The light intensity in the pillow bag experiment was approximately twice that of the lights used in the DTC. Pure dry air from an AADCO air purification system was used for all experiments, and the experiments were carried out at ambient temperature (approximately 295-298^{o}K).

OH Radicals were generated by the photolysis of nitrous acid (HONO). The nitrous acid was prepared using the method of Febo et al (1995), which involves continuously passing low concentrations of gaseous HCl in humidified air through a stirred reactor containing sodium nitrite salt. This produced HONO in ppm quantities with no more than ~2% NO impurity, with no measurable HCl impurities as determined by bubbling the output of the HONO generator through water and analyzing the water for Cl^{-} ions. The output of this HONO generator was flushed into the reactor until the desired initial concentration was achieved, as determined by the flow rates, the HONO concentration output by the generator, and the volume of the reactor. The first kinetic experiments employed approximately 0.5 ppm each of HONO and NO, and the other two employed approximately 1 ppm of HONO without added NO.

All experiments employed approximately 0.1 ppm each of the test and reference organics. The test compounds studied were 2-methyl nonane, 2,6-dimentyl octane, 3,4-diethyl hexane and (for verification purposes) n-octane or n-decane. M-xylene was employed as the reference compound.

After the reactants were injected and mixed, the concentrations of the VOC reactants were monitored by gas chromatography until reproducible concentrations were measured. The analysis methods employed were the same as employed in the reactivity experiments, as described below, and all the VOCs were analyzed simultaneously using the same instrument. Then the lights were turned on for brief periods (5-10 minutes, with the time increasing as the experiment progressed) and then turned off. The reactant concentrations were measured between each irradiation.

Analytical Methods

Ozone and nitrogen oxides (NO_x) were continuously monitored using commercially available continuous analyzers with Teflon sample lines inserted directly into the chambers. The sampling lines from each side of the chamber were connected to solenoids that switched from side to side every 10 minutes, so the instruments alternately collected data from each side. Ozone was monitored using a Dasibi 1003-AH UV photometric ozone analyzer and NO and total oxides of nitrogen (including organic nitrates and perhaps HNO_3) were monitored using a Teco Model 42 chemiluminescent NO/NO_x monitor. The output of these instruments, along with that from the temperature sensors and the formaldehyde instrument, were attached to a computer data acquisition system, which recorded the data at 10 minutes

intervals for ozone, NOx and temperature (and at 15 minutes for formaldehyde), using 30 second averaging times. This yielded a sampling interval of 20 minutes for taking data from each side.

The Teco instrument and Dasibi CO analyzer were calibrated prior to each experiment using a certified NO and CO source and CSI-1700 gas-phase titration calibrator. The Dasibi ozone analyzer was calibrated against a transfer standard ozone analyzer approximately every three months, and was checked with CSI ozone generator for each experiment to assure that the instrument worked properly. The details were discussed elsewhere (Carter et al, 1995c)

Organic reactants other than formaldehyde were measured by gas chromatography with FID detection as described elsewhere (Carter et al. 1993; 1995c). GC samples were taken for analysis at intervals of about 20 minutes using 100 ml gas-tight glass syringes. These samples were taken from ports directly connected to the chamber after injection and before irradiation and at regular intervals after irradiation was started. The sampling method employed for injecting the sample onto the GC column depended on the volatility or "stickiness" of the compound. For analysis of the more volatile species, which includes all the base ROG surrogate and test compounds monitored in this study, the contents of the syringe were flushed through a 10 ml and 5 ml stainless steel or 1/8' Teflon tube loop and subsequently injected onto the column by turning a gas sample valve.

The calibrations for the GC analyses for most compounds were carried out by sampling from chambers or vessels of known volume into which known amounts of the reactants were injected, as described previously (Carter et al, 1995c).

Formaldehyde was monitored using an adaptation of the diffusion scrubber method developed by Dasgupta et al (1988, 1990), as described by Carter et al (1995c). It was calibrated using a formaldehyde diffusion tube whose weight loss was monitored over time. The system cycled between zero, calibrate, and sample modes to correct for zero and span drifts.

Characterization Methods

Temperature

Three temperature thermocouples were used to monitor the chamber temperature, two of which were located in the sampling line of continuous analyzers to monitor the temperature in each side. The third one was located in the outlet of the air conditioning system used to control the chamber temperature. The temperature range in these experiments was typically 25-30 C.

Blacklight Light Source

The light intensity in the DTC chamber was monitored by periodic NO_2 actinometry experiments utilizing the quartz tube method of Zafonte et al (1977), with the data analysis method modified as discussed by Carter et al. (1995c). The results of these experiments were tracked over time, and although there was a gradual decrease in light intensity over time during most of the operational lifetime of this

chamber, the light intensity appeared to be relatively constant during the period of these experiments. Averages of results of actinometry experiments carried out during this period indicated an NO_2 photolysis rate of 0.161 min^{-1}. This was used when modeling all the experiments for this program.

The spectrum of the blacklight light source is periodically measured using a LiCor LI-1800 spectroradiometer, and found to be essentially the same as the general blacklight spectrum recommended by Carter et al (1995c) for use in modeling blacklight chamber experiments.

Dilution

The dilution of the chambers due to sampling is expected to be small because the flexible reaction bags can collapse as samples are withdrawn for analysis. Also, the chambers were designed to operate under slightly positive pressure, so any small leaks would result in reducing the bag volume rather than diluting the contents of the chamber. Information concerning dilution in an experiment can be obtained from relative rates of decay of added VOCs that react with OH radicals with differing rate constants (Carter et al. 1993; 1995c). Most experiments had more reactive compounds such as m-xylene and n-octane present either as a reactant or added in trace amounts to monitor OH radical levels. Trace amounts (~0.1 ppm) of n-butane were also added to experiments if needed to provide a less reactive compound for monitoring dilution. In addition, specific dilution check experiments such as CO irradiations were carried out. Based on these results, the dilution rate was found to be negligible in this chamber in most experiments, generally being less than 0.3% per hour.

Reactivity Data Analysis Methods

As indicated above, most of the experiments for this program consisted of simultaneous irradiation of a "base case" reactive organic gas (ROG) surrogate - NO_x mixture in one of the dual reaction chambers, together with an irradiation, in the other reactor, of the same mixture with the test compound or mixture added. The results were analyzed to yield two measures of VOC reactivity: the effect of the added VOC on the amount of NO reacted plus the amount of ozone formed, and integrated OH radical levels. These are discussed in more detail below.

The first measure of reactivity is the effect of the VOC on the change in the quantity $[O_3]$-[NO], or $\Delta([O_3]$-[NO]). As discussed elsewhere (e.g., Johnson, 1983; Carter and Atkinson, 1987; Carter and Lurmann, 1990, 1991, Carter et al, 1993, 1995a), this gives a direct measure of the amount of conversion of NO to NO_2 by peroxy radicals formed in the photooxidation reactions, which is the process that is directly responsible for ozone formation in the atmosphere. (Johnson calls it "smog produced" or "SP".) The incremental reactivity of the VOC relative to this quantity, which is calculated for each hour of the experiment, is given by

$$IR[\Delta([O_3]-[NO])_t^{VOC}] = \frac{\Delta([O_3]-[NO])_t^{Test} - \Delta([O_3]-[NO])_t^{Base}}{[VOC]_0} \qquad (I)$$

where $\Delta([O3]\text{-}[NO])_t^{Test}$ is the $\Delta([O_3]\text{-}[NO])$ measured at time t from the experiment where the test VOC was added, $\Delta([O3]\text{-}[NO])_t^{Base}$ is the corresponding value from the corresponding base case run, and $[VOC]_0$ is the amount of test VOC added. An estimated uncertainty for IR[$\Delta([O_3]\text{-}[NO])$] is derived based on assuming an ~3% uncertainty or imprecision in the measured $\Delta([O_3]\text{-}[NO])$ values. This is consistent with the results of the side equivalency test, where equivalent base case mixtures are irradiated on each side of the chamber.

Note that reactivity relative to $\Delta([O3]\text{-}[NO])$ is essentially the same as reactivity relative to O_3 in experiments where O_3 levels are high, because under such conditions $[NO]_t^{base}$. $[NO]_t^{test}$. 0, so a change in $\Delta([O3]\text{-}[NO])$ caused by the test compound is due to the change in O_3 alone. However, $\Delta([O3]\text{-}[NO])$ reactivity has the advantage that it provides a useful measure of the effect of the VOC on processes responsible for O_3 formation even in experiments where O_3 formation is suppressed by relatively high NO levels.

The second measure of reactivity is the effect of the VOC on integrated hydroxyl (OH) radical concentrations in the experiment, which is abbreviated as "IntOH" in the subsequent discussion. This is an important factor affecting reactivity because radical levels affect how rapidly all VOCs present, including the base ROG components, react to form ozone. If a compound is present in the experiment that reacts primarily with OH radicals, then the IntOH at time t can be estimated from

$$\text{IntOH}_t = \frac{\ln([\text{tracer}]_0 / [\text{tracer}]_t) - \text{Dt}}{\text{kOH}^{\text{tracer}}} \qquad \text{(II)}$$

where $[tracer]_0$ and $[tracer]_t$ are the initial and time=t concentrations of the tracer compound, kOH^{tracer} its OH rate constant, and D is the dilution rate in the experiments. The latter was found to be small and was neglected in our analysis. The concentration of tracer at each hourly interval was determined by linear interpolation of the experimentally measured values. M-xylene was used as the OH tracer in most of these experiments because it is present as a surrogate component, its OH rate constant is known (the value used was 2.36×10^{-11} cm^3 $molec^{-1}$ s^{-1} [Atkinson, 1989]), and it reacts relatively rapidly. However, for the mini-surrogate experiments for 2,5-dimethyl octane and 3,4-diethyl hexane the m-xylene was replaced with 1,3,5-trimethylbenzene, for which an OH radical rate constant of 5.75×10^{-11} cm^3 $molec^{-1}$ s^{-1} was used (Atkinson, 1989). This was used as an alternative tracer because it might serve as a more sensitive measurement of IntOH because of its higher OH radical rate constant.

The effect of the VOC on OH radicals can thus be measured by its IntOH incremental reactivity, which is defined as

$$\text{IR}[\text{IntOH}]_t = \frac{\text{IntOH}_t^{\text{Test}} - \text{IntOH}_t^{\text{Base}}}{[\text{VOC}]_0} \qquad \text{(III)}$$

where $IntOH^{Test}$ and $IntOH^{Base}$ are the IntOH values measured at time t in the added VOC and the base case experiment, respectively. The results are reported in units of 10^6 min. The uncertainties in IntOH and

IR[IntOH] are estimated based on assuming an ~2% imprecision in the measurements of the m-xylene concentrations. This is consistent with the observed precision of results of replicate analyses of this compound.

CHEMICAL MECHANISMS

General Atmospheric Photooxidation Mechanism

The chemical mechanism evaluated against the environmental chamber data and used in all of the atmospheric model simulations in this study is the "SAPRC-99" mechanism that is documented in detail by Carter (2000). This mechanism represents a complete update of the SAPRC-97 mechanism that was used in our previous study of mineral spirits reactivity (Carter et al, 1997a), and that is documented by Carter et al (1997b). It incorporates recent reactivity data from a wide variety of VOCs, including those discussed in this report. This includes assignments for ~400 types of VOCs, and can be used to estimate reactivities for ~550 VOC categories. A condensed version, developed for use in regional models, is used to represent base case emissions in the atmospheric reactivity simulations discussed in this report. A unique feature of this mechanism is the use of a computerized system to estimate and generate complete reaction schemes for most non-aromatic hydrocarbons and oxygenates in the presence of NO_x, from which condensed mechanisms for the model can be derived. This includes the mechanisms for the higher alkanes discussed in this report and the mechanisms used for their major reactive oxygenated products. The SAPRC-99 mechanism was evaluated against the results of almost 1700 environmental chamber experiments carried out at the University of California at Riverside, including experiments to test ozone reactivity predictions for over 80 types of VOCs. This includes experiments and VOCs discussed in this report.

A listing of the portions of the SAPRC-99 mechanism used in the environmental chamber and mineral spirits reactivity model simulations in this report is given in Appendix A. This consists of the "base mechanism" representing the reactions of the inorganics and common organic products, the reactions of the specific VOCs used in the environmental chamber experiments (including the three test compounds whose mechanisms are discussed in the following sections), and the reactions of the lumped model species used when representing base case VOCs in the ambient reactivity simulations. The mechanisms used for the higher molecular weight alkanes are discussed in more detail below. The report of Carter (2000) can be consulted for a more detailed discussion of the other portions of the mechanism.

In the atmospheric reactivity simulations of the individual alkanes, the mechanisms for the model species used to represent the more reactive oxygenated products (e.g., PROD2 and RCHO) were derived using the "adjusted product" approach as discussed by Carter et al (2000). In this approach, the PROD2 and (where applicable) RCHO model species used to represent the reactions of the more reactive products were replaced by "adjusted mechanism" species whose mechanistic parameters were derived based on the specific product compounds they represented. The mechanisms for these compound-specific product species are given in with the full mechanism listing by Carter et al (2000). This adjusted product approach is not used when representing these compounds in mixtures such as mineral spirits samples, and thus these were not used when modeling the branched alkane experiments or the mineral spirits reactivities. Use of this adjusted product approach usually caused less than ~5% differences in calculated atmospheric

reactivities and had negligible effects in simulations of the environmental chamber experiments. Nevertheless, this approach was used in the atmospheric reactivity simulations for the individual compounds for consistency with the atmospheric reactivity data given by Carter (2000).

Atmospheric Reactions of $C_{\geq 8}$ Alkanes

Available laboratory information concerning the gas-phase atmospheric reactions of the alkanes has been reviewed by Atkinson (1997), and the most recent relevant information is discussed by Carter (2000). The only significant gas-phase atmospheric reaction of alkanes is the reaction with OH radicals. Alkanes do not absorb light in the wavelength region provided by ground-level sunlight ($\lambda \geq 300$ nm) (Calvert and Pitts, 1966), and rate constants for their reactions with other reactive atmospheric species (e.g., O_3, NO_3 radicals, $O(^3P)$ atoms) are too low for them to be of significance (Atkinson 1997, and references therein). Therefore, the current mechanism considers only reactions of alkanes with OH radicals.

Data are available for the OH radical rate constants for all the n-alkanes through n-$C_{16,}$ for various branched alkane isomers up to ~C_{10}, and for various cyclic alkane up to C_{12}. The OH radical rate constants and temperature dependence expressions that are used in the SAPRC-99 mechanism (Carter, 2000) for the higher molecular weight ($C_{\geq 7}$) alkanes for which data are available are summarized on Table 1. Most of the rate constant expressions on Table 1 are those recommended in the review by Atkinson (1997), but a few more recently measured rate constants are also given. Based on the available kinetic data, Atkinson (1987) developed a structure-estimation method that can be used to estimate OH radical rate constants for alkanes and other types of compounds. The performance of this method, as updated by Kwok and Atkinson (1995), in predicting the measured rate constants is shown on Table 1, where it can be seen that the rate constants for most compounds are predicted to within ±25%. Thus, the method of Kwok and Atkinson (1995) serves as a good basis for estimating OH radical rate constants for $C_{\geq 12}$ alkanes whose rate constants have not been measured. The one exception is 3,4-diethyl hexane, where steric effects may be slowing down the rate of reaction at the two tertiary hydrogens in the molecule.

The reaction of OH with alkanes occurs by the abstraction of an H atom from one of the various positions on the molecule, forming H_2O and the corresponding alkyl radical. The alkyl radical can then add O_2 to form the corresponding peroxy radical, which, in the presence of NO_x, will primarily react with NO to form NO_2 and the corresponding alkoxy radical or the corresponding alkyl nitrate. These are shown below in the case of the radical formed from reaction of OH at the 3-position of n-octane.

$$CH_3CH_2CH_2CH_2CH_2CH_2CH_2CH_3 + OH \rightarrow H_2O + CH_3CH_2CH_2CH_2CH_2CH(\cdot)CH_2CH_3 \quad (1)$$

$$CH_3CH_2CH_2CH_2CH_2CH(\cdot)CH_2CH_3 + O_2 \rightarrow CH_3CH_2CH_2CH_2CH_2CH(OO\cdot)CH_2CH_3 \quad (2)$$

$$CH_3CH_2CH_2CH_2CH_2CH(OO\cdot)CH_2CH_3 + NO \rightarrow CH_3CH_2CH(ONO_2)CH_2CH_2CH_2CH_2CH_3 \quad (3)$$

$$CH_3CH_2CH_2CH_2CH_2CH(OO\cdot)CH_2CH_3 + NO \rightarrow NO_2 + CH_3CH_2CH_2CH_2CH_2CH(O\cdot)CH_2CH_3 \quad (4)$$

Table 1. Experimental and estimated rate constants for the reactions of OH radicals with $C_{\geq 7}$ alkanes, as used in the SAPRC-99 mechanism (Carter, 2000). Experimental data are from the evaluation of Atkinson (1997) unless indicated otherwise.

Compound	Model Name	k(300) (cm^3 $molec^{-1}$ s^{-1})	A [a]	B	Ea kcal/mole	Refs [b]	Est'd k(300) k	(diff)
n-Heptane	N-C7	7.04e-12	1.43e-12	2.0	-0.950		6.91e-12	-2%
n-Octane	N-C8	8.76e-12	2.48e-12	2.0	-0.751		8.33e-12	-5%
n-Nonane	N-C9	1.00e-11	2.26e-12	2.0	-0.888		9.75e-12	-3%
n-Decane	N-C10	1.13e-11	2.82e-12	2.0	-0.827		1.12e-11	-1%
n-Undecane	N-C11	1.29e-11					1.26e-11	-2%
n-Dodecane	N-C12	1.39e-11					1.40e-11	1%
n-Tridecane	N-C13	1.60e-11					1.54e-11	-4%
n-Tetradecane	N-C14	1.80e-11					1.69e-11	-6%
n-Pentadecane	N-C15	2.10e-11					1.83e-11	-13%
n-Hexadecane	N-C16	2.30e-11					1.97e-11	-14%
2,2,3-Trimethyl Butane	223TM-C4	4.25e-12	7.61e-13	2.0	-1.025		3.24e-12	-24%
2,2-Dimethyl Pentane	22-DM-C5	3.40e-12					3.26e-12	-4%
2,4-Dimethyl Pentane	24-DM-C5	5.00e-12					6.87e-12	37%
2,2,3,3-Tetrame. Butane	2233M-C4	1.06e-12	1.72e-12	2.0	0.286		1.02e-12	-4%
2,2,4-Trimethyl Pentane	224TM-C5	3.60e-12	1.87e-12	2.0	-0.389		4.66e-12	30%
2,2-Dimethyl Hexane	22-DM-C6	4.80e-12					4.68e-12	-2%
2,3,4-Trimethyl Pentane	234TM-C5	7.10e-12					8.55e-12	20%
2,3,5-Trimethyl Hexane	235TM-C6	7.90e-12					9.97e-12	26%
2-Methyl Octane	2-ME-C8	1.01e-11					9.73e-12	-4%
3,3-Diethyl Pentane	33-DE-C5	4.90e-12					5.31e-12	8%
4-Methyl Octane	4-ME-C8	9.70e-12					1.00e-11	3%
2,6-Dimethyl Octane	26DM-C8	1.29e-11				1	1.14e-11	-12%
2-Methyl Nonane	2-ME-C9	1.28e-11				1	1.12e-11	-12%
3,4-Diethyl Hexane	34-DE-C6	7.40e-12				2	1.25e-11	69%
Cycloheptane	CYCC7	1.30e-11					9.94e-12	-24%
Methyl cyclohexane	ME-CYCC6	1.00e-11					1.02e-11	2%
Cyclooctane	CYCC8	1.40e-11					1.14e-11	-19%
1,1,3-Trimethyl Cyclohexane	113MCYC6	8.70e-12					9.12e-12	5%
Hexyl Cyclohexane	C6-CYCC6	1.78e-11				3	1.77e-11	-1%

[a] Temperature dependence given by $k(T) = A\ (T/300)^B\ e^{-Ea/RT}$, where T is the temperature in ^oK, and R is the gas constant. If no data are given for A, B and Ea, then temperature dependence data are not available.

[b] If no footnote number is given, then the rate constant is recommended by Atkinson (1997). Following are references for rate constants measured subsequently.

1. This work.
2. Atkinson et al. (2000)
3. Carter et al (2000a)

The higher molecular weight alkoxy radical can react either with O_2, by β-scission decomposition, or by 1,4-H shift isomerization via a 6-member ring transition state, e.g.,

$$CH_3CH_2CH_2CH_2CH_2CH(O\cdot)CH_2CH_3 + O_2 \rightarrow CH_3CH_2CH_2CH_2CH_2C(O)CH_2CH_3 + HO_2 \quad (5)$$

$$CH_3CH_2CH_2CH_2CH_2CH(O\cdot)CH_2CH_3 \rightarrow CH_3CH_2CH_2CH_2CH_2CHO + CH_3CH_2\cdot \quad (6)$$

$$CH_3CH_2CH_2CH_2CH_2CH(O\cdot)CH_2CH_3 \rightarrow CH_3CH_2CH(OH)CH_2CH_2CH(\cdot)CH_2CH_3 \quad (7)$$

Based on available information concerning the reactions of alkoxy radicals formed in alkane photooxidation systems, the 1,4-H shift isomerization reaction (e.g., Reaction 7) is expected to be the major process for those long chain alkoxy radicals where it can occur (Atkinson, 1997; Carter, 2000). The subsequent reactions of the bifunctional radical formed in Reaction (7) are expected to be:

$$CH_3CH_2CH(OH)CH_2CH_2CH(\cdot)CH_2CH_3 + O_2 \rightarrow CH_3CH_2CH(OH)CH_2CH_2CH(OO\cdot)CH_2CH_3 \quad (8)$$

$$CH_3CH_2CH(OH)CH_2CH_2CH(OO\cdot)CH_2CH_3 + NO \rightarrow CH_3CH_2CH(OH)CH_2CH_2CH(ONO_2)CH_2CH_3 \quad (9)$$

$$CH_3CH_2CH(OH)CH_2CH_2CH(OO\cdot)CH_2CH_3 + NO \rightarrow NO_2 + CH_3CH_2CH(OH)CH_2CH_2CH(O\cdot)CH_2CH_3 \quad (10)$$

$$CH_3CH_2CH(OH)CH_2CH_2CH(O\cdot)CH_2CH_3 \rightarrow CH_3CH_2CH(OH)CH_2CH_2C(\cdot)(OH)CH_2CH_3 \quad (11)$$

$$CH_3CH_2CH(OH)CH_2CH_2C(\cdot)(OH)CH_2CH_3 + O_2 \rightarrow CH_3CH_2CH(OH)CH_2CH_2C(O)CH_2CH_3 + HO_2\cdot \quad (12)$$

Thus the major products formed after the reaction of OH at the 3-position of n-octane are expected to be 6-hydroxy-3-octanone and HO_2 with two NO to NO_2 conversions, 3-octyl nitrate with the consumption of 1 NO, and 6-hydroxy-2-octyl nitrate with one NO to NO_2 conversion and consumption of an additional NO. Analogous mechanisms and products are expected from the other higher n-alkanes. The predicted formation of these δ-hydroxy carbonyl products from higher molecular weight has been confirmed by recent experimental product data (Eberhard et al, 1995; Kwok et al, 1996; Arey et al, 2000).

Analogous reactions can occur in the case of the higher molecular weight branched and cyclic alkanes if they have sufficiently long chains that the 1,4-H shift can occur. Decompositions to form lower molecular weight oxygenated products and radicals that cause additional NO to NO_2 conversions become relatively more important in the case of the branched alkanes because (1) decompositions forming tertiary radicals or ketones are more favorable than those forming primary radicals or aldehydes (Carter, 2000), and (2) branched alkanes tend to have shorter chains, and the possibility of forming radicals that cannot under go 1,4-H shifts increases. Reactions analogous to Reaction (11) above also cannot occur with radicals formed by reaction of OH at tertiary hydrogens, and the competing processes generally involve more NO to NO_2 conversions. It is also likely that 1,4-H shift isomerizations become relatively less important in the case of the cycloalkanes because the bicyclic transition states required may have greater strain.

For example, in the case of cyclohexane, the initially formed alkoxy radical is estimated to react with O_2 about 70% of the time to form cyclohexanone (Reaction 17), with the remaining 30% reacting by decomposition with ring opening (Reaction 18), to ultimately give rise to polyfunctional products with additional NO to NO_2 conversion and nitrate formation, e.g.,

$$–CH_2CH_2CH_2CH_2CH_2CH_2– + OH \rightarrow –CH_2CH_2CH_2CH_2CH_2CH(\cdot)– \quad (13)$$

$$–CH_2CH_2CH_2CH_2CH_2CH(\cdot)– + O_2 \rightarrow –CH_2CH_2CH_2CH_2CH_2CH(OO\cdot)– \quad (14)$$

$$–CH_2CH_2CH_2CH_2CH_2CH(OO\cdot)– + NO \rightarrow –CH_2CH_2CH_2CH_2CH_2CH(ONO_2)– \quad (15)$$

$$–CH_2CH_2CH_2CH_2CH_2CH(OO\cdot)– + NO \rightarrow NO_2 + –CH_2CH_2CH_2CH_2CH_2CH(O\cdot)– \quad (16)$$

$$–CH_2CH_2CH_2CH_2CH_2CH(O\cdot)– + O_2 \dashrightarrow –CH_2CH_2CH_2CH_2CH_2C(O)– + HO_2 \quad (17)$$

$$–CH_2CH_2CH_2CH_2CH_2CH(O\cdot)– \rightarrow HCOCH_2CH_2CH_2CH_2CH_2\cdot \quad (18)$$

$$HCOCH_2CH_2CH_2CH_2CH_2\cdot + O_2 \rightarrow HCOCH_2CH_2CH_2CH_2CH_2OO\cdot \quad (19)$$

$$HCOCH_2CH_2CH_2CH_2CH_2OO\cdot + NO \rightarrow HCOCH_2CH_2CH_2CH_2CH_2ONO_2 \quad (20)$$

$$HCOCH_2CH_2CH_2CH_2CH_2OO\cdot + NO \rightarrow NO_2 + HCOCH_2CH_2CH_2CH_2CH_2O\cdot \quad (21)$$

$$HCOCH_2CH_2CH_2CH_2CH_2O\cdot \rightarrow HCOCH_2CH(\cdot)CH_2CH_2CH_2OH \quad (22)$$

$$HCOCH_2CH(\cdot)CH_2CH_2CH_2OH + O_2 \rightarrow HCOCH_2CH(OO\cdot)CH_2CH_2CH_2OH \quad (23)$$

$$HCOCH_2CH(OO\cdot)CH_2CH_2CH_2OH + NO \rightarrow HCOCH_2CH(ONO_2)CH_2CH_2CH_2OH \quad (24)$$

$$HCOCH_2CH(OO\cdot)CH_2CH_2CH_2OH + NO \rightarrow NO_2 + HCOCH_2CH(O\cdot)CH_2CH_2CH_2OH \quad (25)$$

$$HCOCH_2CH(O\cdot)CH_2CH_2CH_2OH \rightarrow HCOCH_2CH(OH)CH_2CH_2CH(\cdot)OH \quad (26)$$

$$HCOCH_2CH(OH)CH_2CH_2CH(\cdot)OH + O_2 \rightarrow HCOCH_2CH(OH)CH_2CH_2CHO + HO_2\cdot \quad (27)$$

As discussed by Atkinson (1997) and Carter (2000), except for nitrate yields in the reaction of NO with the initially formed peroxy radicals (discussed below) and qualitative information on bifunctional product formation, there is almost no experimental information on the branching ratios or product yields involved in these reactions. Therefore, the rate constant ratios involved have to be estimated in order to derive overall reaction mechanisms for these alkanes. Estimation methods exist for all the reactions involved (e.g., Carter and Atkinson, 1985; Atkinson, 1987; Carter, 2000) and these can serve as a basis for generating comprehensive detailed mechanisms for the atmospheric reactions of alkanes in the presence of NO_x (Carter, 1990, 2000). The most recent version is incorporated into the SAPRC-99 mechanism generation system that is documented by Carter (2000) and that was used to derive the higher alkane photooxidation mechanisms used in this study.

The major aspects of the mechanisms that affect the overall ozone impacts of these higher alkanes are the overall nitrate yields from the reactions of NO with the higher molecular weight peroxy radicals, and the numbers of NO to NO_2 conversions involved in the overall photooxidation process. The latter are determined by branching ratios involved in the alkoxy radical reactions that determine whether additional radicals are formed that result in multi-step mechanisms. The number of NO to NO_2 conversions is probably not a major uncertainty in the case of the normal alkanes because isomerizations are expected to dominate in almost all cases, but this may be a greater uncertainty in mechanisms for branched and cyclic alkanes where competing decompositions or reactions with O_2 may become relatively more important. Uncertainties in the predictions of product formation are probably not as important a factor affecting reactivity predictions of the alkanes. This is because the most likely mechanisms generally predict similar types of higher molecular weight bi- or polyfunctional oxygenates, and model calculations (at least for single day scenarios) tend to be relatively insensitive to assumptions about these product's mechanisms.

Probably the most important factor affecting predicted reactivities of the higher molecular weight alkanes concerns nitrate formation from the reactions of NO with the higher molecular weight peroxy radicals (e.g., Reactions 3, 19, 15, 20 and 24, above). This reaction, which becomes increasingly important as the size of the molecule increases (Carter and Atkinson, 1989a; Atkinson, 1997), represents both a radical and NO_x sink. If sufficiently important these reactions can cause significant reductions in overall ozone formation potentials of the reacting VOCs, and even ozone inhibition. This is the major reason why high molecular weight alkanes tend to have very low ozone formation potentials, despite their relatively high OH radical rate constants and relatively large number of estimated NO to NO_2 conversions (Carter and Atkinson, 1989b; Carter, 1994a, 2000). Information concerning the relative rates of this reaction compared to the competing formation of the alkoxy radical and NO_2 comes primarily from measurements of yields of the various secondary alkyl nitrates formed from the radicals formed in the initial reactions of the n-alkanes and cyclohexane, and from a very limited number of measurements of primary or tertiary alkyl nitrate yields from branched alkanes (Carter and Atkinson, 1989b; Atkinson, 1997). Yields of substituted nitrates formed from the hydroxy-substituted radicals formed after 1,5-H shift isomerizations (e.g., the rate constant ratio for Reactions 9 vs. 10, 20 vs. 21 and 24 vs. 25, above) are unknown and have to be estimated.

Updates to the Alkane Photooxidation Mechanisms

The nitrate yields used when deriving mechanisms for the higher alkanes in the SAPRC-90 (Carter, 2000) through SAPRC-97 (Carter et. al, 1997b) mechanisms are based on the data and recommendations given by Carter and Atkinson (1989a). These are shown on Figure 1 for the secondary peroxy radicals formed from the normal alkanes. Based on these data, nitrate yields of over 30% were calculated for the radicals initially formed in the oxidation of n-octane. increasing to yields of 40-45% for the initially formed radicals from the $C_{\geq 12}$ n-alkanes. However, the extrapolation above C_8 was uncertain and was determined primarily by the nature of the curve fit parameterization used.

Mechanisms using the nitrate yield data and estimates of Carter and Atkinson (1997a) gave a good fit to the environmental chamber reactivity data for n-octane (Carter et al, 1993, 1995b, 1997b; Carter, 1995), and reasonably good fits to the data for the C_{12} - C_{16} n-alkanes obtained in our Phase 1 study for this project (Carter et al, 1996). However, to obtain these fits it had to be assumed that nitrate formation from the reaction of NO from the hydroxy substituted peroxy radicals formed after the 1,4-H shift isomerization was negligible (e.g., in Reaction 8, above). Otherwise, the predicted total nitrate yields in the overall reaction are increased by a factor of 1.5 or more, and the model predicts much greater inhibitions of radical levels and NO oxidation rates than were consistent with the environmental chamber data. This was a concern because it is not chemically reasonable for the addition of one OH on peroxy radicals four carbons away from the peroxy center with 8 or more carbons to reduce the nitrate yields from 30% or more to negligible levels. In addition, Atkinson et al (2000) observed that measurable amounts of hydroxynitrates are formed in the NO_x -air reactions of n-decane, butyl cyclohexane and 3,4-diethyl hexane, indicating that nitrate formation from the reactions of NO with these radicals does occur to a non-negligible extent. However, there did not appear to be any other way to reconcile the existing

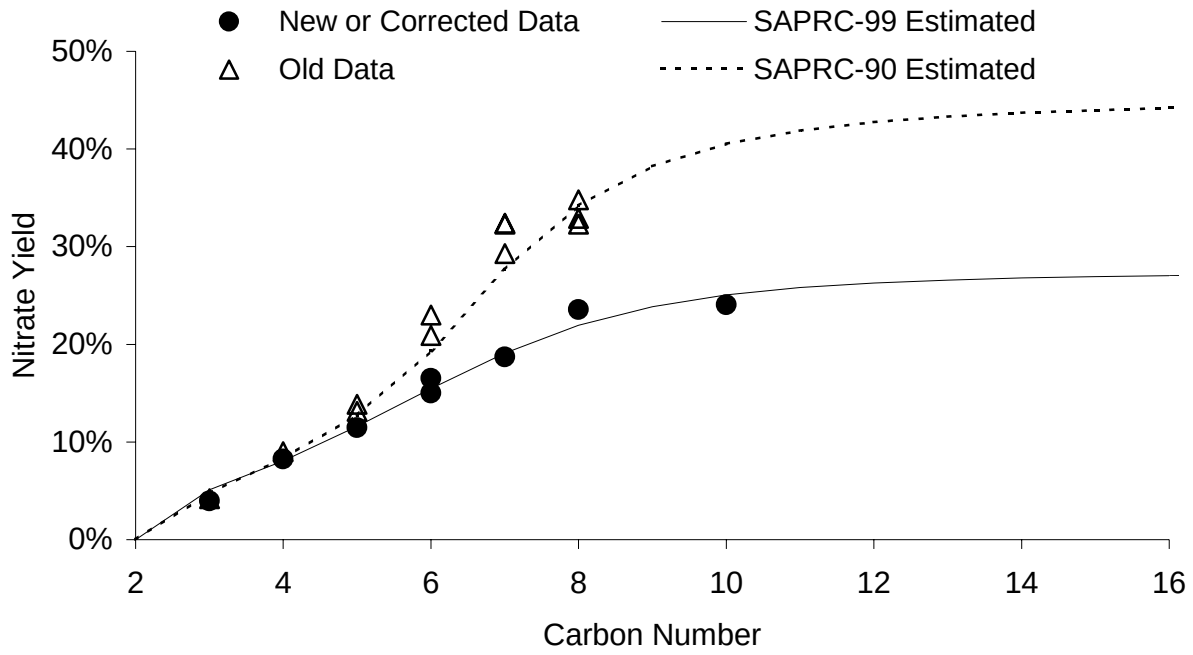

Figure 1. Plots of experimental nitrate yields for reactions of NO with the initially formed secondary peroxy radicals formed from the normal alkanes, and the estimates incorporated in the SAPRC-90 and SAPRC-99 mechanisms derived from these data.

nitrate yield and environmental chamber data into a consistent mechanism for n-alkanes. This assumption was therefore incorporated in the n-alkane mechanism used in our report on the atmospheric ozone impacts of the $C_{\geq 12}$ n-alkanes that was prepared previously (Carter et al, 1996).

The apparent inconsistency between environmental chamber and nitrate yield data was not the only problem associated with the previous mechanisms for the atmospheric reactions of the higher alkanes. Because the limited data indicated lower alkyl nitrate yields from the reactions of NO with primary and tertiary peroxy radicals, the SAPRC-97 and earlier mechanisms predicted that $C_{\geq 8}$ branched and cyclic alkanes tended to have considerably higher ozone reactivities than the normal alkanes with the same carbon numbers. There was limited data available to test this until environmental chamber experiments were carried out using various mineral spirits mixtures, which consist primarily of complex mixtures of $C_{\geq 10}$ alkanes, of which over 75% were branched or cyclic (Carter et al, 1997a). The ozone impacts of these mixtures in the environmental chamber reactivity experiments were very similar to those of n-alkanes in the same carbon number range, and were significantly less than predicted by mechanisms based on their branched and cyclic alkane contents (Carter et al, 1997a). This suggested that the nitrate yields in the reactions of OH radicals with these higher branched and cyclic alkanes may be closer to those for n-alkanes than was being assumed in the mechanism.

Most of the data concerning the effects of nitrate yields on carbon number come from the measurements of Atkinson et al (1982, 1984), and the temperature and pressure effects data come from Atkinson et al (1983b). More recently, using improved chromatographic methods, Arey et al (2000) remeasured the nitrate yields from the C_3-C_8 n-alkanes. They obtained significantly lower nitrate yields for the $C_{\geq 5}$ radicals. In addition, Atkinson and co-workers (unpublished results, 1999) also obtained lower nitrate yields from n-decane than estimated using the parameterization of Carter and Atkinson (1989a). These new data [and old data of Atkinson et al (1982, 1984) corrected using the revised calibration factors as indicated by the results of Arey et al (2000)] are shown on Figure 1, where they can be compared with the previous data and estimates. The revised estimates of these secondary nitrate yields as a function of carbon number, derived by Carter (2000) based on reoptimizing the parameters of Carter and Atkinson (1989a) to fit the new data, are also shown on the figure. It can be seen that the predicted nitrate yields for the higher peroxy radicals are about 40% lower than predicted by the parameterization derived from the older data. In addition, the new data on the nitrate yield for n-decane tended to support the predictions that the rate of increase of the nitrate yields with the size of the molecule will fall off with carbon numbers above 8.

As a result of these reduced nitrate yields from the initially formed peroxy radicals, it is now possible for mechanisms to successfully simulate the $C_{\geq 8}$ normal alkane environmental chamber data without having to make chemically unreasonable assumptions about no nitrate formation from the reactions of NO with OH-substituted peroxy radicals. Only a slight reduction caused by OH substitution is assumed, based on assumed overall nitrate yields that give best fits to the chamber data for a variety of OH-substituted organic compounds (Carter, 2000). Thus it is now possible for model predictions to simulate reactivity data for n-alkanes using a mechanism that is chemically reasonable and consistent with nitrate yield estimates used for other compounds.

This revision in the nitrate yield estimates for secondary peroxy radicals did not totally resolve the problems indicated by the model simulations of the experiments with the mineral spirits mixtures with the branched and cyclic $C_{\geq 8}$ alkanes. As indicated above, the results of these experiments indicated that the $C_{\geq 8}$ branched and cyclic alkanes are much closer in reactivity to the normal alkanes than previously estimated. This is in large part because the reactions of OH radicals with branched and cyclic alkanes are predicted to form nonnegligible amounts of tertiary peroxy radicals, which are predicted to have lower nitrate yields when they react with NO than is the case for the secondary peroxy radicals formed from the n-alkanes. This prediction is based on the limited product data that indicated that nitrate yields from primary and tertiary peroxy radicals are lower than those from the secondary peroxy radicals.

In the previous mechanism, estimates for nitrate yields for these radicals were made by applying a correction factor of 0.4 for primary radicals and 0.3 for tertiary radicals, regardless of the size of the radical. However, an alternative approach can be employed to make this correction for structural effects that is equally consistent with the limited data, but gives much smaller differences in predicted nitrate yields when extrapolated to larger molecules. This is to assume that the structural differences have the effects of changing the effective size of the molecule in terms of affecting predicted nitrate yields, rather

than having the same factor difference regardless of the size of the molecule. In particular, the limited data on primary and tertiary alkyl nitrate yields can be reasonably well predicted by using the nitrate yields predicted for secondary radicals, but with the carbon number reduced by 1.5 (Carter, 2000). This gives about the same predicted nitrate yields for the lower molecular weight primary and tertiary radicals for which there are data (Carter and Atkinson, 1989a), but it also predicts that the differences between the secondary and primary or tertiary radicals decrease with size of the molecule. This is because of the leveling off of the rate of increase in the nitrate yield as the size of the molecule increases, as shown on Figure 1. This prediction is more consistent with the modeling of the mineral spirits reactivity experiments (Carter et al, 1997a), and therefore this approach is adopted for the SAPRC-99 mechanism that is used in this work (Carter, 2000).

Representation of Mineral Spirits Components

The compositions of the four mineral spirits samples that were studied previously for Safety-Kleen (Carter et al, 1997a) are summarized on Table 2. As discussed by Carter et al (1997a), these were derived using carbon number distributions obtained using GC-FID, and normal, branched, and cyclic alkane ratios derived using mass spectral patterns in high-resolution GC-MS analyses carried out by Safety-Kleen Corporation (O'Donnell, personal communication, 1996). Except for Sample "A", which is a recycled material containing small amounts of aromatics and alkenes, they all consisted of mixtures of normal, branched, and cyclic alkanes in the C_8 - C_{15} range. The relative amounts of normal, branched, and cyclic alkanes differed somewhat among the various samples.

The normal alkanes are represented individually in the SAPRC-99 mechanism, but the branched and cyclic components represent complex mixtures of many isomers whose exact structures were not determined. These are represented in the model using selected compounds that are taken as representative of all the isomers with the same carbon number. In our previous calculations (Carter et al, 1997a), a single branched or cyclic compound was taken as representative of all such compounds with the same carbon number, as shown on the left hand columns on Table 3 and Table 4. Note that relatively highly branched compounds were chosen in these assignments. However, GC-MS analyses of mineral spirits samples indicated that less branched compounds, whose mechanisms would be expected to be closer to those of normal alkanes, tend to be relatively more important (O'Donnell, Safety-Kleen Corp., private communication, 1996). Therefore, the assignments of representative compounds used to represent the branched and cyclic alkanes were revised in conjunction with the overall mechanism update. In the revised assignments, the unspeciated branched and cyclic alkanes in complex mixtures are represented using (in most cases) three compounds for each carbon number rather than a single one, and the representative compounds used are generally less highly branched. The revised assignments are also shown on the right hand columns on Table 3 and Table 4. These were used in all the mineral spirits reactivity simulations conducted using the SAPRC-99 mechanism in this work.

Table 2. Compositions of the mineral spirits samples studied by Carter et al (1997a).

Description	Model Species	Weight Percent [a]			
		A	B	C	D
Low reactivity components	INERT	0.17			
n-Octane	N-C8	0.20			
n-Nonane	N-C9	2.36			
n-Decane	N-C10	7.11			
n-Undecane	N-C11	8.29		11.71	14.33
n-Dodecane	N-C12	3.15	1.48	13.59	9.50
n-Tridecane	N-C13	0.23	1.40	0.53	0.21
n-Tetradecane	N-C14		1.71		
Branched C8 Alkanes	BR-C8	0.08			
Branched C9 Alkanes	BR-C9	1.10			
Branched C10 Alkanes	BR-C10	7.89	0.35		
Branched C11 Alkanes	BR-C11	9.52	4.16	2.38	3.33
Branched C12 Alkanes	BR-C12	8.27	11.18	13.30	21.05
Branched C13 Alkanes	BR-C13	2.26	17.69	6.99	5.55
Branched C14 Alkanes	BR-C14	0.10	7.71		
Branched C15 Alkanes	BR-C15		1.33		
Methylcyclohexane	ME-CYCC6	0.01			
Cyclic C8 Alkanes	CYC-C8	0.04			
Cyclic C9 Alkanes	CYC-C9	1.99			
Cyclic C10 Alkanes	CYC-C10	10.45	2.71		
Cyclic C11 Alkanes	CYC-C11	17.32	11.00	12.55	13.40
Cyclic C12 Alkanes	CYC-C12	9.90	19.28	31.26	27.32
Cyclic C13 Alkanes	CYC-C13	1.29	14.37	7.68	5.32
Cyclic C14 Alkanes	CYC-C14		5.04		
Cyclic C15 Alkanes	CYC-C15		0.59		
Aromatic Compounds	See Table 5	6.11			
Alkenes		2.16			

[a] Weight percent for Samples “A”, “B”, “C”, or “D”. See Carter et al (1997a) for a discussion of how the compositions were derived.

Sample “A” differed from the others in that it had small amounts of aromatics and alkenes that also had to be represented. The representation of these constituents used in this work is the same as discussed by Carter et al (1997a), and the specific model species employed and their relative amounts are shown on Table 5. The SAPRC-99 representation of the specific aromatic and alkene model species employed are given by Carter (2000), and were used to derive the lumped “MS-A” aromatic and alkene mechanisms shown in Appendix A.

Table 3. Compounds used to represent branched alkanes when representing mineral spirits samples in atmospheric reactivity model simulations.

Carbon number	1997 Assignments	Current Assignments (SAPRC-99)		Model Species
8	4-Methyl Heptane	50%	2,4-Dimethyl Hexane	24-DM-C6
		25%	4-Methyl Heptane	4-ME-C7
		25%	2-Methyl Heptane	2-ME-C7
9	4-Ethyl Heptane	50%	2,4-Dimethyl Heptane	24-DM-C7
		25%	4-Methyl Octane	4-ME-C8
		25%	2-Methyl Octane	2-ME-C8
10	4-Propyl Heptane	50%	2,6-Dimethyl Octane	26DM-C8
		25%	4-Methyl Nonane	4-ME-C9
		25%	2-Methyl Nonane	2-ME-C9
11	3,5-Diethyl Heptane	50%	2,6-Dimethyl Nonane	26DM-C9
		25%	4-Methyl Decane	4-ME-C10
		25%	3-Methyl Decane	3-ME-C10
12	2,6-Diethyl Octane	50%	3,6-Dimethyl Decane	36DM-C10
		25%	5-Methyl Undecane	5-ME-C11
		25%	3-Methyl Undecane	3-ME-C11
13	3,7-Diethyl Nonane	50%	3,6-Dimethyl Undecane	36DM-C11
		25%	5-Methyl Dodecane	5-ME-C12
		25%	3-Methyl Dodecane	3-ME-C12
14	3,8-Diethyl Decane	50%	3,7-Dimethyl Dodecane	37DM-C12
		25%	6-Methyl Tridecane	6-ME-C13
		25%	3-Methyl Tridecane	3-ME-C13
15	3,9-Diethyl Undecane	50%	3,7-Dimethyl Tridecane	37DM-C13
		25%	6-Methyl Tetradecane	6-ME-C14
		25%	3-Methyl Tetradecane	3-ME-C14

Representation in the SAPRC-99 Mechanism

The detailed mechanisms for the atmospheric reactions of the higher alkanes in the presence of NO_x were derived using the SAPRC-99 mechanism generation and estimation system based on the considerations discussed in the previous sections (see also Carter, 2000). The OH radical rate constants used were either the experimental values as shown on Table 1, above, or, for compounds where reliable experimental data were not available, were estimated using the structure-reactivity method of Kwok and Atkinson (1995). Note that because of the many competing reactions that can occur, the detailed mechanisms produced by the mechanism generation system for the higher molecular weight branched and cyclic alkanes can become quire large, involving hundreds or even thousands of reactions and products. For example, the reactions of 1,3-dipropyl 5-ethyl cyclohexane with OH radicals in the presence of NO_x are predicted to form over 2500 products, with compounds formed in yields of less than 1% contributing almost 50% of the total. This is because of the number of ways that OH can react with the molecule

Table 4. Compounds used to represent cyclic alkanes when representing mineral spirits samples in atmospheric reactivity model simulations.

Carbon number	1997 Assignments	Current Assignments (SAPRC-99)		Model Species
8	Ethylcyclohexane	100%	Ethylcyclohexane	ET-CYCC6
9	1-Ethyl-4-Methyl Cyclohexane	50%	Propyl Cyclohexane	C3-CYCC6
		50%	1-Ethyl-4-Methyl Cyclohexane	1E4MCYC6
10	1,3-Diethyl-Cyclohexane	34%	Butyl Cyclohexane	C4-CYCC6
		33%	1-Methyl-3-Isopropyl Cyclohexane	1M3IPCY6
		33%	1,4-Diethyl-Cyclohexane	14DECYC6
11	13-Diethyl-5-Methyl Cyclohexane	34%	Pentyl Cyclohexane	C5-CYCC6
		33%	13-Diethyl-5-Methyl Cyclohexane	13E5MCC6
		33%	1-Ethyl-2-Propyl Cyclohexane	1E2PCYC6
12	1,3,5-Triethyl Cyclohexane	34%	Hexyl Cyclohexane	C6-CYCC6
		33%	1,3,5-Triethyl Cyclohexane	135ECYC6
		33%	1-Methyl-4-Pentyl Cyclohexane	1M4C5CY6
13	1,3-Diethyl-5-Pentyl Cyclohexane	34%	Heptyl Cyclohexane	C7-CYCC6
		33%	1,3-Diethyl-5-Pentyl Cyclohexane	13E5PCC6
		33%	1-Methyl-2-Hexyl-Cyclohexane	1M2C6CC6
14	1,3-Dipropyl-5-Ethyl Cyclohexane	34%	Octyl Cyclohexane	C8-CYCC6
		33%	1,3-Dipropyl-5-Ethyl Cyclohexane	13P5ECC6
		33%	1-Methyl-4-Heptyl Cyclohexane	1M4C7CC6
15	1,3,5-Tripropyl Cyclohexane	34%	Nonyl Cyclohexane	C9-CYCC6
		33%	1,3,5-Tripropyl Cyclohexane	135PCYC6
		33%	1-Methyl-2-Octyl Cyclohexane	1M2C8CC6

initially, combined with the number of competing alkoxy radical decompositions and isomerizations that are possible with the larger molecules. Various “lumping rules” are applied to these detailed mechanisms to derive their representations in terms of SAPRC-99 model species (Carter, 2000).

The mechanisms used to represent the reactions of these C_8 - C_{15} alkanes are given with the mechanism listing in Appendix A, and their rate constants and radical operator and major product yields are summarized on Table 6. Note that RO2-R· represents the formation of peroxy radicals that ultimately react to convert NO to NO_2 and form HO_2, RO2-N· represents the formation of peroxy radicals that ultimately react with NO to form alkyl nitrates, R2O2· represents extra NO to NO_2 conversions formed by peroxy radicals formed in multi-step mechanisms, CCHO represents acetaldehyde, RCHO represents higher aldehyde products, and PROD2 represents reactive ketones and non-aldehyde bifunctional products that are predicted to be formed. Some of the branched alkanes also form small amounts of acetone and lower reactivity ketone products (MEK) (see Table A-2 in Appendix A), but they are not shown on Table 6 because of their relatively small contributions to the overall reactivity of the alkane.

Table 5. Model species used to represent alkene and aromatic constituents of mineral spirits sample "A" of Carter et al (1997a).

Description	Model Species	Weight Percent
Toluene	TOLUENE	0.12
o-Xylene	O-XYLENE	0.14
m-Xylene	M-XYLENE	0.08
p-Xylene	P-XYLENE	0.08
Cumene	I-C3-BEN	0.02
Naphthalene	NAPHTHAL	0.19
Monosubstituted C9 Alkylbenzenes	C9-BEN1	0.05
Monosubstituted C10 Alkylbenzenes	C10-BEN1	0.09
Monosubstituted C11 Alkylbenzenes	C11-BEN1	0.10
Monosubstituted C12 Alkylbenzenes	C12-BEN1	0.03
Monosubstituted C13 Alkylbenzenes	C13-BEN1	0.00
Disubstituted C9 Alkylbenzenes	C9-BEN2	0.24
Disubstituted C10 Alkylbenzenes	C10-BEN2	0.44
Disubstituted C11 Alkylbenzenes	C11-BEN2	0.52
Disubstituted C12 Alkylbenzenes	C12-BEN2	0.16
Disubstituted C13 Alkylbenzenes	C13-BEN2	0.01
Polysubstituted C9 Alkylbenzenes	C9-BEN3	0.66
Polysubstituted C10 Alkylbenzenes	C10-BEN3	1.23
Polysubstituted C11 Alkylbenzenes	C11-BEN3	1.47
Polysubstituted C12 Alkylbenzenes	C12-BEN3	0.45
Polysubstituted C13 Alkylbenzenes	C13-BEN3	0.02
C8 Terminal Alkenes	C8-OLE1	0.00
C9 Terminal Alkenes	C9-OLE1	0.08
C10 Terminal Alkenes	C10-OLE1	0.44
C11 Terminal Alkenes	C11-OLE1	0.73
C12 Terminal Alkenes	C12-OLE1	0.42
C13 Terminal Alkenes	C13-OLE1	0.05
C8 Internal Alkenes	C8-OLE2	0.00
C9 Internal Alkenes	C9-OLE2	0.02
C10 Internal Alkenes	C10-OLE2	0.11
C11 Internal Alkenes	C11-OLE2	0.18
C12 Internal Alkenes	C12-OLE2	0.10
C13 Internal Alkenes	C13-OLE2	0.01

Table 6. Summary of OH radical rate constants and radical operator and product yields used when representing the C_8 - C_{15} normal, branched, and cyclic alkanes in the SAPRC-99 mechanism

Model Species	kOH [a]	Radical Operator or Product Yields						
		RO2-R·	RO2-N·	R2O2·	HCHO	CCHO	RCHO	PROD2
				Normal Alkanes				
N-C8	8.74e-12	0.65	0.35	0.79			0.02	0.62
N-C9	1.00e-11	0.60	0.40	0.78			0.02	0.58
N-C10	1.13e-11	0.57	0.43	0.77			0.01	0.56
N-C11	1.29e-11	0.55	0.45	0.77			0.01	0.54
N-C12	1.39e-11	0.54	0.46	0.77			0.01	0.53
N-C13	1.60e-11	0.53	0.47	0.77			0.01	0.52
N-C14	1.80e-11	0.53	0.47	0.76			0.01	0.52
N-C15	2.10e-11	0.53	0.47	0.76			0.01	0.52
				Branched Alkanes				
24-DM-C6	8.57e-12	0.65	0.35	1.35	0.16	0.33	0.31	0.29
4-ME-C7	8.59e-12	0.68	0.32	0.87			0.38	0.38
2-ME-C7	8.31e-12	0.66	0.34	0.88	0.02	0.03	0.16	0.55
24-DM-C7	9.99e-12	0.60	0.40	1.18	0.10	0.01	0.41	0.38
4-ME-C8	9.70e-12	0.61	0.39	0.89		0.03	0.13	0.56
2-ME-C8	1.01e-11	0.59	0.41	0.91			0.06	0.54
26DM-C8	1.29e-11	0.57	0.43	1.10		0.11	0.31	0.28
4-ME-C9	1.14e-11	0.57	0.43	0.88		0.02	0.14	0.52
2-ME-C9	1.28e-11	0.55	0.45	0.89			0.04	0.52
34-DE-C6 [b]	7.40e-12	0.62	0.38	1.11	0.01	0.34	0.32	0.13
26DM-C9	1.28e-11	0.53	0.47	1.04			0.22	0.38
4-ME-C10	1.29e-11	0.53	0.47	0.91			0.08	0.50
3-ME-C10	1.29e-11	0.53	0.47	0.92		0.03	0.04	0.49
36DM-C10	1.45e-11	0.49	0.51	1.08		0.09	0.11	0.46
5-ME-C11	1.43e-11	0.52	0.48	0.87		0.01	0.06	0.50
3-ME-C11	1.43e-11	0.52	0.48	0.90		0.03	0.03	0.48
36DM-C11	1.60e-11	0.49	0.51	1.05		0.07	0.12	0.44
5-ME-C12	1.57e-11	0.51	0.49	0.86		0.01	0.04	0.50
3-ME-C12	1.57e-11	0.51	0.49	0.88		0.02	0.03	0.48
37DM-C12	1.74e-11	0.50	0.50	0.98		0.06	0.11	0.44
6-ME-C13	1.71e-11	0.51	0.49	0.85		0.01	0.04	0.50
3-ME-C13	1.71e-11	0.51	0.49	0.87		0.02	0.01	0.49
37DM-C13	1.88e-11	0.49	0.51	0.98		0.04	0.09	0.44
6-ME-C14	1.85e-11	0.51	0.49	0.84		0.01	0.04	0.50
3-ME-C14	1.85e-11	0.50	0.50	0.86		0.02	0.01	0.49

Table 6 (continued)

Model Species	kOH [a]	Radical Operator or Product Yields						
		RO2-R·	RO2-N·	R2O2·	HCHO	CCHO	RCHO	PROD2
				Cyclic Alkanes				
ET-CYCC6	1.20e-11	0.62	0.38	1.05		0.15	0.33	0.30
C3-CYCC6	1.34e-11	0.61	0.39	0.86			0.36	0.39
1E4MCYC6	1.37e-11	0.52	0.48	1.34	0.03	0.14	0.41	0.14
C4-CYCC6	1.49e-11	0.58	0.42	0.83		0.02	0.18	0.47
1M3IPCY6	1.51e-11	0.54	0.46	1.20	0.01		0.26	0.29
14DECYC6	1.55e-11	0.51	0.49	1.23	0.02	0.23	0.33	0.21
C5-CYCC6	1.63e-11	0.56	0.44	0.81		0.02	0.15	0.46
13E5MCC6	1.72e-11	0.43	0.57	1.37	0.02	0.17	0.35	0.09
1E2PCYC6	1.70e-11	0.46	0.54	1.20	0.01	0.03	0.19	0.35
C6-CYCC6	1.78e-11	0.53	0.47	0.85			0.09	0.46
135ECYC6	1.90e-11	0.42	0.58	1.35	0.01	0.22	0.31	0.12
1M4C5CY6	1.80e-11	0.48	0.52	1.05		0.02	0.21	0.33
C7-CYCC6	1.91e-11	0.51	0.48	0.85			0.07	0.46
13E5PCC6	2.05e-11	0.43	0.56	1.24	0.01	0.13	0.34	0.19
1M2C6CC6	1.94e-11	0.46	0.54	1.08		0.01	0.13	0.38
C8-CYCC6	2.05e-11	0.51	0.49	0.85			0.06	0.46
13P5ECC6	2.19e-11	0.45	0.55	1.16	0.01	0.06	0.38	0.23
1M4C7CC6	2.08e-11	0.46	0.54	1.06			0.13	0.35
C9-CYCC6	2.20e-11	0.51	0.49	0.84			0.06	0.47
135PCYC6	2.33e-11	0.45	0.55	1.11			0.42	0.26
1M2C8CC6	2.22e-11	0.46	0.54	1.03		0.01	0.10	0.39

[a] OH radical rate constant in units of cm^3 $molec^{-1}$ s^{-1}.

[b] 3,4-Diethyl hexane not used when representing mixtures, but is one of the representative branched alkanes studied for this program.

The two major factors that affect the overall impacts of these alkanes are the total organic nitrate yields and the extra NO to NO_2 conversions caused by multi-step mechanisms, which are represented by the yields of the RO2-N· and the R2O2· model species respectively. A graphical comparison of how these factors vary with carbon number for the different types of alkanes is shown on Figure 2. Note that the $C_{\geq 8}$ normal alkanes have very similar overall mechanisms, other than the predicted increase in the overall nitrate yield with the size of the molecule, leveling off at about C_{13}. The predicted nitrate yields and the extra NO to NO_2 conversions tend to be more variable with the branched and cyclic alkanes, as might be expected due to the structural variations that are possible. The variability in the extra NO to NO_2 conversions is considerably more than the variability in nitrate yields. The greatest variability appears to be with the cyclic alkanes, with the compounds with the most substituents around the rings tending to have the highest nitrate yields and also the largest number of NO to NO_2 conversions. Note that for cyclic compounds with 11 or more carbons and branched compounds with 12 or more carbons the variability with structure becomes greater than the effect of carbon number in determining the overall nitrate yields.

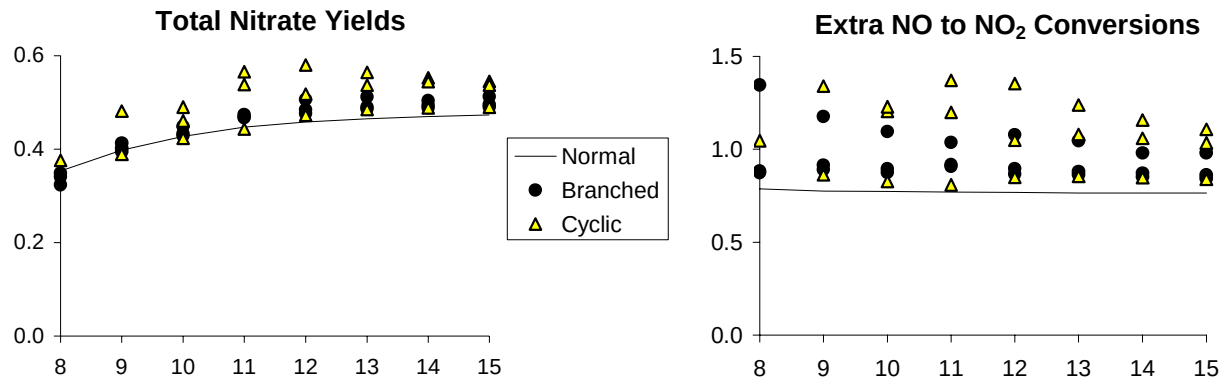

Figure 2. Plots of total nitrate yields and extra NO to NO_2 conversions for the normal, branched, and cyclic C_8 - C_{15} alkanes against carbon number.

It is interesting to note that, in contrast with the previous version of the mechanism, the overall nitrate yields in the branched and cyclic alkanes tend to be *higher* than with the normal alkanes with the same carbon number. This is despite the fact that the reactions of these compounds involve more formation of tertiary peroxy radicals, which are predicted to have lower nitrate yields when they react with NO. This can be attributed to the prediction of more complex mechanisms for the branched and cyclic alkanes, involving more peroxy radical formation in secondary reactions, and thus the additional extra NO to NO_2 conversions that is represented by higher R2O2· yields. In addition to causing extra NO to NO_2 conversions, these secondarily-formed peroxy radicals also react with NO to cause additional nitrate formation. For example, compare the sequence of reactions typical of a normal alkane mechanism (Reactions 1 - 12, above), with the sequence representative of a cyclic alkane mechanism (Reactions 13 - 27, above). The latter involves more steps and peroxy radicals, thus more overall NO to NO_2 conversions and higher overall nitrate yields.

The higher nitrate yields predicted for the branched and cyclic alkanes would tend to cause reduced predicted reactivities for these compounds because of the radical and NO_x inhibition effects. However, this is countered by the effect of the higher predicted NO to NO_2 conversions, which tend to cause increased predicted ozone formation due to the alkane's direct reactions. As can be seen by the results of the atmospheric reactivity calculations discussed later in this report, the differences in the extra NO to NO_2 conversions appears to be the relatively more important factor in determining the effects of structure on overall reactivities in most of these cases.

EXPERIMENTAL RESULTS

Relative Rate Constant Measurements

The rate constants for the reactions of OH radicals with 2-methyl nonane, 2,5-dimethyl octane, 3,4-diethyl hexane and (for control purposes) n-octane and n-decane were measured using a relative rate method, with m-xylene used as the reference compound. The relative rate method employed has been used extensively in other laboratories for many years [see references cited by Atkinson (1989), e.g., Atkinson et al, 1981)], and involves measurements of the consumption of the various compounds in the presence of OH radicals. In this work, the OH radicals were generated by the photolysis of nitrous acid,

$$HONO + h\nu \rightarrow OH + NO$$

which photolyzes with half life of less than 5 minutes with the light source that was employed.

Assuming that the organics react only with OH radicals, the kinetic differential equations for the organics can be solved and rearranged to yield

$$\ln(\frac{[Organic]_{t0}}{[Organic]_t}) - D_t = \frac{k_{Organic}}{k_{Reference}} \ln\left[(\frac{[Reference]_{t0}}{[Reference]_t}) - D_t \right] \qquad (IV)$$

where $[Organic]_{t0}$ and $[Organic]_t$, $[Reference]_{t0}$, and $[Reference]_t$ are the initial and time=t concentrations of the test and reference compounds, respectively, $k_{Organic}$ and $k_{Reference}$ are the test and reference compound's OH rate constant, and D_t is a factor added to account for dilution due to reactant injections, leaks, etc, from the beginning of the experiment up to time t. Since no reactant injections were made during the experiments and the leaks in this chamber are believed to be negligible during the time period of the experiments, D_t is assumed to be negligible in our analysis. Therefore plots of $\ln([Organic]_{t0}/[Organic]_t)$ against $\ln([Reference]_{t0}/[Reference]_t)$ should yield a straight line with intercept of approximately zero and a slope that is the ratio of rate constants. Given the known value of $k_{Reference}$, then $k_{Organic}$ can then be derived. In principle all of the compounds could be present in the same experiment but because of GC interferences and other factors generally only 2-4 test compounds are present in any given experiment.

To verify the method as employed in this study, relative rate constants were also determined for n-octane and n-decane. These were used because their rate constants have already been measured, their physical characteristics and volatilities are similar to the test compounds of interest, and the same analytical methods are employed. Thus if there are analytical or wall loss problems associated with conducting the experiments with the test compounds, they should also show up and yield incorrect results for these control compounds as well.

Three kinetic experiments were carried out for this project, and their conditions and detailed measurement data are given on Table 7. Plots of Equation (IV) are shown on Figure 3 for each of the five

test compounds. Note that the initial reactant concentrations used when deriving these plots were determined using a least squares optimization method to minimize least squares errors in fits of the data to Equation (IV), with the initial reactant concentrations as well as the ratios of rate constants being simultaneously optimized during this process. This procedure minimizes biases introduced by experimental uncertainties in the initial reactant measurements, and allows all of the measurements to be weighted equally when determining rate constant ratios according to Equation (IV). The results are summarized on Table 8.

Figure 3 shows that good precision was obtained in all the relative rate constant measurements in this study, and that the rate constants derived for n-octane and n-decane were in good agreement with the literature values. The rate constant for 3,4-diethyl hexane was recently measured by Atkinson et al (2000), and the value obtained in this work is also consistent with that result. The Atkinson et al (2000) value is used in our model simulations for this compound because only one experiment was carried out for this compound in this study. There are no known previous measurements for the rate constants for 2-methyl nonane and 2,6-dimethyl octane, but the measurements obtained in this work are in good agreement with the rate constants estimated using the structure-reactivity methods of Kwok and Atkinson (1995). These rate constants were used in the model simulations for these two compounds in this work.

Environmental Chamber Experiments

Summary of Experiments and Characterization Results

Table 9 gives a chronological listing of all the experiments carried out for this program. These consisted primarily of the experiments with the three branched alkanes, whose results are summarized in the following section. In addition, several characterization runs were carried out to determine the chamber-dependent inputs needed for the model simulations of the experiments. Table 9 summarizes the purposes and relevant results from these runs. Except as discussed below, the results of most of these experiments were as expected based on our previous experience with these and similar chambers in our laboratories (Carter et al., 1995c and references therein; Carter et al, 2000b). Carter et al (2000b) gives a more detailed more discussion of the characterization results for these chambers during this time period, particularly with respect to light intensity and the chamber radical source.

The one problem observed with the chamber conditions during the course of this study was that there was apparent chamber contamination by chlorine atom sources caused by an attempt to inject too much HONO in side B in run DTC742, as indicated on Table 9. The n-butane - NO_x experiment carried out immediately after that indicated a much higher apparent chamber radical source in the side that was exposed to the apparent contamination from the reactants in the previous run. However, subsequent n-butane - NO_x irradiations apparently cleaned up the contamination, since after two such experiments the results were in the normal range.

Table 7. Measurement data for the kinetic experiments carried out for this program.

	m-Xylene	n-Octane	n-Decane	2-Methyl Nonane	2,6-Dimethyl Octane	3,4-Diethyl Hexane
			Run 1. 0.5 ppm HONO, 0.5 ppm NO			
Init.	0.208	0.165		0.193	0.232	
Init.	0.219	0.167		0.208	0.244	
.	0.107	0.125		0.142	0.163	
	0.105	0.124		0.139	0.162	
	0.083	0.113		0.123	0.142	
	0.084	0.114		0.122	0.143	
	0.071	0.108		0.114	0.133	
	0.070	0.108		0.111	0.131	
	0.060	0.101		0.104	0.118	
	0.057	0.097		0.097	0.113	
			Run 2. 1 ppm HONO			
Init.	0.098		0.086	0.110	0.100	
Init.	0.099		0.084	0.109	0.099	
	0.067		0.074	0.092	0.083	
	0.068		0.075	0.094	0.083	
	0.040		0.059	0.072	0.063	
	0.040		0.059	0.073	0.063	
	0.029		0.051	0.062	0.053	
	0.028		0.049	0.060	0.052	
	0.023		0.045	0.054	0.046	
	0.022		0.043	0.052	0.045	
	0.019		0.042	0.050	0.041	
	0.017		0.039	0.046	0.038	
			Run 3. 1 ppm HONO			
Init.	0.100		0.086	0.108		0.125
Init.	0.095		0.076	0.097		0.119
	0.062		0.062	0.077		0.103
	0.060		0.061	0.076		0.103
	0.037		0.049	0.058		0.089
	0.038		0.050	0.060		0.093
	0.027		0.043	0.049		0.081
	0.028		0.044	0.050		0.082
	0.020		0.034	0.038		0.068
	0.021		0.038	0.042		0.075
	0.018		0.033	0.037		0.068
	0.015		0.031	0.033		0.064

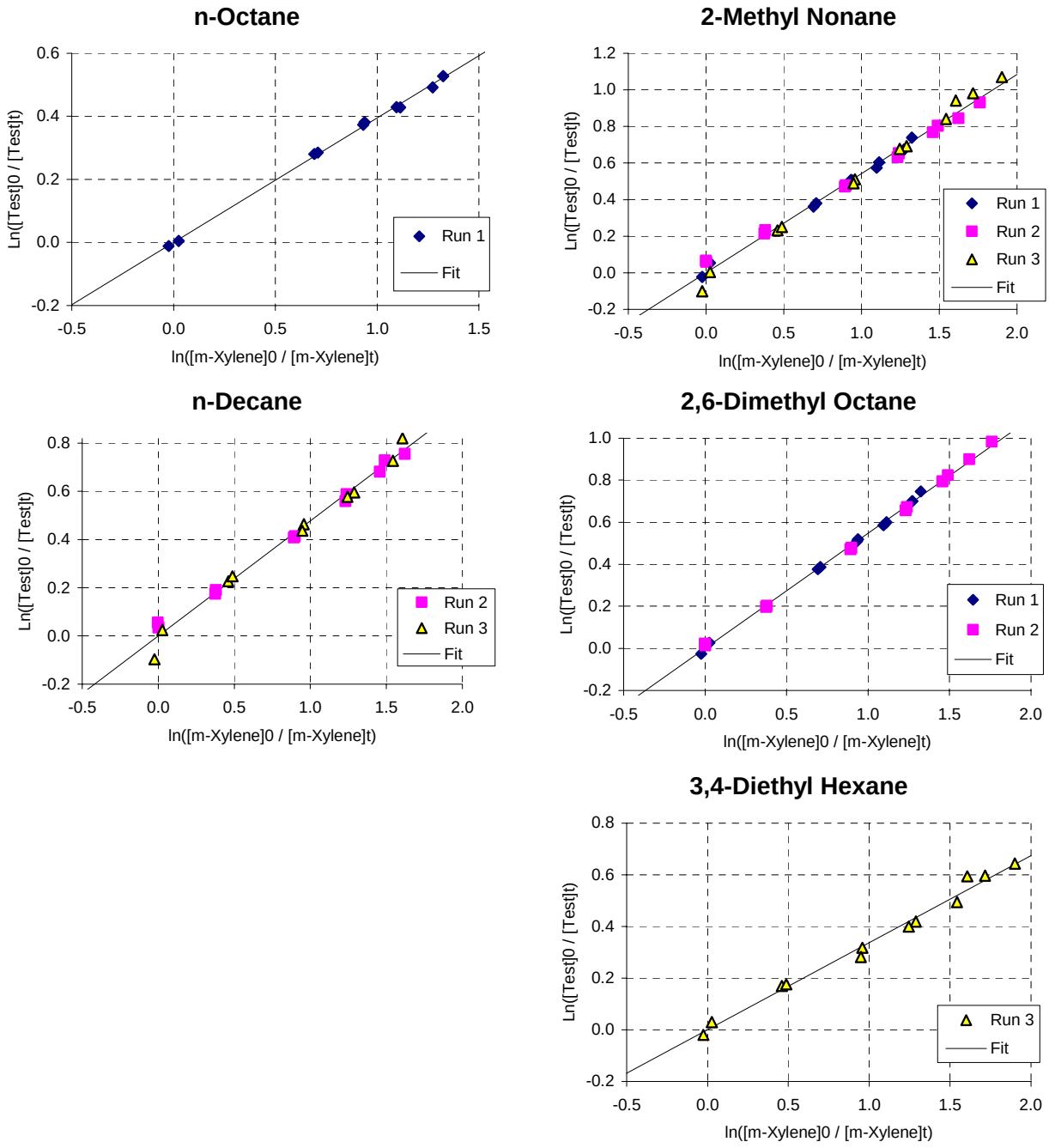

Figure 3. Plots of Equation (IV) for n-octane, n-decane, 2-methyl nonane, 2,6-dimethyl octane, and 3,4-diethyl hexane, with m-xylene as the test compound.

Table 8. Summary of Results of OH Radical Rate Constant Measurements.

Compound	kOH / kOH (m-Xylene) [a]	kOH (cm^3 $molec^{-1}$ s^{-1})		
		This Work [b]	Literature	Reference
n-Octane	0.39 ± 0.01	9.32×10^{-12}	8.83×10^{-12}	Atkinson (1989)
n-Decane	0.48 ± 0.02	1.13×10^{-11}	1.14×10^{-11}	Atkinson (1989)
2-Methyl Nonane	0.54 ± 0.02	1.28×10^{-11}	1.14×10^{-11}	Kwok and Atkinson (1995) (Estimated)
2,6-Dimethyl Octane	0.55 ± 0.01	1.29×10^{-11}	1.14×10^{-11}	Kwok and Atkinson (1995) (Estimated)
3,4-Diethyl Hexane	0.34 ± 0.02	7.96×10^{-12}	7.40×10^{-12}	Atkinson et al. (2000)

[a] Rate constant ratio determined to minimize least squares errors between $\ln([VOC]_0/[VOC]_t)$ calculated using Equation (IV) and the experimentally measured values. The initial m-xylene and test VOC concentrations in each experiment were also optimized as part of this determination, to avoid biases introduced by uncertainties in initial reactant concentrations used in Equation (IV). Dilution is assumed to be negligible in all experiments. The stated error limits reflect precision on measurement only. Uncertainties for n-dodecane and hexyl cyclohexane based on (2 σ) standard deviations of least squares fits of lines to data.

[b] Placed on an absolute basis using kOH for m-xylene of 2.36×10^{-11} cm^3 $molec^{-1}$ s^{-1} at 298K (Atkinson, 1989).

The results of these characterization experiments were taken into account when deriving the chamber dependent parameters used in the model simulations of these experiments, as discussed below and indicated on Table A-4 in Appendix A.

Reactivity Experiments

As indicated on Table 9, at least five incremental reactivity experiments were carried out for each of the three branched alkanes, consisting of two experiments for each compound using the mini-surrogate and high NO_x full surrogate, and at least one experiment using the low NO_x full surrogate. The initial reactant concentrations and results of these experiments are summarized on Table 10. Concentration-time plots of selected data are given in the following section, in conjunction with the discussion of the results of the model simulations of these and the mineral spirits experiments.

The results of these experiments indicate that the reactivity characteristics of these branched alkanes are qualitatively similar to the other higher alkanes (Carter et al, 1996, 2000a) and the mineral spirits samples (Carter et al, 1997a) that we have studied. All compounds inhibit OH radical levels in the experiments, and they also have negative effects on NO oxidation and O_3 formation rates in the mini-surrogate experiments. However, the magnitudes of the negative IntOH and mini-surrogate $\Delta([O_3]-[NO])$ incremental reactivities are generally less than observed in comparable experiments with the $C_{\geq 12}$ normal (Carter et al, 1996) and cyclic (Carter et al, 2000a) alkanes. This suggests that the amount of inhibition caused by the reactions of the branched alkanes is less than those for the normal alkanes and alkyl cyclohexanes in similar size ranges. The inhibition is also somewhat less (on a per-carbon basis) than

Table 9. Chronological listing of the environmental chamber experiments carried out to evaluate the ozone formation potentials of the selected branched alkanes.

Run No.	Date	Title	Comments
DTC704	8/31/98	NO_2 Actinometry	NO_2 photolysis rate measured using the quartz tube method was 0.165 min^{-1}, in good agreement with the trend observed with the other such runs.
DTC718	10/30/98	n-Butane - NO_x	Run to measure the rate of the chamber radical source, as discussed by Carter et al (1995c). The NO oxidation rate was slightly higher on Side A, but the results were in the normal range and were well simulated using the standard chamber model assigned to this series of experiments.
DTC725	11/13/98	Modified Mini-Surrogate + 3,4-Diethyl hexane	Modified mini-surrogate reactivity experiment with 0.24 ppm 3,4-diethyl hexane injected in Side A. Results summarized on Table 10.
DTC726	11/16/98	Full Surrogate + 3,4-Diethyl Hexane	High NO_x full surrogate reactivity experiment with 0.24 ppm 3,4-diethyl hexane injected in Side B. Results summarized on Table 10.
DTC727	11/17/98	Pure Air Irradiation	Control run to test for chamber background effects. Only about 10 ppb of O_3 was formed on both sides of the chamber, about half the amount predicted by the standard chamber wall model.
DTC729	11/19/98	Full Surrogate + 3,4-Diethyl Hexane	High NO_x full surrogate reactivity experiment with 0.5 ppm 3,4-diethyl hexane injected in Side B. Results summarized on Table 10.
DTC730	11/20/98	Modified Mini-Surrogate + 3,4-Diethyl-Hexane	Modified mini-surrogate reactivity experiment with 1 ppm 3,4-diethyl hexane injected in Side A. Results summarized on Table 10.
DTC731	11/21/98	Pure Air Irradiation	Pure air irradiation carried out to determine the results of improvements made to clean air system to reduce the background NO_x levels that have been periodically observed. Approximately 19 ppb of O_3 was observed on both sides after 6 hours of irradiation, compared to ~35 ppb of O_3 predicted by the standard chamber effects model. Therefore, the improvements reduced the background O_3 formed in these experiments. This has no significant results on results of experiments where NO_x is injected, as is the case for the mechanism evaluation runs for this program.
DTC732	11/23/98	Low NO_x Full Surrogate + 3,4-Diethyl Hexane	Low NO_x full surrogate reactivity experiment with 1.2 ppm 3,4-diethyl hexane injected in Side B. Results summarized on Table 10.
DTC733	11/24/98	Modified Mini-Surrogate + 2,6-Dimethyl Octane	Modified mini-surrogate reactivity experiment with 1 ppm 2,6-dimethyl octane injected in Side A. Results summarized on Table 10.
DTC734	11/25/98	Mini-Surrogate + 2-Methyl Nonane	Modified mini-surrogate reactivity experiment with 1 ppm 2-methyl nonane injected in Side B. Results summarized on Table 10.

Table 9 (continued)

Run No.	Date	Title	Comments
DTC735	11/29/98	Pure Air Irradiation	Pure air irradiation to test for background effects after the improvements in the pure air system. Approximately 8 ppb of O_3 was found after 5 hours of irradiation on both sides, which was slightly less than was the case in run DTC731.
DTC736		NO_2 Actinometry	NO_2 photolysis rate measured using the quartz tube method was 0.162 min^{-1}, suggesting that the light intensity is becoming approximately constant during this period.
DTC737	12/1/98	Full Surrogate + 2-Methyl Nonane	High NO_x full surrogate reactivity experiment with 0.5 ppm 2-methyl nonane injected in Side A. Results summarized on Table 10.
DTC738	12/2/98	Full Surrogate + 2,6-Dimethyl Octane	High NO_x full surrogate reactivity experiment with 0.6 ppm 2,6-dimethyl octane injected in Side B. Results summarized on Table 10.
DTC739	12/5/98	Low NO_x Full Surrogate + 2,6-Dimethyl Octane	Low NO_x full surrogate reactivity experiment with 0.5 ppm 2,6-dimethyl octane injected in Side A. Results summarized on Table 10.
DTC740	12/7/98	Low NO_x Full Surrogate + 2-Methyl Nonane	Low NO_x full surrogate reactivity experiment with 0.6 ppm 2-methyl nonane injected in Side B. Results summarized on Table 10.
DTC741	12/8/98	Mini-Surrogate + 2-Methyl Nonane	Mini-surrogate reactivity experiment with 0.5 ppm 2-methyl nonane injected in Side A. Results summarized on Table 10.
DTC742	12/10/98	kOH Determination with HONO	An attempted kinetic experiment was carried out with HONO, various alkanes, and m-xylene injected into Side B. A high flow rate was used in the HONO generator in an attempt to get the desired amount of HONO into the chamber. The alkane rate constant ratios relative to m-xylene were high, suggesting possible contamination by chlorine atom sources (either HCl or NOCl). This apparently resulted from incomplete reaction of the HCl with the $NaNO_2$ in the HONO generator (Febo et al, 1995). The data were rejected.
DTC743	12/11/98	n-Butane - NO_x	Run to test for chamber effects after apparent HCl or NOCl contamination in Side B in the chamber. The NO oxidation rate in Side B was about twice as high as that on Side A, which was in the normal range. Leaks were found on Side B, which were fixed.
DTC744	12/12/98	n-Butane - NO_x conditioning	The n-butane run was repeated to condition the chamber after the apparent contamination of Side B. The NO oxidation rate on Side B was still higher than on Side A, but it was less than in the previous run.

Table 9 (continued)

Run No.	Date	Title	Comments
DTC745	12/14/98	n-Butane - NO_x	The n-butane run was repeated to further condition the chamber after the apparent contamination of Side B, and to test whether the chamber has been restored to normal. The NO oxidation rate on Side B was only slightly higher than on Side A, and the NO oxidation rates on both sides were somewhat lower than predicted by the standard chamber model, but the results were in the normal range. Since the contamination caused higher than normal NO oxidation rates, and the side differences are now relatively small, it was concluded that the chamber has been adequately reconditioned.
DTC746	12/15/98	Full Surrogate + 2-Methyl Nonane	High NO_x full surrogate reactivity experiment with 1 ppm 2-methyl nonane injected in Side B. Results summarized on Table 10.
DTC747	12/16/98	Full Surrogate + 2,6-Dimethyl Octane	High NO_x full surrogate reactivity experiment with 1 ppm 2,6-dimethyl octane injected in Side A. Results summarized on Table 10.
DTC748	12/17/98	Low NO_x Full Surrogate + 3,4-Diethyl Hexane	Low NO_x full surrogate reactivity experiment with 2 ppm 3,4-diethyl hexane injected in Side B. Results summarized on Table 10.
DTC749	12/18/98	Modified Mini-Surrogate + 2,6-Dimethyl Octane	Modified mini-surrogate reactivity experiment with 0.5 ppm 2,6-dimethyl octane injected in Side A. Results summarized on Table 10.
DTC751	12/22/98	n-Butane - Chlorine Actinometry	Run to measure the light intensity by determining the Cl_2 photolysis rate, as discussed by Carter et al (1995c). The results yielded a calculated NO_2 photolysis rate of 0.153 min-1, which is reasonably consistent with the results of the quartz tube Actinometry experiments carried out previously, which indicated an NO_2 photolysis rate of ~0.16 min-1.
DTC752	1/5/99	n-Butane - NO_x	Run to measure the rate of the chamber radical source. Results are reasonably well simulated using the standard chamber model, though Side B still had a somewhat higher radical source than Side A.
DTC761	1/20/99	Propene - NO_x	Standard propene - NO_x control run for comparison with other such runs in this and other chambers. Results in normal range. Good side equivalency observed.
DTC764	1/26/99	Acetaldehyde + air	Run to test for NO_x wall offgasing effects. Approximately 17 ppb of O_3 and 4 ppb of PAN formed after six hours of irradiation, with similar results on both sides. Results in good agreement with predictions of standard chamber wall model.

Table 10 Summary of conditions and selected results of the environmental chamber experiments with the selected C_{10} cycloalkanes.

Run	Test VOC (ppm)	NO_x (ppm)	Surg. (ppm C)	Δ([O_3]-[NO]) (ppm) 2nd Hour Base	2nd Hour Test	2nd Hour IR [a]	6th Hour Base	6th Hour Test	6th Hour IR [a]	5th Hour IntOH (10^{-6} min) Base	5th Hour IntOH Test	5th Hour IntOH IR [a]
2-Methyl Nonane												
Mini-Surrogate												
DTC734B	1.08	0.40	5.59	0.10	0.05	-0.05	0.43	0.18	-0.23	9.4	1.9	-7
DTC741A	0.53	0.38	5.35	0.09	0.05	-0.09	0.38	0.20	-0.33	9.2	2.7	-12
High NO_x Full Surrogate												
DTC737A	0.49	0.32	4.37	0.24	0.17	-0.14	0.46	0.48	0.03	19.6	11.2	-17
DTC746B	1.10	0.30	4.38	0.25	0.13	-0.10	0.48	0.46	-0.01	21.2	7.8	-12
Low NO_x Full Surrogate												
DTC740B	0.55	0.10	3.98	0.26	0.24	-0.03	0.29	0.28	-0.01	22.1	14.4	-14
2,6-Dimethyl Octane												
Mini-Surrogate [b]												
DTC733A	1.01	0.30	6.44	0.09	0.04	-0.05	0.36	0.17	-0.19	10.7	2.1	-9
DTC749A	0.52	0.38	6.48	0.12	0.06	-0.10	0.44	0.28	-0.30	12.4	5.1	-14
High NO_x Full Surrogate												
DTC738B	0.56	0.31	4.19	0.25	0.18	-0.13	0.49	0.49	0.01	19.7	10.0	-17
DTC747A	0.98	0.29	4.26	0.24	0.16	-0.08	0.47	0.52	0.05	21.1	7.9	-13
Low NO_x Full Surrogate												
DTC739A	0.54	0.10	4.22	0.26	0.27	0.01	0.28	0.31	0.05	20.2	9.9	-19
3,4-Diethyl Hexane												
Mini-Surrogate [b]												
DTC725A	0.24	0.37	6.00	0.10	0.09	-0.03	0.39	0.38	-0.05	-	-	-
DTC730A	1.10	0.30	6.21	0.09	0.06	-0.02	0.34	0.25	-0.09	10.1	4.1	-5
High NO_x Full Surrogate												
DTC726B	0.24	0.29	4.32	0.24	0.22	-0.10	0.49	0.49	-0.02	19.3	16.7	-11
DTC729B	1.15	0.24	4.04	0.18	0.15	-0.02	0.42	0.46	0.03	16.2	9.9	-5
Low NO_x Full Surrogate												
DTC732B	1.24	0.08	4.12	0.26		-	0.29	0.29	0.00	23.4	10.6	-10
DTC748B	2.05	0.09	4.09	0.25	0.25	0.00	0.26	0.28	0.01	19.8	11.1	-4

[a] IR = Incremental Reactivity = ([Test] - [Base]) / [Test Compound Added]

[b] Modified mini-surrogate used, with m-xylene replaced by toluene and 1,3,5-trimethylbenzene.

observed in the experiments with the mineral spirits samples (Carter et al, 1997a). As with the other higher alkanes and the mineral spirits samples, the effects of these branched alkanes on NO oxidation and O_3 formation was less in the full surrogate experiments, with their negative effect on O_3 declining essentially to zero or becoming slightly positive by the end of the irradiations.

The results of the experiments with 2-methyl nonane and 2,6-dimethyl octane are very similar to each other, suggesting similar reactivity characteristics for these two isomers. On the other hand, the inhibiting characteristics of 3,4-diethyl hexane is considerably less than the other two isomers, having much lower $\Delta([O_3]-[NO])$ inhibition in the mini-surrogate experiments, and somewhat less negative IntOH reactivities. However all three isomers were similar in that all isomers had very small effects on $\Delta([O_3]-[NO])$ in the full surrogate experiments.

The radical inhibiting effects in the reactions of these higher molecular weight alkanes can be attributed to the relatively high nitrate formation in the reactions of the peroxy radicals with NO, as discussed above. The NO oxidation and O_3 formation rates in the mini-surrogate experiments tend to be the most sensitive to radical inhibition or initiation effects (Carter et al, 1995a), and consequently the $\Delta([O_3]-[NO])$ reactivities are also highly negative in these experiments. On the other hand the full surrogate experiments are relatively more sensitive to the effects of the NO to NO_2 conversions involved in the alkane photooxidation mechanisms, which tend to work in the opposite direction. For alkanes such as n-octane, with lower overall nitrate yields, this is sufficient to counteract the inhibiting effect of the radical inhibition involved with nitrate formation and result in positive $\Delta([O_3]-[NO])$ reactivities in the full surrogate experiments (Carter et al, 1995a). In the case of the higher alkanes the positive effects of the NO to NO_2 conversions almost counter the radical inhibiting effects in the full surrogate experiments, so the magnitudes of the $\Delta([O_3]-[NO])$ reactivities are generally quite small.

The mechanistic implications of these results will be discussed further in the following section, in conjunction with the discussion of the model simulations of these experiments.

MECHANISM EVALUATION

The abilities of the current SAPRC-99 chemical mechanism to appropriately simulate the atmospheric impacts of the representative branched alkanes studied was evaluated by conducting model simulations of the environmental chamber experiments carried out for this project. This is compared with the performance of the SAPRC-97 mechanism used in the previous study of Carter et al (1997a). In addition, since changes were made to the mechanisms and model species used to represent the constituents of the mineral spirits samples studied by Carter et al (1997a), the ability of the current mechanism to simulate these mineral spirits experiments is also examined in this work, and compared with the results of the previous evaluation. The methods and results of this mechanism evaluation are discussed in this section.

Methods

The environmental chamber modeling methods used in this work are based on those discussed in detail by Carter and Lurmann (1990, 1991), updated as discussed by Carter et al. (1995c; 1997b, 2000b). Model simulations of environmental chamber experiments requires including in the model appropriate representations of chamber-dependent effects such as wall reactions and characteristics of the light source. The photolysis rates were derived from results of NO_2 actinometry experiments and measurements of the relative spectra of the light source. The thermal rate constants were calculated using the temperatures measured during the experiments, with the small variations in temperature with time during the experiment being taken into account. The computer programs and modeling methods employed are discussed in more detail elsewhere (Carter et al, 1995c). The specific values of the chamber-dependent parameters used in the model simulations of the experiments for this study are given in Table A-4 in Appendix A.

The experiments modeled in this study included most of the mineral spirits reactivity experiments studied by Carter et al (1997a) as well as the branched alkane reactivity experiments carried out for the current project. The mineral spirits reactivity experiments were also carried out in the same chamber employed in this study, though several years previously. The chamber-dependent parameters used when modeling these are also given in Table A-4 in Appendix A. As indicated there, most of the chamber-dependent parameters used when modeling those experiments were the same as used in modeling the experiments for the current study. However, the light intensities as determined by the results of the actinometry experiments and the chamber radical source parameters as determined by the butane - NO_x or CO - NO_x irradiations carried out during those periods were somewhat different. Table A-4 indicates those cases where different values were used for chamber-dependent parameters for runs carried out during different periods.

As indicated above, the chemical mechanism used in most of the model simulations in this work was the SAPRC-99 mechanism documented by Carter (2000). The species, reactions, rate constants, and

parameters used to calculate photolysis rates are listed in Tables A-1 through A-3 in Appendix A. Note that the mechanisms used for the higher alkanes are those derived using the SAPRC-99 mechanism generation system, as discussed above. No adjustments were made to improve the fits of model calculations to the chamber data, except for some sensitivity calculations in the simulations of the branched alkane experiments where the overall nitrate yield and the total number of NO to NO_2 conversions were both reduced by 25%. When reducing the nitrate yields in these sensitivity calculations, the RO2-R· yield was increased by the appropriate amount to account for radical balance, and the yields of the oxygenated products formed along with RO2-R· was increased by the same factor.

For comparison purposes, the chamber experiments were also simulated using the SAPRC-97 mechanism that was employed in the previous study of Carter et al (1997a). This version of the mechanism is documented by Carter et al (1997b). The SAPRC-97 mechanism did not include assignments for 2-methyl nonane, 2,6-dimethyl octane and 3,4-diethyl hexane, so these had to be derived for this work for the alkane mechanism estimation procedures associated with this version of the mechanism (Carter and Atkinson, 1985; Carter and Atkinson, 1989a; Carter, 1990), and the measured OH radical rate constants. Therefore, the mechanisms used for those compounds are the same as they would have been had they been derived at the time of the Carter et al (1997a) study, had the OH radical rate constants been known[1]. These calculations employed the chamber effects model appropriate for that version of the mechanism, which were generally the same as those used for this version of the mechanism as shown on Table A-4, except that slightly different radical source rates were used, as given by Carter et al (1997a,b).

Because of the relative large number of components in the mineral spirit samples, the constituents of the mineral spirits samples were represented using lumped model species whose rate constants and product yield parameters were derived by averaging those of the constituents they represented. All $C_{\geq 8}$ alkane constituents were lumped into a single model species with, for sample "A", separate model species being used for the aromatics and for the olefins. This is the same as the approach that would be used when representing such complex mixtures when present in emissions.

Results

Simulations of the Branched Alkane Experiments

The results of the model simulations of the experiments with the branched alkanes are shown in Figure 4 through Figure 6, which give plots of the experimental and calculated $\Delta([O_3]\text{-}[NO])$ data and $\Delta([O_3]\text{-}[NO])$ and IntOH incremental reactivities for the experiments using the three compounds. The solid lines show model calculations using the branched alkane mechanisms derived using the SAPRC-99 mechanism, and the darker dashed lines show the calculations using the SAPRC-97 mechanism that was

[1] The measured OH rate constants for 2-methyl nonane and 2,6-dimethyl octane are very similar to the measured values, so the use of the measured values would not significantly affect the results. However, as indicated on Table 1, the use of the measured rate constant for 3,4-diethyl hexane will affect the reactivity predictions for that compound.

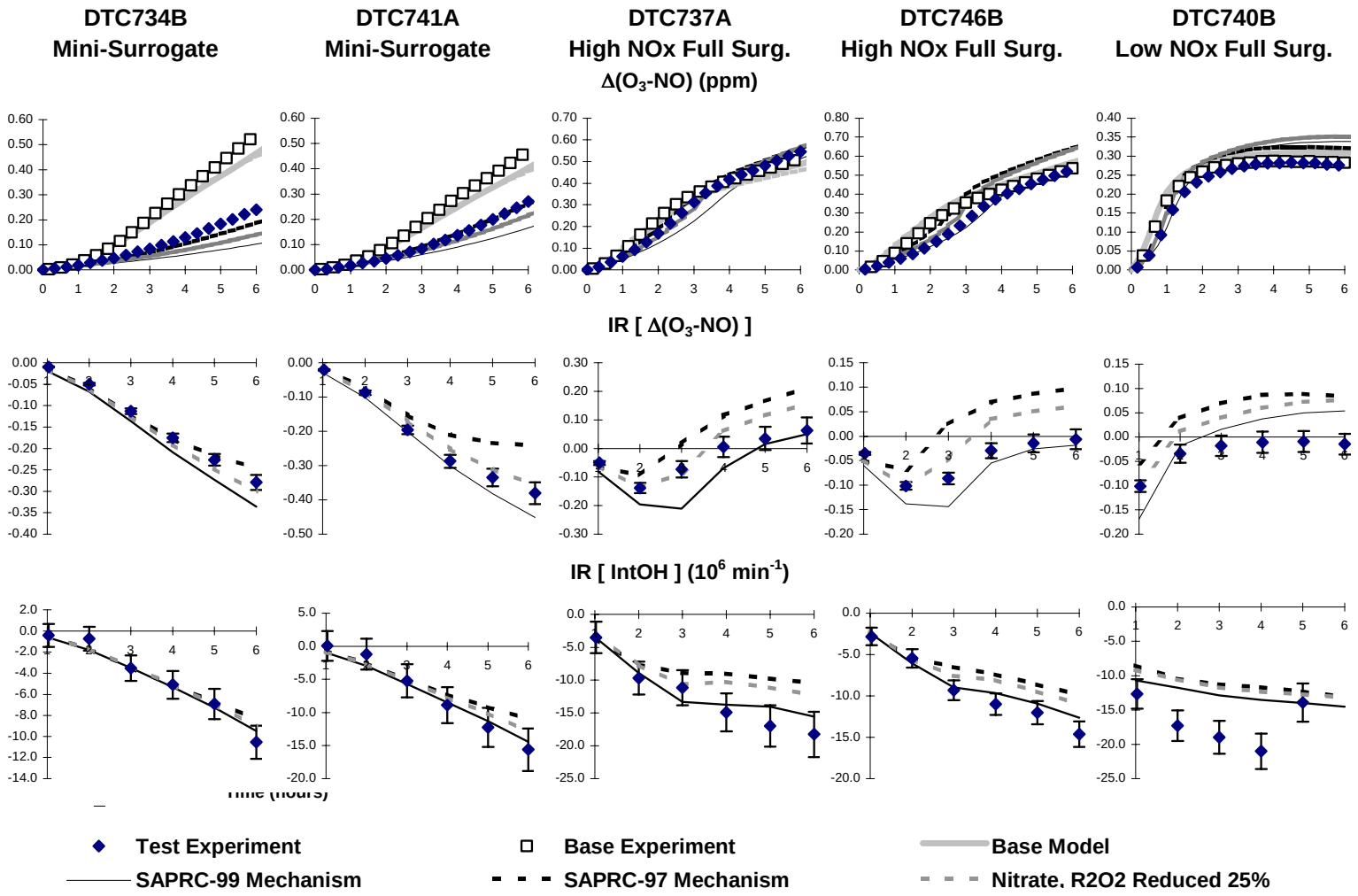

Figure 4. Selected experimental and calculated results of the incremental reactivity experiments with 2-methyl nonane.

employed in the previous study of Carter et al (1997a). In addition, the lighter dashed lines show the calculations with the SAPRC-99 mechanism, but with the overall organic nitrate yields and numbers of extra NO to NO_2 conversions (the R2O2· yield) reduced by 25%.

The results show that the model using the SAPRC-99 mechanism is able to simulate the major reactivity characteristics of these branched alkanes, correctly predicting the inhibition of IntOH in all experiments and of $\Delta([O_3]-[NO])$ in the mini-surrogate runs, and the relatively small effects on $\Delta([O_3]-[NO])$ in the full surrogate experiments. It also correctly predicts that the inhibition of IntOH and mini-surrogate $\Delta([O_3]-[NO])$ is less in the case of 3,4-diethyl hexane than it is for the other two isomers. The mechanism gives good simulations of the magnitude of the IntOH inhibition in most of the experiments, but its performance in simulating the $\Delta([O_3]-[NO])$ reactivity data is more variable. It simulates the $\Delta([O_3]-[NO])$ reactivity data within experimental uncertainty for all the 2-methyl nonane experiments, for the full surrogate experiments for 2,6-dimethyl octane, and for the high NO_x full surrogate experiments for 3,4-diethyl hexane. On the other hand, it tends to overpredict the $\Delta([O_3]-[NO])$ inhibition in the mini-surrogate experiments with 2,6-dimethyl octane and 3,4-diethyl hexane, and overpredict the $\Delta([O_3]-[NO])$ reactivities in the low NO_x full surrogate experiments with 3,4-diethyl hexane.

Although the performance of the SAPRC-99 mechanism in simulating these data is not prefect in all cases, the figures show that it is significantly better overall than the SAPRC-97 mechanism used in the study of Carter et al (1997a). That SAPRC-97 mechanism tends to underpredict the $\Delta([O_3]-[NO])$ inhibition in the mini-surrogate experiments and significantly overpredicts the $\Delta([O_3]-[NO])$ reactivities in essentially all of the full surrogate runs. The poor performance of the SAPRC-97 mechanism in simulating these C_{10} branched alkane experiments is similar to its poor performance in simulating the mineral spirits experiments of Carter et al (1997a) (see also below).

As discussed above, the overall nitrate yields derived for the branched alkane are quite uncertain, based on extrapolating corrections for tertiary nitrate yields from lower molecular weight compounds to compounds in this molecular weight range. Therefore, the tendency of the SAPRC-99 mechanism to overpredict $\Delta([O_3]-[NO])$ inhibition in the mini-surrogate experiments may be due to the nitrate yields being overestimated. However, if overall the nitrate yields are adjusted so the model simulations fit the mini-surrogate experiments and no other modifications are made to the mechanism, then the model significantly overpredicts the $\Delta([O_3]-[NO])$ reactivities in the full surrogate experiments, similar to the results obtained using the SAPRC-97 mechanism. This discrepancy can be reduced by also reducing the extra NO to NO_2 conversions in the mechanism, since the full surrogate experiments are relatively more sensitive to this aspect of the mechanism than are the mini-surrogate runs.

The effects of making these two adjustments to the estimated branched alkane mechanisms are shown by the lighter dotted lines on Figure 4 through Figure 6, which shows model calculations where both the overall nitrate yields and the extra NO to NO_2 conversions are reduced by 25%. This adjustment causes generally better fits to the $\Delta([O_3]-[NO])$ reactivity data, and somewhat improves the model performance in simulating the full surrogate experiments for 2,6-dimethyl octane. On the other hand, the

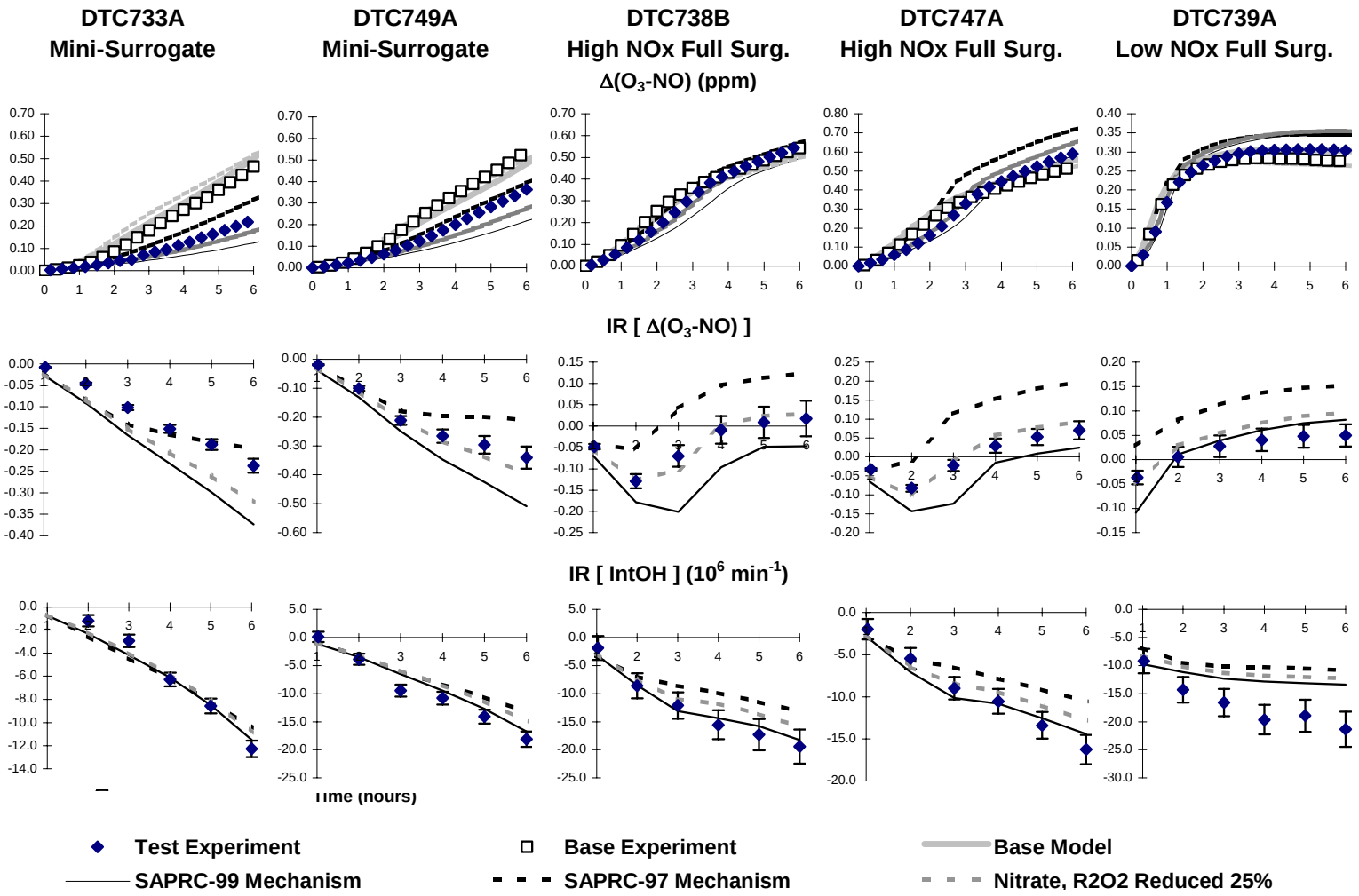

Figure 5. Selected experimental and calculated results of the incremental reactivity experiments with 2,6-dimethyl octane.

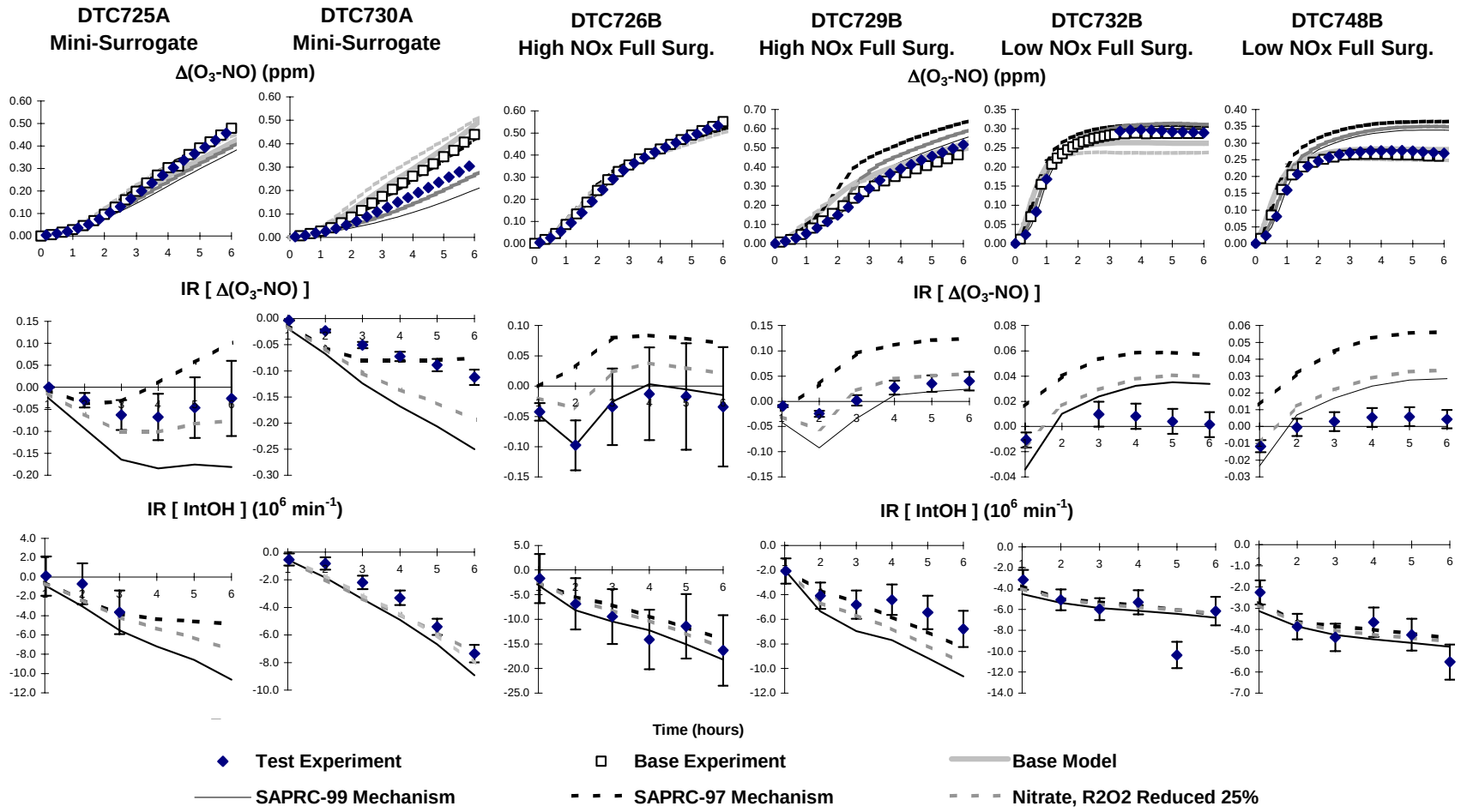

Figure 6. Selected experimental and calculated results of the incremental reactivity experiments with 3,4-diethyl hexane.

adjustment causes somewhat less satisfactory simulations of the full surrogate experiments for 2-methyl nonane and the low NO_x full surrogate experiments for 3,4-diethyl hexane. Overall, the adjustment improves the simulations for 2,6-dimethyl octane and 3,4-diethyl hexane, but the unadjusted mechanism performs better in simulating the data for 2-methyl nonane.

The overall nitrate yields in the atmospheric reactions of branched alkanes are highly uncertain, and reducing these yields to improve fits to these chamber data would not be inappropriate. However, simultaneously reducing the numbers of NO to NO_2 conversions in the model to fit the data is more difficult to justify. It is not clear what reasonable modifications to the estimation methods used for the photooxidation mechanisms for these compounds should be made to reduce the overall number of NO to NO_2 conversions. The estimated number of NO to NO_2 conversions are affected primarily by the branching ratios in the alkoxy radical reactions, but for these compounds making alternative estimates in this regard generally result in similar, or even larger, numbers of such conversions. Also, the influential branching ratios involved for each compound are different, and any adjustments affecting NO to NO_2 conversions would be applicable only to the individual compound. For these reasons, no adjustments were made to the branched alkane mechanisms for general reactivity assessment purposes. Results of ongoing mechanistic studies for atmospheric reactions of branched alkanes may provide data to suggest what improvements to the alkane mechanism estimation methods might be appropriate.

Simulations of the Mineral Spirits Experiments

The conditions and selected results of the mineral spirits reactivity experiments that were modeled in this work are summarized on Table 11. As indicated there, they consist of one each of the three types of incremental reactivity experiments for the four types of mineral spirits samples that were studied by Carter et al (1997a). The experimental and calculated $\Delta([O_3]-[NO])$ data and the $\Delta([O_3]-[NO])$ and the IntOH incremental reactivity data for these experiments are shown on Figure 7 and Figure 8. The solid lines on these figures show the calculations using the current mechanism and model species assignments, and the dashed lines show the calculations using the mechanism and model species assignments employed by Carter et al (1997a). The branched and cyclic alkane constituents were represented in the model calculations using the representative individual species as indicated on Table 3 and Table 4, with the SAPRC-97 assignments in the left-hand columns and the current assignments on the right. No adjustments were made to the mechanisms or assignments to achieve the fits that are obtained.

In contrast with the results obtained using the mechanism and assignments of Carter et al (1997a), the current mechanism and assignments give excellent fits to the results of these experiments without the need for any adjustments. The only systematic discrepancy is the underprediction of IntOH reactivities in the low NO_x full surrogate experiments. However, this is seen for many VOCs (including those with very simple mechanisms, such as CO), and is more likely due to a problem with the base mechanism than the mechanisms for the mineral spirits constituents (Carter et al, 1995b; Carter, 2000). Indeed, the model performance in simulating the results of these experiments is better than its performance in simulating the

Table 11 Summary of conditions and selected results of the selected environmental chamber experiments with the mineral spirits samples. The data are from Carter et al. (1997a).

Run	MS Sample [a]	NO_x (ppm)	Surg. (ppm C)	$\Delta([O_3]-[NO])$ (ppm) 2nd Hour			$\Delta([O_3]-[NO])$ (ppm) 6th Hour			5th Hour IntOH (10^{-6} min)		
				Base	Test	IR [b]	Base	Test	IR [b]	Base	Test	IR [b]
Mini-Surrogate, High NO_x Full Surrogate, and low NO_x Full Surrogate + MS Sample "A" [c]												
DTC442A	1.8	0.35	5.97	0.07	0.05	-0.009	0.31	0.23	-0.042	12.0	7.4	-2.6
DTC486A	3.7	0.30	4.38	0.33	0.33	0.002	0.59	0.65	0.017	24.3	15.4	-2.4
DTC487B	3.7	0.13	4.17	0.37	0.36	-0.003	0.43	0.43	0.000	25.5	12.5	-3.5
Mini-Surrogate, High NO_x Full Surrogate, and low NO_x Full Surrogate + MS Sample "B" [c]												
DTC441B	1.8	0.35	5.61	0.09	0.06	-0.016	0.33	0.21	-0.066	8.6	5.2	-1.9
DTC480A	3.8	0.30	4.21	0.33	0.27	-0.015	0.59	0.58	-0.002	25.5	13.7	-3.2
DTC481B	3.8	0.13	4.32	0.37	0.34	-0.006	0.42	0.42	0.001	26.2	14.0	-3.3
Mini-Surrogate, High NO_x Full Surrogate, and low NO_x Full Surrogate + MS Sample "C" [c]												
DTC440A	1.8	0.35	5.44	0.10	0.06	-0.022	0.40	0.25	-0.079	12.1	6.6	-3.0
DTC478A	3.7	0.31	4.54	0.34	0.30	-0.012	0.61	0.60	-0.002	24.4	14.0	-2.8
DTC479B	3.7	0.14	4.57	0.37	0.36	-0.003	0.44	0.46	0.005	27.0	15.3	-3.2
Mini-Surrogate, High NO_x Full Surrogate, and low NO_x Full Surrogate + MS Sample "D" [c]												
DTC439B	1.8	0.35	5.49	0.11	0.07	-0.020	0.41	0.29	-0.068	10.5	7.2	-1.8
DTC476A	3.7	0.31	4.28	0.33	0.30	-0.009	0.60	0.61	0.003	25.2	14.3	-3.0
DTC477B	3.7	0.13	4.74	0.38	0.36	-0.006	0.43	0.43	0.002	25.9	14.4	-3.1

[a] Initial mineral spirits components in ppm carbon.

[b] IR = Incremental Reactivity = ([Test] - [Base]) / [Test Compound Added]

[c] First run is mini-surrogate, second run is high NO_x full surrogate, and third run is low NO_x full surrogate in each case.

experiments with the individual branched alkanes studied in this project, and is comparable or better than the performance in simulating the individual $C_{\geq 12}$ normal and cyclic alkanes carried out for separate programs (Carter et al, 2000a; Carter, 2000). Clearly, the changes to the alkane mechanisms and the mineral spirits constituent assignments incorporated in the SAPRC-99 mechanism has resolved the problems observed by Carter et al (1997a) in the model simulations of these experiments.

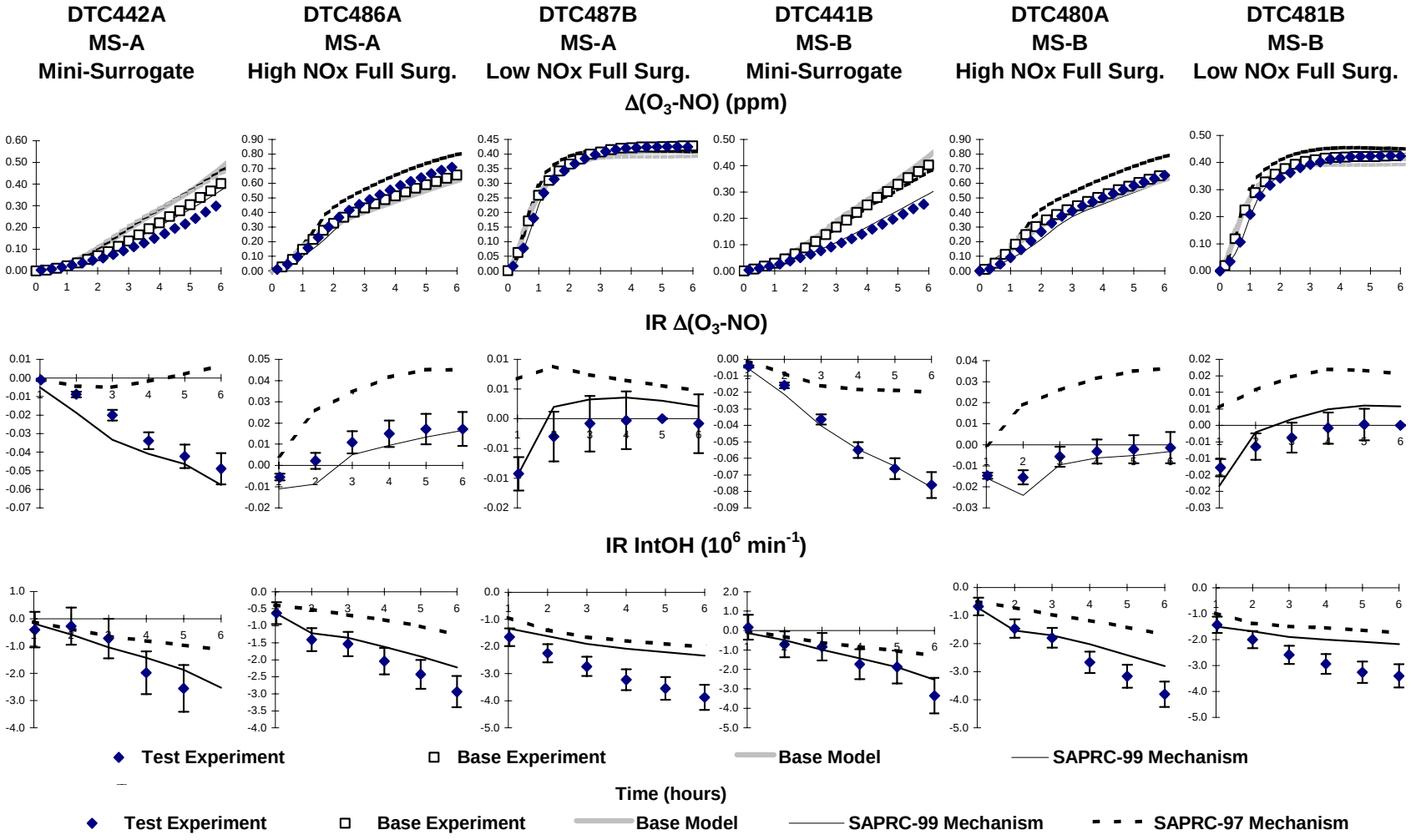

Figure 7. Selected experimental and calculated results of the experiments from the mineral spirits samples "A" and "B" studied by Carter et al (1997a).

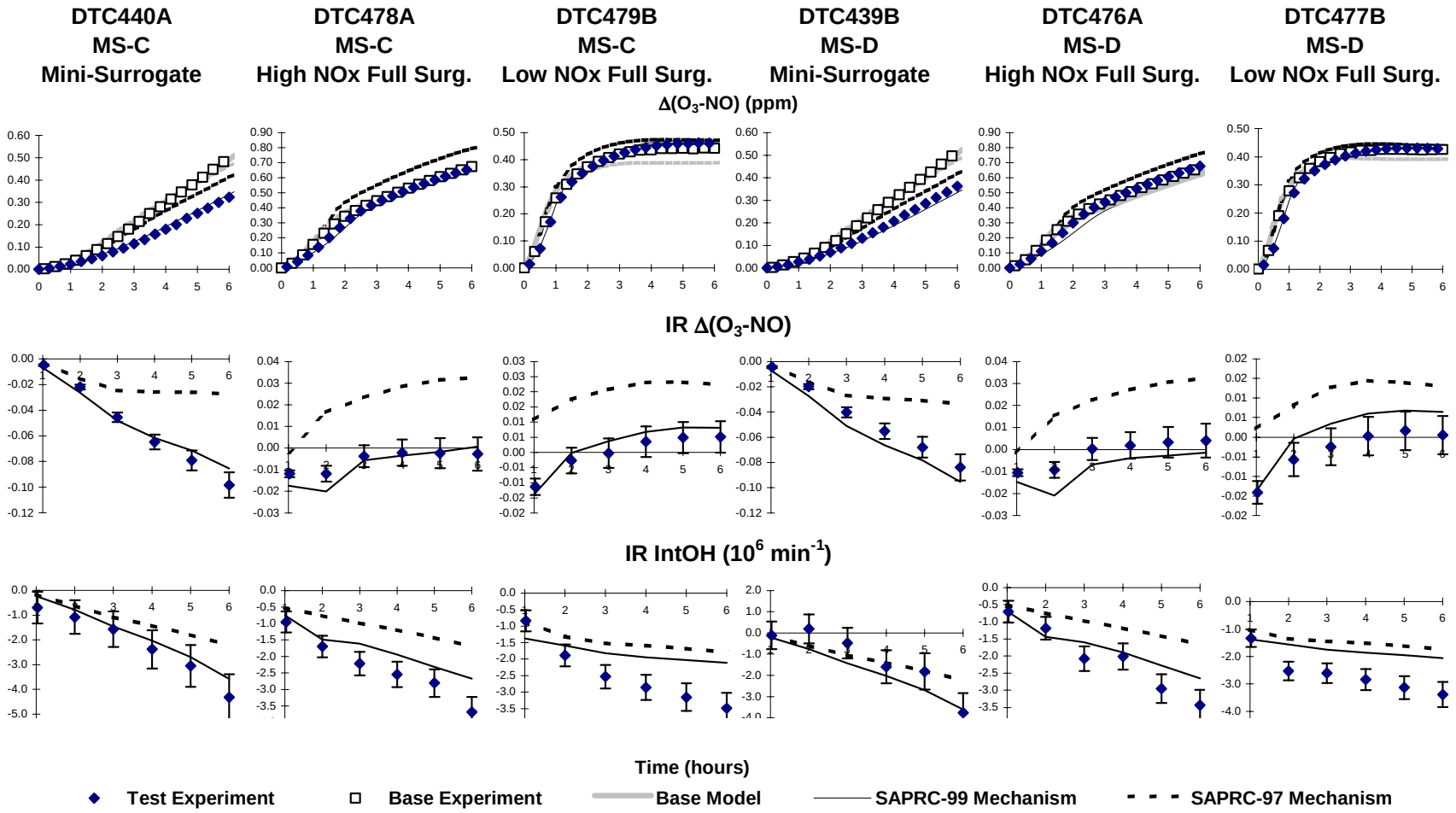

Figure 8. Selected experimental and calculated results of the experiments from the mineral spirits samples "C" and "D" studied by Carter et al (1997a).

ATMOSPHERIC REACTIVITY CALCULATIONS

Incremental reactivities of VOCs have been shown to be highly dependent on environmental conditions, so reactivities measured in environmental chamber experiments cannot necessarily be assumed to be the same as those under atmospheric conditions (Carter and Atkinson, 1989b; Carter et al, 1995b). Because of this, the only method available to obtain quantitative estimates of incremental reactivities of VOCs in ambient air pollution episodes is to conduct airshed model simulations of the episodes. Since these simulations cannot be any more reliable than the chemical mechanisms, the major objective of our studies of the mineral spirits samples and representative constituent compounds has been to assess the reliability of the mechanisms for the compounds and mixtures of interest for use in such calculations. The results of this study, and our studies of representative $C_{\geq 12}$ normal and cyclic alkanes carried out under separate funding (Carter et al, 2000a; Carter, 2000) suggest that the SAPRC-99 mechanism serves as an appropriate basis for estimating the effects of four mineral spirits samples and their major constituents on ozone under atmospheric conditions. The atmospheric reactivity estimates using this mechanism are discussed in this section.

Scenarios Used for Reactivity Assessment

The set of airshed scenarios employed to assess the reactivities for this study is the same as those used for calculating the MIR and other reactivity scales in our previous work (Carter, 1994a), and also in the update using the SAPRC-99 mechanism (Carter, 2000). These scenarios, and the reasons for using them, are briefly described below. Note that the scenarios used in this work are exactly the same as used in the atmospheric reactivity estimates in our Phase 1 study (Carter et al, 1996).

The objective is to use a set of scenarios that represents, as much as possible, a comprehensive distribution of the environmental conditions where unacceptable levels of ozone are formed. Although a set of scenarios has not been developed for the specific purpose of VOC reactivity assessment, the EPA developed an extensive set of scenarios for conducting analyses of effects of ROG and NO_x controls on ozone formation using the EKMA modeling approach (Gipson et al. 1981; Gipson and Freas, 1983; EPA, 1984; Gery et al. 1987; Baugues, 1990). The EKMA approach involves the use of single-cell box models to simulate how the ozone formation in one day episodes is affected by changes in ROG and NO_x inputs. Although single-cell models cannot represent realistic pollution episodes in great detail, they can represent dynamic injection of pollutants, time-varying changes of inversion heights, entrainment of pollutants from aloft as the inversion height raises, and time-varying photolysis rates, temperatures, and humidities (Gipson and Freas, 1981; EPA, 1984; Gipson, 1984; Hogo and Gery, 1988). Thus, they can be used to simulate a wide range of the chemical conditions which affect ozone formation from ROG and NO_x, and which affect VOC reactivity. Therefore, at least to the extent they are suitable for their intended purpose, an appropriate set of EKMA scenarios should also be suitable for assessing reactivities over a wide range of conditions.

Base Case Scenarios

The set of EKMA scenarios used in this study were developed by the United States EPA for assessing how various ROG and NO_x control strategies would affect ozone nonattainment in various areas of the country (Baugues, 1990). The characteristics of these scenarios and the methods used to derive their input data are described in more detail elsewhere (Baugues, 1990; Carter, 1994b). Briefly, 39 urban areas in the United States were selected based on geographical representativeness of ozone nonattainment areas and data availability, and a representative high ozone episode was selected for each. The initial non-methane organic carbon (NMOC) and NO_x concentrations, the aloft O_3 concentrations, and the mixing height inputs were based on measurement data for the various areas. The hourly emissions in the scenarios were obtained from the National Acid Precipitation Assessment Program emissions inventory (Baugues, 1990), and biogenic emissions were also included. Table 12 gives a summary of the urban areas represented and other selected characteristics of the scenarios.

Several changes to the scenario inputs were made based on discussions with the California ARB staff and others (Carter, 1994a,b). Two percent of the initial NO_x and 0.1% of the emitted NO_x in all the scenarios was assumed to be in the form of HONO. The photolysis rates were calculated using solar light intensities and spectra calculated by Jeffries (1991) for 640 meters, the approximate mid-point of the mixed layer during daylight hours. The composition of the non-methane organic pollutants entrained from aloft was based on the analysis of Jeffries et al. (1989). The composition of the initial and emitted reactive organics was derived as discussed below. Complete listings of the input data for the scenarios are given elsewhere (Carter, 1994b).

This set of 39 EKMA scenarios are referred to as “base case” to distinguish them from the scenarios derived from them by adjusting NO_x inputs to yield standard conditions of NO_x availability as discussed below. No claim is made as to the accuracy of these scenarios in representing any real episode, but they are a result of an effort to represent, as accurately as possible given the available data and the limitations of the formulation of the EKMA model, the range of conditions occurring in urban areas throughout the United States. When developing general reactivity scales it is more important that the scenarios employed represent a realistic distribution of chemical conditions than accurately representing the details of any one particular episode.

The Base ROG mixture is the mixture of reactive organic gases used to represent the chemical composition of the initial and emitted anthropogenic reactive organic gases from all sources in the scenarios. Consistent with the approach used in the original EPA scenarios, the same mixture was used for all scenarios. The speciation for this mixture was derived by Croes (1991) based on an analysis of the EPA database (Jeffries et al. 1989) for the hydrocarbons and the 1987 Southern California Air Quality Study (SCAQS) database for the oxygenates (Croes et al. 1994; Lurmann and Main. 1992). This mixture consists of 52% (by carbon) alkanes, 15% alkenes, 27% aromatics, 1% formaldehyde, 2% higher aldehydes, 1% ketones, and 2% acetylene. The detailed composition of this mixture is given elsewhere (Carter, 1994b; Carter, 2000).

Table 12. Summary of the conditions of the scenarios used for atmospheric reactivity assessment.

	Scenario	Max O_3 (ppb)	Max 8-Hr Avg O_3 (ppb)	ROG / NO_x	NO_x / MOIR NO_x	Height (kM)	Init., Emit ROG (m. mol m^{-2})	O_3 aloft (ppb)	Integrated OH (ppt-min)
Avg.	MIR	187	119	3.1	1.5	1.8	15	70	128
Cond.	MOIR	239	165	4.5	1.0	1.8	15	70	209
	EBIR	227	172	6.4	0.7	1.8	15	70	210
Base	Atlanta, GA	179	132	7.3	0.7	2.1	12	63	200
Case	Austin, TX	175	144	9.3	0.5	2.1	11	85	179
	Baltimore, MD	334	215	5.2	1.1	1.2	17	84	186
	Baton Rouge, LA	241	173	6.8	0.9	1.0	11	62	186
	Birmingham, AL	244	202	6.9	0.5	1.8	13	81	208
	Boston, MA	197	167	6.5	0.6	2.6	14	105	262
	Charlotte, NC	143	126	7.8	0.3	3.0	7	92	212
	Chicago, IL	278	226	11.6	0.5	1.4	25	40	164
	Cincinnati, OH	205	153	6.4	0.7	2.8	17	70	220
	Cleveland, OH	252	179	6.6	0.9	1.7	16	89	187
	Dallas, TX	208	141	4.7	1.2	2.3	18	75	176
	Denver, CO	204	139	6.3	1.1	3.4	29	57	143
	Detroit, MI	246	177	6.8	0.7	1.8	17	68	235
	El Paso, TX	182	135	6.6	1.0	2.0	12	65	138
	Hartford, CT	172	144	8.4	0.5	2.3	11	78	220
	Houston, TX	312	217	6.1	0.9	1.7	25	65	225
	Indianapolis, IN	212	148	6.6	0.9	1.7	12	52	211
	Jacksonville, FL	155	115	7.6	0.6	1.5	8	40	206
	Kansas City, MO	159	126	7.1	0.6	2.2	9	65	233
	Lake Charles, LA	286	209	7.4	0.6	0.5	7	40	233
	Los Angeles, CA	568	406	7.6	1.0	0.5	23	100	134
	Louisville, KY	212	155	5.5	0.8	2.5	14	75	260
	Memphis, TN	229	180	6.8	0.6	1.8	15	58	249
	Miami, FL	132	111	9.6	0.4	2.7	9	57	181
	Nashville, TN	167	138	8.0	0.4	1.6	7	50	225
	New York, NY	365	294	8.1	0.7	1.5	39	103	159
	Philadelphia, PA	247	169	6.2	0.9	1.8	19	53	227
	Phoenix, AZ	277	193	7.6	1.0	3.3	40	60	153
	Portland, OR	166	126	6.5	0.7	1.6	6	66	233
	Richmond, VA	242	172	6.2	0.8	1.9	16	64	217
	Sacramento, CA	204	142	6.6	0.8	1.1	7	60	209
	St Louis, MO	324	209	6.1	1.1	1.6	26	82	176
	Salt Lake City, UT	186	150	8.5	0.6	2.2	11	85	182
	San Antonio, TX	133	98	3.9	1.0	2.3	6	60	192
	San Diego, CA	193	150	7.1	0.9	0.9	8	90	146
	San Francisco, CA	229	126	4.8	1.8	0.7	25	70	61
	Tampa, FL	230	153	4.4	1.0	1.0	8	68	211
	Tulsa, OK	231	160	5.3	0.9	1.8	15	70	264
	Washington, DC	283	209	5.3	0.8	1.4	13	99	239

Adjusted NO_x scenarios

Incremental reactivities in the base case scenarios would be expected to vary widely, since incremental reactivities depend on the ROG/NO_x ratio, and that ratio varies widely among the base case scenarios. To obtain reactivity scales for specified NO_x conditions, separate scenarios, designated MIR (for maximum incremental reactivity), MOIR (for maximum ozone incremental reactivity), and Equal Benefit Incremental Reactivity (EBIR) were developed (Carter, 1994a). In the MIR scenarios, the NO_x inputs were adjusted so the base ROG mixture (and most other VOCs) has its highest incremental reactivity. This is representative of the highest NO_x conditions of relevance to VOC reactivity assessment because at higher NO_x levels O_3 yields become significantly suppressed, but is also the condition where O_3 is most sensitive to VOC emissions. In the MOIR scenarios, the NO_x inputs were adjusted to yield the highest ozone concentration. In the EBIR scenarios, the NO_x inputs were adjusted so that the relative effects of NO_x reductions and total ROG reductions on peak ozone levels were equal. This represents the lowest NO_x condition of relevance for VOC reactivity assessment, because O_3 formation becomes more sensitive to NO_x emissions than VOC emissions at lower NO_x levels. As discussed by Carter (1994a) the MIR and EBIR ROG/NO_x ratios are respectively ~1.5 and ~0.7 times those for the MOIR scenarios in all cases.

NO_x Conditions in the Base Case Scenarios

The variability of ROG/NO_x ratios in the base case scenarios suggests a variability of reactivity characteristics in those scenarios. However, as discussed previously (Carter, 1994a), the ROG/NO_x ratio is also variable in the MIR or MOIR scenarios, despite the fact that the NO_x inputs in these scenarios are adjusted to yield a specified reactivity characteristic. Thus, the ROG/NO_x ratio, by itself, is not necessarily a good predictor of reactivity characteristics of a particular scenario. The NO_x/NO_x^{MOIR} ratio is a much better predictor of this, with values greater than 1 indicating relatively high NO_x conditions where ozone formation is more sensitive to VOCs, and values less than 1 indicating NO_x-limited conditions. NO_x/NO_x^{MOIR} ratios less than 0.7 represent conditions where NO_x control is a more effective ozone control strategy than ROG control (Carter, 1994a). These rations are shown on Table 12 for the various base case scenarios. Note that more than half of the base case scenarios represent NO_x-limited conditions, and ~25% of them represent conditions where NO_x control is more beneficial than VOC control. A relatively small number of scenarios represent MIR or near MIR conditions. However, as discussed elsewhere (Carter, 1994a), this set of scenarios is based on near-worst-case conditions for ozone formation in each of the airsheds. Had scenarios representing less-than-worst-case conditions been included, one might expect a larger number of MIR or near MIR scenarios. This is because NO_x is consumed more slowly on days with lower light intensity or temperature, and thus the scenario is less likely to become NO_x-limited.

Quantification of Atmospheric Reactivity

The reactivity of a VOC in an airshed scenario is measured by its incremental reactivity. For ambient scenarios, this is defined as the change in ozone caused by adding the VOC to the emissions,

divided by the amount of VOC added, calculated for sufficiently small amounts of added VOC that the incremental reactivity is independent of the amount added[2].

$$\mathrm{IR(VOC, Scenario)} = \lim_{\mathrm{VOC}\to 0}\left[\frac{\mathrm{O_3\,(Scenario\ with\ VOC\ added) - O_3\,(Base\ Scenario)}}{\mathrm{Amount\ of\ VOC\ Added}}\right] \qquad \text{(V)}$$

The specific calculation procedure is discussed in detail elsewhere (Carter, 1994a,b).

Incremental reactivities derived as given above tend to vary from scenario to scenario because they differ in their overall sensitivity of O_3 formation to VOCs. These differences can be factored out to some extent by using "relative reactivities", which are defined as ratios of incremental reactivities to the incremental reactivity of the base ROG mixture, which is used to represent emissions of reactive VOCs from all sources.

$$\mathrm{RR(VOC, Scenario)} = \frac{\mathrm{IR(VOC, Scenario)}}{\mathrm{IR\ (Base\ ROG, Scenario)}} \qquad \text{(VI)}$$

These relative reactivities can also be thought of as the relative effect on O_3 of controlling emissions of the particular VOC by itself, compared to controlling emissions from all VOC sources equally. Thus, they are more meaningful in terms of control strategy assessment than absolute reactivities, which can vary greatly depending on the episode and local meteorology.

In addition to depending on the VOC and the scenario, the incremental and relative reactivities depend on how the amounts of VOC added are quantified. In this work, this is quantified on a mass basis, since this is how VOCs are regulated, and generally approximates how VOC substitutions are made in practice. Note that relative reactivities will be different if they are quantified on a molar basis, with VOCs with higher molecular weight having higher reactivities on a mole basis than a gram basis.

Relative reactivities can also depend significantly on how ozone impacts are quantified (Carter, 1994a). Two different ozone quantification methods are used in this work, as follows:

"Ozone Yield" reactivities measure the effect of the VOC on the total amount of ozone formed in the scenario at the time of its maximum concentration. Incremental reactivities are quantified as grams O_3 formed per gram VOC added. Most previous recent studies of ozone reactivity (Dodge, 1984; Carter and Atkinson, 1987, 1989, Chang and Rudy, 1990; Jeffries and Crouse, 1991) have been based on this quantification method. The MIR, MOIR, and EBIR scales of Carter (1994a) also use this quantification.

"Maximum 8 Hour Average Ozone" reactivities measure the effect of the VOC on the average ozone concentration during the 8-hour period when the average ozone concentration was the greatest, which in these one-day scenarios was the last 8 hours of the simulation. This provides a measure of ozone

[2] Note that this differs from how the term "incremental reactivity" is used in the context of chamber experiments. In that case, the incremental reactivity refers to the relative change observed in the individual experiments, which in general depends on the amount added.

impact that is more closely related to the new Federal ozone standard that is given in terms of an 8 hour average. This quantification is used for relative reactivities in this work.

In previous reports, we have reported reactivities in terms of integrated O_3 over a standard concentration of 0.09 or 0.12 ppm. This provides a measure of the effect of the VOC on exposure to unacceptable levels of ozone. This is replaced by the maximum 8 hour average reactivities because it is more representative of the proposed new Federal ozone standard and because reactivities relative to integrated O_3 over a standard tend to be between those relative to ozone yield and those relative to 8-hour averages. Therefore, presenting both ozone yield and maximum 8-hour average relative reactivities should be sufficient to provide information on how relative reactivities vary with ozone quantification method. Incremental reactivities are quantified as ppm O_3 per milligram VOC emitted per square meter, but maximum 8 hour average reactivities are usually quantified as relative reactivities quantified on a mass basis.

Note that incremental reactivities are calculated for a total of 156 scenarios, consisting of the 39 base case scenarios and the three adjusted NO_x scenarios for each of the 39 base case scenarios. However, the incremental reactivities in the MIR, MOIR, or EBIR scales are reported as averages of the incremental reactivities in the corresponding adjusted NO_x scenarios, because adjusting the NO_x conditions reduces the scenario variability, and this allows for derivation of single reactivity scales representing each type of NO_x condition. On the other hand, the individual scenario results for the base case scenarios give an indication of the scenario-to-scenario variability of the calculated reactivity results.

Results

Table 13 lists the ozone yield incremental reactivities calculated for the set of C_8 - C_{15} normal, branched, and cyclic alkanes that are used to represent the various alkane mineral spirits constituents, as well as the reactivities calculated for the four mineral spirits samples studied by Carter et al (1997a). For comparison purposes, the incremental reactivities for ethane and the base ROG mixture that is used to represent reactive VOC emissions from all sources are also shown on the table. Table 14 shows both the ozone yield and maximum 8-hour average ozone reactivities for these compounds and mixtures relative to the base ROG mixture, and plots of these relative reactivities against carbon number are shown on Figure 9. Note that the values given are averages of the incremental or relative reactivities calculated for the various adjusted NO_x and the base case scenarios. Note also that the relative reactivities on Table 14 and Figure 9 can be thought of as the relative ozone benefits resulting from regulating emissions of these compounds or mixtures alone, compared to regulating VOC emissions from all sources equally.

It can be seen that the reactivities of the $C_{\geq 8}$ alkanes decrease with carbon number, as is expected due to the increase in nitrate yields with carbon number. As also expected based on their variable mechanistic parameters (see Table 6 and Figure 2, above) the reactivities of the branched and cyclic

Table 13. Atmospheric incremental reactivities calculated for the C_8 - C_{15} alkanes, the mineral spirits samples, the base ROG mixture, and ethane.

Compound or Mixture	Model Name	Ozone Yield Incremental Reactivities (grams O_3 / grams VOC or mixture)			
		MIR	MOIR	EBIR	Average Base Case
	Normal Alkanes				
n-Octane	N-C8	1.11	0.71	0.41	0.43
n-Nonane	N-C9	0.95	0.62	0.34	0.35
n-Decane	N-C10	0.83	0.54	0.28	0.28
n-Undecane	N-C11	0.74	0.48	0.24	0.24
n-Dodecane	N-C12	0.66	0.43	0.21	0.21
n-Tridecane	N-C13	0.62	0.41	0.20	0.20
n-Tetradecane	N-C14	0.58	0.38	0.19	0.19
n-Pentadecane	N-C15	0.56	0.37	0.19	0.19
	Branched Alkanes				
2,4-Dimethyl Hexane	24-DM-C6	1.80	1.01	0.63	0.68
4-Methyl Heptane	4-ME-C7	1.48	0.86	0.52	0.56
2-Methyl Heptane	2-ME-C7	1.20	0.74	0.43	0.45
2,4-Dimethyl Heptane	24-DM-C7	1.49	0.84	0.49	0.53
4-Methyl Octane	4-ME-C8	1.08	0.67	0.37	0.39
2-Methyl Octane	2-ME-C8	0.96	0.60	0.32	0.34
2,6-Dimethyl Octane	26DM-C8	1.27	0.72	0.41	0.44
4-Methyl Nonane	4-ME-C9	0.99	0.61	0.33	0.34
2-Methyl Nonane	2-ME-C9	0.86	0.55	0.29	0.29
2,6-Dimethyl Nonane	26DM-C9	0.95	0.56	0.30	0.32
4-Methyl Decane	4-ME-C10	0.80	0.51	0.26	0.26
3-Methyl Decane	3-ME-C10	0.77	0.49	0.25	0.25
3,6-Dimethyl Decane	36DM-C10	0.88	0.54	0.29	0.30
5-Methyl Undecane	5-ME-C11	0.72	0.46	0.23	0.23
3-Methyl Undecane	3-ME-C11	0.70	0.45	0.23	0.23
3,6-Dimethyl Undecane	36DM-C11	0.82	0.50	0.26	0.27
5-Methyl Dodecane	5-ME-C12	0.64	0.42	0.20	0.21
3-Methyl Dodecane	3-ME-C12	0.64	0.41	0.21	0.20
3,7-Dimethyl Dodecane	37DM-C12	0.74	0.46	0.24	0.24
6-Methyl Tridecane	6-ME-C13	0.62	0.40	0.20	0.20
3-Methyl Tridecane	3-ME-C13	0.57	0.37	0.18	0.18
3,7-Dimethyl Tridecane	37DM-C13	0.64	0.41	0.21	0.21
6-Methyl Tetradecane	6-ME-C14	0.57	0.38	0.18	0.18
3-Methyl Tetradecane	3-ME-C14	0.53	0.35	0.17	0.17
	Cyclic Alkanes				
Ethylcyclohexane	ET-CYCC6	1.75	0.99	0.59	0.63
Propyl Cyclohexane	C3-CYCC6	1.47	0.84	0.48	0.51
1-Ethyl-4-Methyl Cyclohexane	1E4MCYC6	1.63	0.89	0.52	0.56

Table 13 (continued)

Compound or Mixture	Model Name	Ozone Yield Incremental Reactivities (grams O_3 / grams VOC or mixture)			
		MIR	MOIR	EBIR	Average Base Case
Butyl Cyclohexane	C4-CYCC6	1.07	0.64	0.35	0.36
1-Methyl-3-Isopropyl Cyclohexane	1M3IPCY6	1.26	0.72	0.41	0.43
1,4-Diethyl-Cyclohexane	14DECYC6	1.49	0.82	0.47	0.50
Pentyl Cyclohexane	C5-CYCC6	0.91	0.55	0.29	0.30
1,3-Diethyl-5-Methyl Cyclohexane	13E5MCC6	1.11	0.62	0.33	0.35
1-Ethyl-2-Propyl Cyclohexane	1E2PCYC6	0.95	0.58	0.31	0.31
Hexyl Cyclohexane	C6-CYCC6	0.75	0.47	0.24	0.24
1,3,5-Triethyl Cyclohexane	135ECYC6	1.06	0.60	0.32	0.34
1-Methyl-4-Pentyl Cyclohexane	1M4C5CY6	0.81	0.49	0.26	0.27
Heptyl Cyclohexane	C7-CYCC6	0.66	0.42	0.21	0.21
1,3-Diethyl-5-Pentyl Cyclohexane	13E5PCC6	0.99	0.56	0.30	0.32
1-Methyl-2-Hexyl-Cyclohexane	1M2C6CC6	0.70	0.44	0.22	0.22
Octyl Cyclohexane	C8-CYCC6	0.60	0.39	0.19	0.19
1,3-Dipropyl-5-EthylCyclohexane	13P5ECC6	0.94	0.53	0.29	0.30
1-Methyl-4-Heptyl Cyclohexane	1M4C7CC6	0.58	0.38	0.20	0.19
Nonyl Cyclohexane	C9-CYCC6	0.54	0.36	0.17	0.17
1,3,5-Tripropyl Cyclohexane	135PCYC6	0.90	0.51	0.28	0.29
1-Methyl-2-Octyl Cyclohexane	1M2C8CC6	0.60	0.39	0.20	0.20
	Mineral Spirit Samples				
Mineral Spirits "A" (Type I-B, 91% Alkanes)	MS-A	1.27	0.65	0.35	0.39
Mineral Spirits "B" (Type II-C)	MS-B	0.78	0.48	0.25	0.26
Mineral Spirits "C" (Type II-C)	MS-C	0.78	0.48	0.26	0.26
Mineral Spirits "D" (Type II-C)	MS-D	0.79	0.49	0.26	0.26
	Others				
Ethane	ETHANE	0.31	0.20	0.15	0.15
Base ROG Mixture	ARBROG	3.71	1.46	0.85	1.03

alkanes are variable, with the variability being somewhat greater with the cyclic alkanes[3]. It can also be seen that the reactivities of the branched and cyclic alkanes tend to be higher than those for the normal alkanes, though this is not true for all isomers. In general, the more branched the isomer the higher the reactivity, with the most reactive compounds relative to their isomers being the cyclohexanes, and with the monomethyl alkanes having about the same reactivities as their normal alkane isomers.

[3] This may be due to the greater variability in degree of branching in the set of representative cycloalkanes than is the case for the set of representative branched alkanes.

Table 14. Atmospheric relative reactivities calculated for the C_8 - C_{15} alkanes, the mineral spirits samples, and ethane. Reactivities are relative to the base ROG mixture, quantified on an ozone formed per unit mass basis.

Model Name	Ozone Yield Relative Reactivities				Max 8-Hour Average Relative Reactivities			
	MIR	MOIR	EBIR	Average Base Case	MIR	MOIR	EBIR	Average Base Case
				Normal Alkanes				
N-C8	0.30	0.49	0.48	0.41	0.24	0.26	0.22	0.20
N-C9	0.26	0.42	0.39	0.33	0.20	0.20	0.15	0.14
N-C10	0.22	0.37	0.32	0.27	0.17	0.16	0.10	0.09
N-C11	0.20	0.33	0.28	0.23	0.15	0.13	0.06	0.05
N-C12	0.18	0.30	0.25	0.21	0.13	0.11	0.04	0.03
N-C13	0.17	0.28	0.24	0.19	0.12	0.09	0.03	0.02
N-C14	0.16	0.26	0.22	0.18	0.11	0.08	0.02	0.01
N-C15	0.15	0.25	0.22	0.18	0.10	0.07	0.01	0.00
				Branched Alkanes				
24-DM-C6	0.49	0.69	0.74	0.66	0.41	0.44	0.43	0.41
4-ME-C7	0.40	0.59	0.61	0.54	0.33	0.35	0.32	0.30
2-ME-C7	0.32	0.50	0.50	0.44	0.26	0.28	0.25	0.23
24-DM-C7	0.40	0.57	0.58	0.51	0.33	0.33	0.29	0.28
4-ME-C8	0.29	0.46	0.44	0.37	0.23	0.23	0.18	0.17
2-ME-C8	0.26	0.41	0.38	0.33	0.20	0.20	0.15	0.13
26DM-C8	0.34	0.49	0.48	0.42	0.28	0.26	0.20	0.19
4-ME-C9	0.27	0.42	0.38	0.33	0.20	0.20	0.13	0.12
2-ME-C9	0.23	0.38	0.34	0.28	0.17	0.16	0.09	0.08
26DM-C9	0.26	0.39	0.35	0.31	0.20	0.18	0.11	0.11
4-ME-C10	0.22	0.35	0.30	0.26	0.16	0.14	0.07	0.06
3-ME-C10	0.21	0.34	0.29	0.25	0.15	0.13	0.06	0.06
36DM-C10	0.24	0.37	0.34	0.29	0.18	0.15	0.08	0.07
5-ME-C11	0.19	0.32	0.27	0.22	0.14	0.12	0.04	0.04
3-ME-C11	0.19	0.31	0.27	0.22	0.14	0.11	0.04	0.04
36DM-C11	0.22	0.35	0.31	0.26	0.16	0.13	0.06	0.06
5-ME-C12	0.17	0.29	0.24	0.20	0.12	0.10	0.02	0.02
3-ME-C12	0.17	0.28	0.24	0.20	0.12	0.10	0.02	0.02
37DM-C12	0.20	0.31	0.28	0.23	0.15	0.11	0.04	0.04
6-ME-C13	0.17	0.28	0.23	0.19	0.12	0.09	0.02	0.01
3-ME-C13	0.15	0.26	0.22	0.18	0.11	0.08	0.01	0.00
37DM-C13	0.17	0.28	0.24	0.20	0.12	0.09	0.02	0.01
6-ME-C14	0.15	0.26	0.22	0.18	0.11	0.08	0.01	0.00
3-ME-C14	0.14	0.24	0.20	0.16	0.10	0.07	0.00	0.00
				Cyclic Alkanes				
ET-CYCC6	0.47	0.68	0.70	0.61	0.40	0.40	0.35	0.34
C3-CYCC6	0.40	0.57	0.57	0.50	0.33	0.31	0.25	0.24
1E4MCYC6	0.44	0.61	0.61	0.54	0.36	0.34	0.27	0.25

Table 14 (continued)

Model Name	Ozone Yield Relative Reactivities				Max 8-Hour Average Relative Reactivities			
	MIR	MOIR	EBIR	Average Base Case	MIR	MOIR	EBIR	Average Base Case
C4-CYCC6	0.29	0.44	0.41	0.35	0.23	0.21	0.13	0.12
1M3IPCY6	0.34	0.49	0.49	0.42	0.28	0.26	0.20	0.19
14DECYC6	0.40	0.56	0.56	0.49	0.33	0.29	0.21	0.21
C5-CYCC6	0.25	0.38	0.34	0.29	0.19	0.16	0.08	0.07
13E5MCC6	0.30	0.42	0.39	0.34	0.24	0.18	0.08	0.08
1E2PCYC6	0.26	0.40	0.36	0.30	0.19	0.16	0.07	0.06
C6-CYCC6	0.20	0.32	0.28	0.23	0.15	0.11	0.03	0.03
135ECYC6	0.29	0.41	0.38	0.32	0.22	0.17	0.07	0.07
1M4C5CY6	0.22	0.33	0.31	0.26	0.16	0.13	0.05	0.05
C7-CYCC6	0.18	0.29	0.24	0.20	0.13	0.09	0.01	0.01
13E5PCC6	0.27	0.38	0.36	0.31	0.20	0.15	0.05	0.05
1M2C6CC6	0.19	0.30	0.26	0.21	0.13	0.09	0.01	0.00
C8-CYCC6	0.16	0.27	0.23	0.19	0.11	0.08	0.00	0.00
13P5ECC6	0.25	0.36	0.34	0.29	0.19	0.14	0.05	0.05
1M4C7CC6	0.16	0.26	0.23	0.19	0.11	0.08	0.00	-0.01
C9-CYCC6	0.15	0.24	0.21	0.17	0.10	0.06	-0.01	-0.02
135PCYC6	0.24	0.35	0.33	0.28	0.19	0.13	0.04	0.04
1M2C8CC6	0.16	0.26	0.24	0.19	0.11	0.07	0.00	0.00
				Mineral Spirits Samples				
MS-A	0.34	0.45	0.42	0.37	0.29	0.27	0.20	0.19
MS-B	0.21	0.33	0.30	0.25	0.15	0.13	0.06	0.05
MS-C	0.21	0.33	0.30	0.25	0.16	0.14	0.06	0.06
MS-D	0.21	0.33	0.30	0.26	0.16	0.14	0.07	0.06
				Ethane				
ETHANE	0.08	0.14	0.17	0.15	0.07	0.09	0.10	0.09

The higher reactivities of the branched and cycloalkanes relative to the normal alkanes can be attributed to the effects of the additional NO to NO_2 conversions in their predicted mechanisms, as indicated on Table 6 and Figure 2, above. This apparently is more important than the effect of the higher predicted overall nitrate yields for these compounds, which tends to reduce predicted reactivities. This can be attributed at least in part to the greater effect of structure on NO to NO_2 conversions compared to their effects on overall nitrate yields. For example, the most reactive C_{11} tabulated, 1,3-diethyl-5-methyl cyclohexane, has an 80% higher number of extra NO to NO_2 conversions, but only a 26% higher nitrate yield, compared to n-undecane. In addition, atmospheric reactivity simulations tend to be relatively more sensitive to NO to NO_2 conversions, and somewhat less sensitive to overall nitrate yields, than is the case for simulations of environmental chamber reactivity experiments.

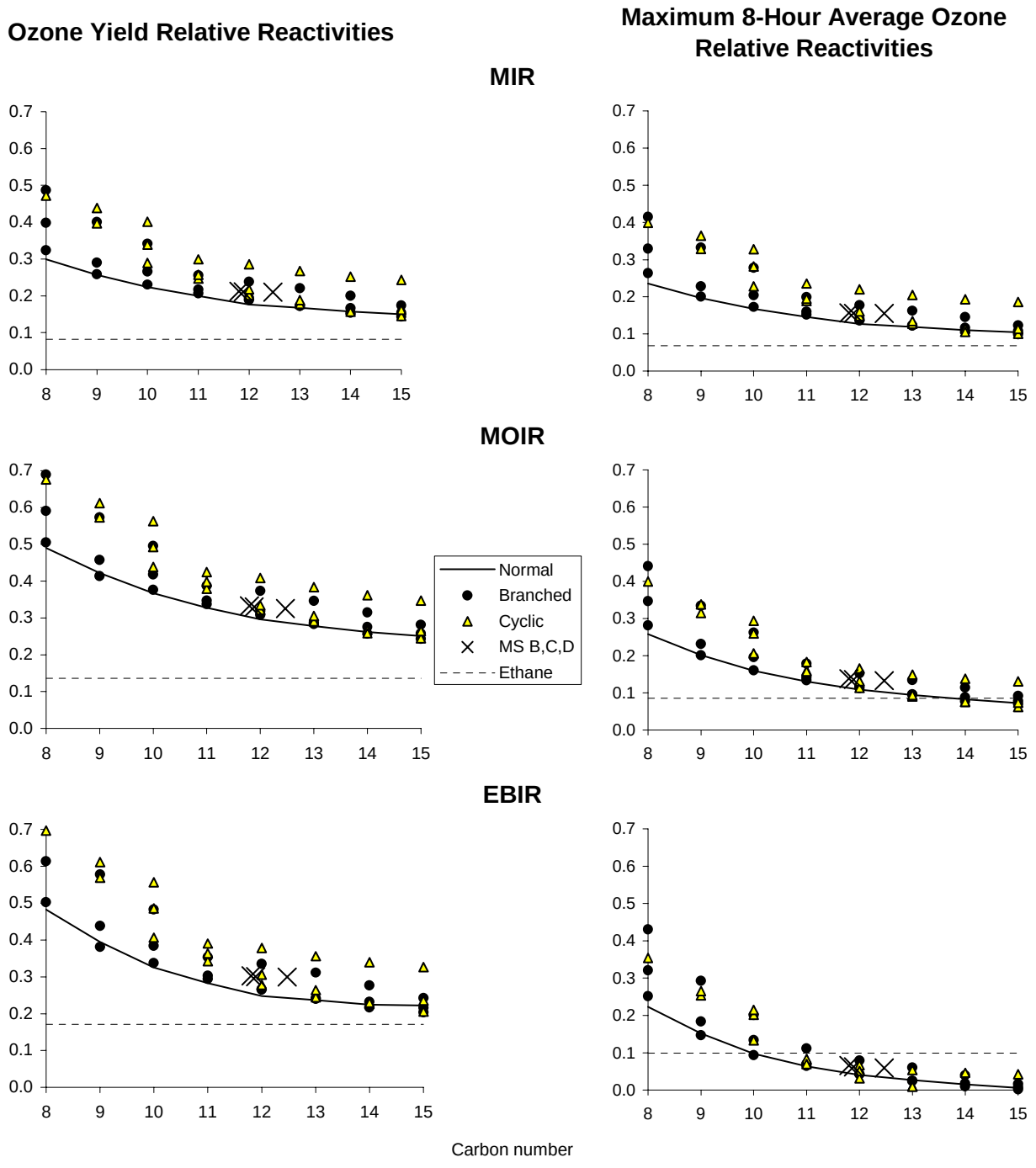

Figure 9. Plots of MIR, MOIR and EBIR ozone yield and maximum 8-hour average ozone relative reactivities against carbon number. Reactivities are relative to the base ROG mixture, quantified on a mass basis. Relative reactivities of ethane are shown for comparison.

The calculated reactivities of the all-alkane mineral spirits samples (Samples "B", "C", and "D") are very similar, and are in the middle of the range of the reactivities of the alkanes with the same carbon number range. This is as expected based on their assumed composition. Sample "A" is calculated to have 2-3 times higher reactivities than the other samples, with its reactivity relative to the all-alkane samples increasing as NO_x levels decrease. Its higher reactivity can be attributed in part to its higher average carbon number, but primarily to the contributions of the aromatic and alkene constituents. Although the aromatic and alkene fractions are relatively small (weight fractions being 6% and 2%, respectively), these constituents are much more reactive on a mass basis than the higher molecular weight alkanes (Carter, 1994a, 2000).

The ozone impacts of the higher molecular weight alkanes and the all-alkane mineral spirits samples are relatively low compared to the emissions of VOCs from all sources, indicating that regulating emissions of these substances is less effective than regulating emissions of VOCs from all sources equally. Their relative impacts on maximum 8-hour average ozone tend to be less than their impacts on peak ozone yields, particularly in scenarios with lower NO_x levels, such as the EBIR scenarios or many of the base case scenarios. Their relative impacts on peak ozone yields tend to be less dependent on NO_x conditions than their impacts on maximum 8-hour average ozone. The ozone yield reactivities of the all alkane mineral spirits samples relative to the base ROG are in the 20-30% range, while their 8-hour average ozone relative reactivities decline from ~15% in the MIR scenarios to ~6% in the lower NO_x EBIR and average base case scenarios.

The reactivities of the mineral spirits relative to ethane are of interest because ethane has been used by the EPA as the informal standard for determining "negligible" ozone impact for VOC exemption purposes (Dimitriades, 1999). Although their mass-based ozone yield reactivities are somewhat higher than those of ethane, their maximum 8-hour average reactivities are comparable to or lower than those of ethane in scenarios with NO_x levels lower than MOIR.

As is the case with the higher molecular weight normal alkanes (Carter, 2000a), the relative reactivities of the all-alkane mineral spirits samples are highly variable from scenario to scenario. This is shown on Figure 10, which shows distribution plots of reactivities of two representative all-alkane mineral spirits samples relative to the base ROG mixture for the base case scenarios and the three types of adjusted NO_x scenarios. The relative reactivities for ethane are also shown, for comparison. It can be seen that the relative reactivities of these samples are quite varied even in the adjusted NO_x scenarios, especially the maximum 8-hour average relative reactivities and the relative reactivities in the lower NO_x scenarios. Note, however, that there are very little differences in the distribution of reactivities of the two mineral spirits samples shown; the same is the case for sample "C", whose distributions are not shown. The relative reactivities of ethane (and many other types of VOCs) are much less varied in the adjusted NO_x scenarios. This shows that the ozone impacts of these higher alkane mixtures are significantly affected by environmental factors other than NO_x conditions. A systematic assessment of the other scenario conditions that may be important has not been carried out.

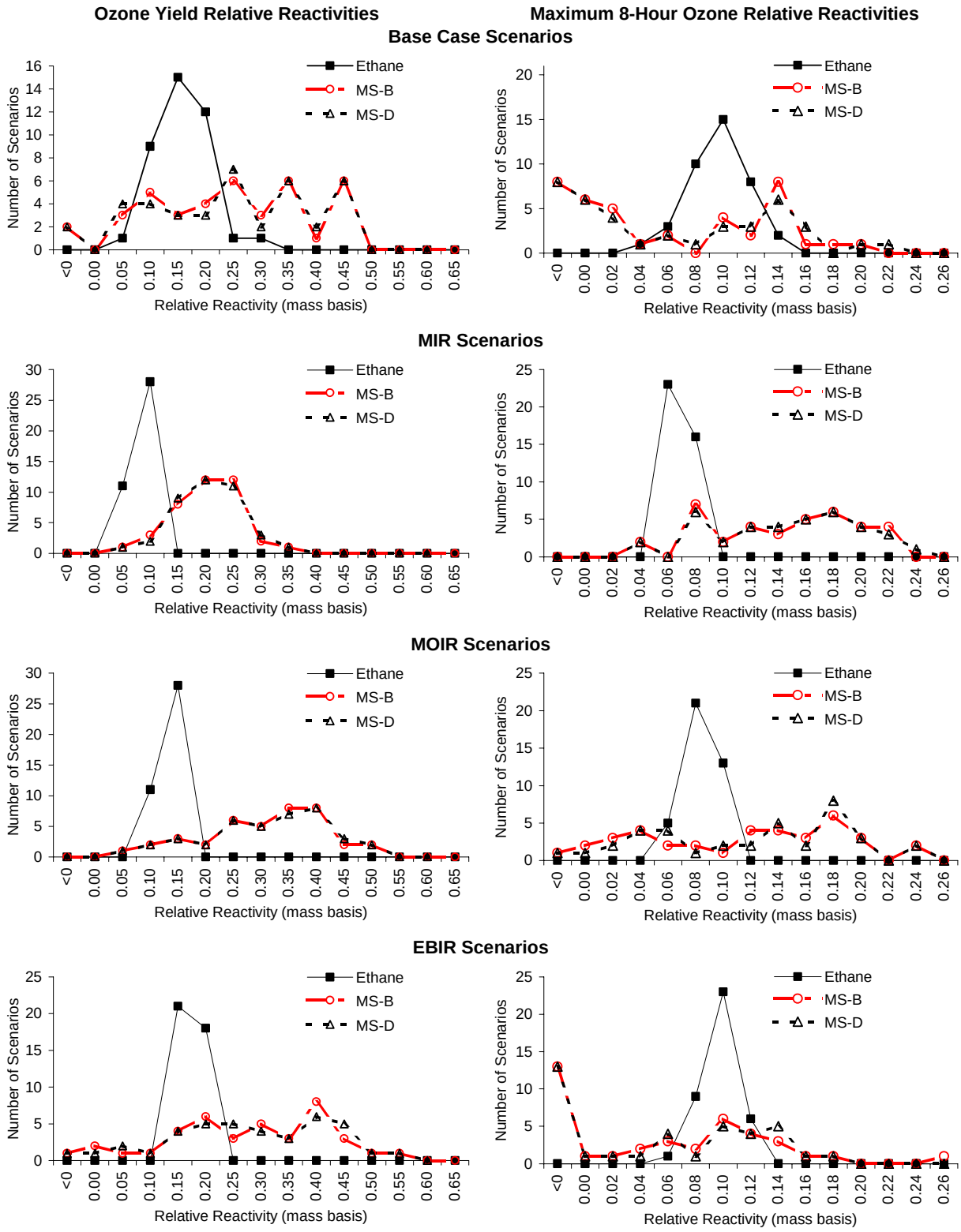

Figure 10. Distribution plots of relative reactivities of ethane and two representative all-alkane mineral spirits samples in the various types of scenarios. Reactivities are relative to the base ROG mixture.

DISCUSSION AND CONCLUSIONS

The overall objective of our two projects with Safety-Kleen Corporation was to assess whether current methods for assessing the compositions and ozone formation potentials for mineral spirits could be used to predict atmospheric ozone impacts for several representative mineral spirits samples. The results of the first project indicated that with high resolution GC-MS techniques, combined with FIA type analysis, GC fractionation, and elemental analysis data, it is possible to characterize their compositions reasonably well in terms of the model species currently used to assess ozone reactivities in airshed model calculations (Carter et al, 1997a). However, the chemical mechanism used at the time performed poorly in simulating the environmental chamber results, and probably overpredicted the atmospheric reactivities of these samples by at least a factor of two. This was believed to be due to problems with the estimated atmospheric reaction mechanisms derived for the $C_{\geq 9}$ branched and/or cyclic alkane constituents, which represent ~70-95% of the mass of these samples. Much better simulations of the data were obtained if it was assumed that the branched and cyclic alkanes had the same ozone impacts as the corresponding normal alkanes, contrary to the predictions of the estimated mechanisms used at that time. Inappropriate choices of compounds to represent the unspeciated branched and cyclic alkane constituents may also have contributed to the problem.

The major objective of this second project for Safety-Kleen was to provide data needed to assess the possible sources of the problems observed in the first project, and to update our assessment of mineral spirits reactivities based on any new information obtained. It was determined that addressing the problem required obtaining environmental chamber data to evaluate mechanisms for representative branched and cyclic alkanes, obtaining improved kinetic and mechanistic data on relevant atmospheric reactions of higher molecular weight alkanes, particularly concerning alkyl nitrate yields, and obtaining mechanism evaluation data for other types of mineral spirits samples. Some of this information was obtained under separate funding. Environmental chamber experiments on cycloalkanes were carried out under funding from the Aluminum Association (Carter et al, 2000a). The California Air Resources Board (CARB) funded mechanistic studies on the higher alkanes (Arey et al, 2000; Atkinson et al, 2000, unpublished data). Exxon Corporation (now ExxonMobil) funded environmental chamber studies of other types of hydrocarbon solvents in this molecular weight range, though the analysis of the results is still underway (Carter et al, 2000c). In addition, the CARB also funded a complete update of the SAPRC atmospheric chemical mechanism that was used in our previous project (Carter, 2000). However, these projects did not provide the chamber data needed to evaluate mechanisms for individual representative branched alkanes, so obtaining such data was therefore included in this project for Safety-Kleen.

The CARB-funded projects resulted in major revisions to the methods used for estimating nitrate yields in the atmospheric reactions of the alkanes, which are incorporated in the current SAPRC-99 mechanism that is used to predict their atmospheric impacts. These revisions did not significantly affect the overall predicted mechanisms for the normal alkanes, but resulted in significant increases in estimated nitrate yields for the higher molecular weight branched and cyclic alkanes. This resulted in predicted

reactivities of the branched and cyclic alkanes being closer to the normal alkanes, as suggested by the reactivity data obtained for the mineral spirits samples. These predictions were supported by the environmental chamber experiments on hexyl cyclohexane and octyl cyclohexane carried out for the Aluminum Association, whose results were very well simulated by the current SAPRC-99 mechanism (Carter et al, 2000a). These predictions are also largely supported by the results of the branched alkane experiments carried out for this project.

The current mechanism gave good predictions of the ozone impacts and other measures of reactivity for 2-methyl nonane. This suggests that the current alkane mechanisms should perform well for alkanes with relatively low degrees of branching, which are believed to be important in mineral spirits samples (O'Donnell, Safety-Kleen Corp., private communication, 1996). The mechanism does not perform quite as well for the more branched alkanes that were studied, tending to underpredict the inhibition effects of these compounds in the experiments that are sensitive to these effects. Adjusting the nitrate yields downward towards the levels estimated in the previous mechanism does not give satisfactory fits to the data unless the number of NO to NO_2 conversions was also adjusted, by an equal or greater factor. This suggests that refinements in the estimation methods may be appropriate to improve overall model performance in predicting overall reactivities of highly branched alkanes, though additional data are needed before the appropriate area for refinements are identified. Nevertheless, even for these compounds the current mechanism performs significantly better in simulating the data than did the mechanism employed in the previous study (Carter et al, 1997a). This indicates that overall the current SAPRC-99 mechanism represents a significant improvement in our ability to simulate ozone impacts for the branched alkanes.

The major conclusion obtained from this program is that the updates to the mechanism and the mineral spirits component assignments has completely eliminated the discrepancies in the model simulations of the experiments using the four mineral spirits we studied previously (Carter et al, 1997a). In particular, the data obtained in that study are now well simulated by the current mechanism. The major reason for this improvement is probably the changes in the estimation methods for nitrate yields for the reactions of peroxy radicals with NO, resulting in predicted nitrate yields for branched and cyclic alkanes being closer to those for the corresponding normal alkanes. This is based in part on the new data obtained by Atkinson and co-workers (Arey et al, 2000; Atkinson et al, 2000), and in part on a revised method to estimate structural effects on nitrate yields. However, the revised assignments of compounds used to represent unspeciated branched and cyclic alkane isomers, based on using more varied and generally less branched compounds as indicated by results of GC-MS analyses, may also be contributing to this improved model performance.

Based on these results, it can be concluded that model calculations using the current SAPRC-99 mechanism can provide a reasonable basis for estimating the impacts of the four mineral spirits samples on ozone formation in the atmosphere. The ozone impacts for the all-alkane mineral spirits samples studied by Carter et al (1997a) were found to be relatively low, with the effect on peak ozone yields being 20-30% that of VOC emissions from all sources, on a mass basis. The impacts of the mineral spirits

sample containing ~8% aromatics or were about a factor of 2 or 3 higher than the all-alkane samples. The all-alkane mineral spirit samples tended to have less of an impact on maximum 8-hour average ozone yields than on peak ozone yields, particularly in lower NO_x scenarios. The mass-based ozone impacts of the all-alkane mineral spirits samples were generally somewhat greater than those of ethane, the compound used by the EPA to define "negligible" reactivity for VOC exemption purposes, except for impacts on maximum 8-hour average ozone in the lower NO_x scenarios. However, the relative impacts of the mineral spirits samples were found to be quite variable from scenario to scenario. This means that it is important that the model appropriately represent scenario conditions in assessments of relative ozone impacts of mineral spirits emissions.

Since a wide variety of hydrocarbon solvents are in use and emitted into the atmosphere, it is important to assess whether the methods used to evaluate the ozone impacts of the four samples studied for Safety-Kleen can be reliably applied for other such materials. Under funding from ExxonMobil we found that the mechanism and assignments used for the Safety-Kleen samples performed well in simulating chamber data for ExxonMobil D95®, a complex mixture of alkanes similar to mineral spirits but with a carbon number range of 11-16 (Carter et al, 2000c). The mechanism also performed reasonably well in simulating data for ExxonMobil Isopar-M®, a C_{11} - C_{16} mixture of primarily branched alkanes (Carter et al, 2000c), though not quite as well as is the case for the mineral spirits or D95 samples that were studied. However, no data are yet available concerning commercial non-dearomatized mineral spirits samples, which may not be well represented by the recycled material that was studied by Safety-Kleen.

Additional work is also needed to improve experimental atmospheric reactivity assessment methods for these types of substances. The environmental chamber experiments as employed in this and our previous studies are expensive, do not give fully unambiguous tests of aspects of the mechanisms concerning numbers of NO to NO_2 conversion, which are important in affecting predictions of ozone formation in the atmosphere, and are difficult to carry out reliably for very low volatility compounds. New methods to address these problems are being developed under CARB funding, but additional work is needed to determine if they can be applied to mineral spirits and similar substances.

REFERENCES

Arey, J., S. M. Aschmann, E. S. C. Kwok, and R. Atkinson (2000): Alkyl nitrate, hydroxyalkyl nitrate, and hydroxycarbonyl formation from the NO_x-air photooxidations of C_5-C_{10} n-alkanes. J. Phys. Chem. A, to be submitted for publication.

Atkinson, R. (1987): "A Structure-Activity Relationship for the Estimation of Rate Constants for the Gas-Phase Reactions of OH Radicals with Organic Compounds," Int. J. Chem. Kinet., 19, 799-828.

Atkinson, R. (1989): "Kinetics and Mechanisms of the Gas-Phase Reactions of the Hydroxyl Radical with Organic Compounds," J. Phys. Chem. Ref. Data, Monograph no 1.

Atkinson, R. (1997): "Gas Phase Tropospheric Chemistry of Volatile Organic Compounds: 1. Alkanes and Alkenes," J. Phys. Chem. Ref. Data, 26, 215-290.

Atkinson, R., S. M. Aschmann, W. P. L. Carter, A. M. Winer and J. N. Pitts, Jr. (1982): "Alkyl Nitrate Formation from the NO_x-Air Photooxidations of C_2-C_8 n-Alkanes," J. Phys. Chem. 86, 4562-4569.

Atkinson, R. and W. P. L. Carter (1984): "Kinetics and Mechanisms of the Gas-Phase Reactions of Ozone with Organic Compounds under Atmospheric Conditions," Chem. Rev. 84, 437-470.

Atkinson, R. et al. (2000) Manuscript on OH rate constants for branched alkanes. In preparation.

Baugues, K. (1990): "Preliminary Planning Information for Updating the Ozone Regulatory Impact Analysis Version of EKMA," Draft Document, Source Receptor Analysis Branch, Technical Support Division, U. S. Environmental Protection Agency, Research Triangle Park, NC, January.

Calvert, J. G., and J. N. Pitts, Jr. (1966): "Photochemistry," John Wiley and Sons, New York.

Carter, W. P. L. (1990): "A Detailed Mechanism for the Gas-Phase Atmospheric Reactions of Organic Compounds," Atmos. Environ., 24A, 481-518.

Carter, W. P. L. (1994a): "Development of Ozone Reactivity Scales for Volatile Organic Compounds," J. Air & Waste Manage. Assoc., 44, 881-899.

Carter, W. P. L. (1994b): "Calculation of Reactivity Scales Using an Updated Carbon Bond IV Mechanism," Report Prepared for Systems Applications International Under Funding from the Auto/Oil Air Quality Improvement Research Program, April 12. Available at http://helium.ucr.edu/~carter/absts.htm#cb4rct.

Carter, W. P. L. (2000): "Documentation of the SAPRC-99 Chemical Mechanism for VOC Reactivity Assessment," Report to the California Air Resources Board, Contracts 92-329 and 95-308, May 8. Available at http://helium.ucr.edu/~carter/absts.htm#saprc99.

Carter, W. P. L., and R. Atkinson (1985): "Atmospheric Chemistry of Alkanes", J. Atmos. Chem., 3, 377-405, 1985.

Carter, W. P. L. and R. Atkinson (1987): "An Experimental Study of Incremental Hydrocarbon Reactivity," Environ. Sci. Technol., 21, 670-679

Carter, W. P. L. and R. Atkinson (1989a): "Alkyl Nitrate Formation from the Atmospheric Photooxidation of Alkanes; a Revised Estimation Method," J. Atm. Chem. 8, 165-173.

Carter, W. P. L. and R. Atkinson (1989b): "A Computer Modeling Study of Incremental Hydrocarbon Reactivity", Environ. Sci. Technol., 23, 864.

Carter, W. P. L., and F. W. Lurmann (1990): "Evaluation of the RADM Gas-Phase Chemical Mechanism," Final Report, EPA-600/3-90-001.

Carter, W. P. L. and F. W. Lurmann (1991): "Evaluation of a Detailed Gas-Phase Atmospheric Reaction Mechanism using Environmental Chamber Data," Atm. Environ. 25A, 2771-2806.

Carter, W. P. L., J. A. Pierce, I. L. Malkina, D. Luo and W. D. Long (1993): "Environmental Chamber Studies of Maximum Incremental Reactivities of Volatile Organic Compounds," Report to Coordinating Research Council, Project No. ME-9, California Air Resources Board Contract No. A032-0692; South Coast Air Quality Management District Contract No. C91323, United States Environmental Protection Agency Cooperative Agreement No. CR-814396-01-0, University Corporation for Atmospheric Research Contract No. 59166, and Dow Corning Corporation. April 1. Available at http://helium.ucr.edu/~carter/absts.htm#rct1rept.

Carter, W. P. L., J. A. Pierce, D. Luo, and I. L. Malkina (1995a): "Environmental Chamber Studies of Maximum Incremental Reactivities of Volatile Organic Compounds," Atmos. Environ. 29, 2499-2511.

Carter, W. P. L., D. Luo, I. L. Malkina, and J. A. Pierce (1995b): "Environmental Chamber Studies of Atmospheric Reactivities of Volatile Organic Compounds. Effects of Varying ROG Surrogate and NO_x," Final report to Coordinating Research Council, Inc., Project ME-9, California Air Resources Board, Contract A032-0692, and South Coast Air Quality Management District, Contract C91323. March 24. Available at http://helium.ucr.edu/~carter/absts.htm#rct2rept.

Carter, W. P. L., D. Luo, I. L. Malkina, and D. Fitz (1995c): "The University of California, Riverside Environmental Chamber Data Base for Evaluating Oxidant Mechanism. Indoor Chamber Experiments through 1993," Report submitted to the U. S. Environmental Protection Agency, EPA/AREAL, Research Triangle Park, NC., March 20. Available at http://helium.ucr.edu/~carter/absts.htm#databas.

Carter, W. P. L., D. Luo, and I. L. Malkina (1996): "Investigation of Atmospheric Ozone Formation Potentials of C_{12} - C_{16} n-Alkanes," Report to the Aluminum Association, October 28. Available at http://cert.ucr.edu/~carter/absts.htm#alkrept.

Carter, W. P. L., D. Luo, and I. L. Malkina (1997a): "Investigation of the Atmospheric Ozone Formation Potentials of Selected Mineral Spirits Mixtures," Report to Safety-Kleen Corporation, July 25. Available at http://cert.ucr.edu/~carter/absts.htm#msrept.

Carter, W. P. L., D. Luo, and I. L. Malkina (1997b): "Environmental Chamber Studies for Development of an Updated Photochemical Mechanism for VOC Reactivity Assessment," Final report to the California Air Resources Board, the Coordinating Research Council, and the National Renewable Energy Laboratory, November 26. Available at http://helium.ucr.edu/~carter/absts.htm#rct3rept.

Carter, W. P. L., D. Luo, and I. L. Malkina (2000a): "Investigation of the Atmospheric Ozone Formation Potentials of Selected $C_{\geq 12}$ Normal and Cyclic Alkanes," Draft Report to the Aluminum Association, August 9.

Carter. W. P. L., D. Luo and I. L. Malkina (2000b): "Investigation of Atmospheric Reactivities of Selected Consumer Product VOCs," Report to California Air Resources Board, May 30. Available at http://helium.ucr.edu/~carter/absts.htm#cpreport.

Carter, W. P. L., D. Luo, and I. L. Malkina (2000c): "Investigation of the Atmospheric Ozone Formation Potentials of D95®, Isopar-M® and Exxate-1000® Fluids," Report to ExxonMobile Chemical Company, in preparation.

Chang, T. Y. and S. J. Rudy (1990): "Ozone-Forming Potential of Organic Emissions from Alternative-Fueled Vehicles," Atmos. Environ., 24A, 2421-2430.

Croes, B. E., Technical Support Division, California Air Resources Board, personal communication (1991).

Croes, B. E., et al. (1994): "Southern California Air Quality Study Data Archive," Research Division, California Air Resources Board.

Dasgupta, P. K, Dong, S. and Hwang, H. (1988): "Continuous Liquid Phase Fluorometry Coupled to a Diffusion Scrubber for the Determination of Atmospheric Formaldehyde, Hydrogen Peroxide, and Sulfur Dioxide," Atmos. Environ. 22, 949-963.

Dasgupta, P.K, Dong, S. and Hwang, H. (1990): Aerosol Science and Technology 12, 98-104

Dimitriades, B. (1999): "Scientific Basis of an Improved EPA Policy on Control of Organic Emissions for Ambient Ozone Reduction," J. Air & Waste Manage. Assoc. 49, 831-838

Dodge, M. C. (1984): "Combined effects of organic reactivity and NMHC/NOx ratio on photochemical oxidant formation -- a modeling study," Atmos. Environ., 18, 1657.

Eberhard, J., C. Muller, D. W. Stocker and J. A. Kerr (1995): "Isomerization of Alkoxy Radicals under Atmospheric Conditions," Environ. Sci. Technol. 29, 232.

EPA (1984): "Guideline for Using the Carbon Bond Mechanism in City-Specific EKMA," EPA-450/4-84-005, February.

Febo, A., C. Perrino, M. Gerardi and R. Sparapini (1995): "Evaluation of a High-Purity and High Stability Continuous Generation System for Nitrous Acid," Environ. Sci. Technol. 29, 2390-2395.

Gery, M. W., R. D. Edmond and G. Z. Whitten (1987): "Tropospheric Ultraviolet Radiation. Assessment of Existing Data and Effects on Ozone Formation," Final Report, EPA-600/3-87-047, October.

Gipson, G. L., W. P. Freas, R. A. Kelly and E. L. Meyer (1981): "Guideline for Use of City-Specific EKMA in Preparing Ozone SIPs, EPA-450/4-80-027, March.

Gipson, G. L. and W. P. Freas (1983): "Use of City-Specific EKMA in the Ozone RIA," U. S. Environmental Protection Agency, July.

Johnson, G. M. (1983): "Factors Affecting Oxidant Formation in Sydney Air," in "The Urban Atmosphere -- Sydney, a Case Study." Eds. J. N. Carras and G. M. Johnson (CSIRO, Melbourne), pp. 393-408.

Jeffries, H. E. (1991): "UNC Solar Radiation Models," unpublished draft report for EPA Cooperative Agreements CR813107, CR813964 and CR815779".

Jeffries, H. E., K. G. Sexton, J. R. Arnold, and T. L. Kale (1989): "Validation Testing of New Mechanisms with Outdoor Chamber Data. Volume 2: Analysis of VOC Data for the CB4 and CAL Photochemical Mechanisms," Final Report, EPA-600/3-89-010b.

Jeffries, H. E. and R. Crouse (1991): "Scientific and Technical Issues Related to the Application of Incremental Reactivity. Part II: Explaining Mechanism Differences," Report prepared for Western States Petroleum Association, Glendale, CA, October.

Kwok, E. S. C., and R. Atkinson (1995): "Estimation of Hydroxyl Radical Reaction Rate Constants for Gas-Phase Organic Compounds Using a Structure-Reactivity Relationship: An Update," Atmos. Environ 29, 1685-1695.

Kwok, E. S. C., J. Arey and R. Atkinson (1996): "Alkoxy radical isomerization in the OH radical-initiated reactions of C4-C8 n-alkanes," J. Phys. Chem., 100, 214-219.

Lurmann, F. W. and H. H. Main (1992): "Analysis of the Ambient VOC Data Collected in the Southern California Air Quality Study," Final Report to California Air Resources Board Contract No. A832-130, February.

Zafonte, L., P. L. Rieger, and J. R. Holmes (1977): "Nitrogen Dioxide Photolysis in the Los Angeles Atmosphere," Environ. Sci. Technol. 11, 483-487.

APPENDIX A.
MECHANISM LISTING AND TABULATIONS

This Appendix gives a complete listing of the mechanisms used in the SAPRC-99 model simulations of the environmental chamber experiments and the mineral spirits atmospheric reactivity simulations in this report. Table A-1 contains a list of all the model species used, and Table A-2 lists all the reactions and rate parameters, Table A-3 lists the absorption cross sections and photolysis reactions used in the mechanism. In addition, Table A-4 gives the chamber-dependent parameters used in the model simulations of the chamber experiments.

Table A-1. Listing of the model species in the mechanism used in the model simulations discussed in this report.

Type and Name	Description
	Species used in Base Mechanism
Constant Species.	
O2	Oxygen
M	Air
H2O	Water
H2	Hydrogen Molecules
HV	Light
Active Inorganic Species.	
O3	Ozone
NO	Nitric Oxide
NO2	Nitrogen Dioxide
NO3	Nitrate Radical
N2O5	Nitrogen Pentoxide
HONO	Nitrous Acid
HNO3	Nitric Acid
HNO4	Peroxynitric Acid
HO2H	Hydrogen Peroxide
CO	Carbon Monoxide
SO2	Sulfur Dioxide
Active Radical Species and Operators.	
HO.	Hydroxyl Radicals
HO2.	Hydroperoxide Radicals
C-O2.	Methyl Peroxy Radicals
RO2-R.	Peroxy Radical Operator representing NO to NO2 conversion with HO2 formation.
R2O2.	Peroxy Radical Operator representing NO to NO2 conversion without HO2 formation.
RO2-N.	Peroxy Radical Operator representing NO consumption with organic nitrate formation.
CCO-O2.	Acetyl Peroxy Radicals

Table A-1 (continued)

Type and Name	Description
RCO-O2.	Peroxy Propionyl and higher peroxy acyl Radicals
BZCO-O2.	Peroxyacyl radical formed from Aromatic Aldehydes
MA-RCO3.	Peroxyacyl radicals formed from methacrolein and other acroleins.
Steady State Radical Species	
O3P	Ground State Oxygen Atoms
O*1D2	Excited Oxygen Atoms
TBU-O.	t-Butoxy Radicals
BZ-O.	Phenoxy Radicals
BZ(NO2)-O.	Nitro-substituted Phenoxy Radical
HOCOO.	Radical formed when Formaldehyde reacts with HO2
PAN and PAN Analogues	
PAN	Peroxy Acetyl Nitrate
PAN2	PPN and other higher alkyl PAN analogues
PBZN	PAN analogues formed from Aromatic Aldehydes
MA-PAN	PAN analogue formed from Methacrolein
Explicit and Lumped Molecule Reactive Organic Product Species	
HCHO	Formaldehyde
CCHO	Acetaldehyde
RCHO	Lumped C3+ Aldehydes
ACET	Acetone
MEK	Ketones and other non-aldehyde oxygenated products that react with OH radicals slower than 5 x 10^{-12} cm^3 $molec^{-2}$ sec^{-1}.
MEOH	Methanol
COOH	Methyl Hydroperoxide
ROOH	Lumped higher organic hydroperoxides
GLY	Glyoxal
MGLY	Methyl Glyoxal
BACL	Biacetyl
PHEN	Phenol
CRES	Cresols
NPHE	Nitrophenols
BALD	Aromatic aldehydes (e.g., benzaldehyde)
METHACRO	Methacrolein
MVK	Methyl Vinyl Ketone
ISO-PROD	Lumped isoprene product species
Lumped Parameter Products	
PROD2	Ketones and other non-aldehyde oxygenated products that react with OH radicals faster than 5 x 10^{-12} cm^3 $molec^{-2}$ sec^{-1}.
RNO3	Lumped Organic Nitrates

Table A-1 (continued)

Type and Name	Description
Uncharacterized Reactive Aromatic Ring Fragmentation Products	
DCB1	Reactive Aromatic Fragmentation Products that do not undergo significant photodecomposition to radicals.
DCB2	Reactive Aromatic Fragmentation Products which photolyze with alpha-dicarbonyl-like action spectrum.
DCB3	Reactive Aromatic Fragmentation Products which photolyze with acrolein action spectrum.
Non-Reacting Species	
CO2	Carbon Dioxide
XC	Lost Carbon
XN	Lost Nitrogen
SULF	Sulfates (SO_3 or H_2SO_4)
Low Reactivity Compounds or Unknown Products Represented as Unreactive	
H2	Hydrogen
HCOOH	Formic Acid
CCO-OH	Acetic Acid
RCO-OH	Higher organic acids
CCO-OOH	Peroxy Acetic Acid
RCO-OOH	Higher organic peroxy acids
NROG	Unspecified Unreactive Carbon
	Base ROG VOC Species used in the Chamber Simulations
N-C4	n-Butane
N-C6	n-Hexane
N-C8	n-Octane
ETHENE	Ethene
PROPENE	Propene
T-2-BUTE	*Trans*-2-Butene
TOLUENE	Toluene
M-XYLENE	m-Xylene
135-TMB	1,3,5-Trimethyl Benzene
	Normal Alkane Mineral Spirit Constituents
N-C8	n-Octane
N-C9	n-Nonane
N-C10	n-Decane
N-C11	n-Undecane
N-C12	n-Dodecane
N-C13	n-Tridecane
N-C14	n-Tetradecane
N-C15	n-Pentadecane
	Branched Alkane Mineral Spirit Constituents
24-DM-C6	2,4-Dimethyl Hexane
4-ME-C7	4-Methyl Heptane
2-ME-C7	2-Methyl Heptane
24-DM-C7	2,4-Dimethyl Heptane

Table A-1 (continued)

Type and Name	Description
4-ME-C8	4-Methyl Octane
2-ME-C8	2-Methyl Octane
26DM-C8	2,6-Dimethyl Octane
4-ME-C9	4-Methyl Nonane
2-ME-C9	2-Methyl Nonane
26DM-C9	2,6-Dimethyl Nonane
34-DE-C6	3,4-Diethyl Hexane
4-ME-C10	4-Methyl Decane
3-ME-C10	3-Methyl Decane
36DM-C10	3,6-Dimethyl Decane
5-ME-C11	5-Methyl Undecane
3-ME-C11	3-Methyl Undecane
36DM-C11	3,6-Dimethyl Undecane
5-ME-C12	5-Methyl Dodecane
3-ME-C12	3-Methyl Dodecane
37DM-C12	3,7-Dimethyl Dodecane
6-ME-C13	6-Methyl Tridecane
3-ME-C13	3-Methyl Tridecane
37DM-C13	3,7-Dimethyl Tridecane
6-ME-C14	6-Methyl Tetradecane
3-ME-C14	3-Methyl Tetradecane
	Cyclic Alkane Mineral Spirit Constituents
ET-CYCC6	Ethylcyclohexane
C3-CYCC6	Propyl Cyclohexane
1E4MCYC6	1-Ethyl-4-Methyl Cyclohexane
C4-CYCC6	Butyl Cyclohexane
1M3IPCY6	1-Methyl-3-Isopropyl Cyclohexane
14DECYC6	1,4-Diethyl-Cyclohexane
C5-CYCC6	Pentyl Cyclohexane
13E5MCC6	1,3-Diethyl-5-Methyl Cyclohexane
1E2PCYC6	1-Ethyl-2-Propyl Cyclohexane
C6-CYCC6	Hexyl Cyclohexane
135ECYC6	1,3,5-Triethyl Cyclohexane
1M4C5CY6	1-Methyl-4-Pentyl Cyclohexane
C7-CYCC6	Heptyl Cyclohexane
13E5PCC6	1,3-Diethyl-5-Pentyl Cyclohexane
1M2C6CC6	1-Methyl-2-Hexyl-Cyclohexane
C8-CYCC6	Octyl Cyclohexane
13P5ECC6	1,3-Dipropyl-5-EthylCyclohexane
1M4C7CC6	1-Methyl-4-Heptyl Cyclohexane
C9-CYCC6	Nonyl Cyclohexane
135PCYC6	1,3,5-Tripropyl Cyclohexane
1M2C8CC6	1-Methyl-2-Octyl Cyclohexane

Table A-1 (continued)

Type and Name	Description
	Aromatic and Alkene Constituents of Mineral Spirits Sample "A" [a]
MS-A-ARO	Lumped aromatics in Sample "A" (parameters derived from weighed averages of those for all the aromatic constituents listed on Table 5)
MS-A-OLE	Lumped alkanes in Sample "A" (parameters derived from weighed averages of those for all the alkene constituents listed on Table 5)
	Explicit and Lumped VOC Species used in the Ambient Simulations
Primary Organics Represented explicitly	
CH4	Methane
ETHENE	Ethene
ISOPRENE	Isoprene
Example Test VOCs not in the Base Mechanism	
ETHANE	Ethane
Lumped Parameter Species	
ALK1	Alkanes and other non-aromatic compounds that react only with OH, and have kOH < 5 x 10^2 ppm-1 min-1. (Primarily ethane)
ALK2	Alkanes and other non-aromatic compounds that react only with OH, and have kOH between 5 x 10^2 and 2.5 x 10^3 ppm-1 min-1. (Primarily propane and acetylene)
ALK3	Alkanes and other non-aromatic compounds that react only with OH, and have kOH between 2.5 x 10^3 and 5 x 10^3 ppm-1 min-1.
ALK4	Alkanes and other non-aromatic compounds that react only with OH, and have kOH between 5 x 10^3 and 1 x 10^4 ppm-1 min-1.
ALK5	Alkanes and other non-aromatic compounds that react only with OH, and have kOH greater than 1 x 10^4 ppm-1 min-1.
ARO1	Aromatics with kOH < 2x10^4 ppm-1 min-1.
ARO2	Aromatics with kOH > 2x10^4 ppm-1 min-1.
OLE1	Alkenes (other than ethene) with kOH < 7x10^4 ppm-1 min-1.
OLE2	Alkenes with kOH > 7x10^4 ppm-1 min-1.
TERP	Terpenes

[a] See Carter (2000) for the mechanisms or model representations used for these constituents.

Table A-2. Listing of the reactions in the mechanism used in the model simulations discussed in this report. See Carter (2000) for documentation.

Label	Rate Parameters [a] k(298)	A	Ea	B	Reaction and Products [b]
Inorganic Reactions					
1		Phot Set= NO2			NO2 + HV = NO + O3P
2	5.79e-34	5.68e-34	0.00	-2.8	O3P + O2 + M = O3 + M
3	7.96e-15	8.00e-12	4.09		O3P + O3 = #2 O2
4	1.01e-31	1.00e-31	0.00	-1.6	O3P + NO + M = NO2 + M
5	9.72e-12	6.50e-12	-0.24		O3P + NO2 = NO + O2
6	1.82e-12	Falloff, F=0.80			O3P + NO2 = NO3 + M
	0:	9.00e-32	0.00	-2.0	
	inf:	2.20e-11	0.00	0.0	
8	1.81e-14	1.80e-12	2.72		O3 + NO = NO2 + O2
9	3.52e-17	1.40e-13	4.91		O3 + NO2 = O2 + NO3
10	2.60e-11	1.80e-11	-0.22		NO + NO3 = #2 NO2
11	1.95e-38	3.30e-39	-1.05		NO + NO + O2 = #2 NO2
12	1.54e-12	Falloff, F=0.45			NO2 + NO3 = N2O5
	0:	2.80e-30	0.00	-3.5	
	inf:	2.00e-12	0.00	0.2	
13	5.28e-2	Falloff, F=0.45			N2O5 = NO2 + NO3
	0:	1.00e-3	21.86	-3.5	
	inf:	9.70e+14	22.02	0.1	
14	2.60e-22	2.60e-22			N2O5 + H2O = #2 HNO3
15		(Slow)			N2O5 + HV = NO3 + NO + O3P
16		(Slow)			N2O5 + HV = NO3 + NO2
17	6.56e-16	4.50e-14	2.50		NO2 + NO3 = NO + NO2 + O2
18		Phot Set= NO3NO			NO3 + HV = NO + O2
19		Phot Set= NO3NO2			NO3 + HV = NO2 + O3P
20		Phot Set= O3O3P			O3 + HV = O3P + O2
21		Phot Set= O3O1D			O3 + HV = O*1D2 + O2
22	2.20e-10	2.20e-10			O*1D2 + H2O = #2 HO.
23	2.87e-11	2.09e-11	-0.19		O*1D2 + M = O3P + M
24	7.41e-12	Falloff, F=0.60			HO. + NO = HONO
	0:	7.00e-31	0.00	-2.6	
	inf:	3.60e-11	0.00	-0.1	
25		Phot Set= HONO-NO			HONO + HV = HO. + NO
26		Phot Set= HONO-NO2			HONO + HV = HO2. + NO2
27	6.46e-12	2.70e-12	-0.52		HO. + HONO = H2O + NO2
28	8.98e-12	Falloff, F=0.60			HO. + NO2 = HNO3
	0:	2.43e-30	0.00	-3.1	
	inf:	1.67e-11	0.00	-2.1	
29	2.00e-11	2.00e-11			HO. + NO3 = HO2. + NO2
30	1.47e-13	k = k0+k3M/(1+k3M/k2)			HO. + HNO3 = H2O + NO3
	k0:	7.20e-15	-1.56	0.0	
	k2:	4.10e-16	-2.86	0.0	
	k3:	1.90e-33	-1.44	0.0	
31		Phot Set= HNO3			HNO3 + HV = HO. + NO2
32	2.09e-13	k = k1 + k2 [M]			HO. + CO = HO2. + CO2
	k1:	1.30e-13	0.00	0.0	
	k2:	3.19e-33	0.00	0.0	
33	6.63e-14	1.90e-12	1.99		HO. + O3 = HO2. + O2

Table A-2 (continued)

Label	Rate Parameters [a] k(298)	A	Ea	B	Reaction and Products [b]
34	8.41e-12	3.40e-12	-0.54		HO2. + NO = HO. + NO2
35	1.38e-12	Falloff, F=0.60			HO2. + NO2 = HNO4
	0:	1.80e-31	0.00	-3.2	
	inf:	4.70e-12	0.00	0.0	
36	7.55e-2	Falloff, F=0.50			HNO4 = HO2. + NO2
	0:	4.10e-5	21.16	0.0	
	inf:	5.70e+15	22.20	0.0	
37	Phot Set= HO2NO2				HNO4 + HV = #.61 {HO2. + NO2} + #.39 {HO. + NO3}
38	5.02e-12	1.50e-12	-0.72		HNO4 + HO. = H2O + NO2 + O2
39	1.87e-15	1.40e-14	1.19		HO2. + O3 = HO. + #2 O2
40A	2.87e-12	k = k1 + k2 [M]			HO2. + HO2. = HO2H + O2
	k1:	2.20e-13	-1.19	0.0	
	k2:	1.85e-33	-1.95	0.0	
40B	6.46e-30	k = k1 + k2 [M]			HO2. + HO2. + H2O = HO2H + O2 + H2O
	k1:	3.08e-34	-5.56	0.0	
	k2:	2.59e-54	-6.32	0.0	
41	4.00e-12	4.00e-12			NO3 + HO2. = #.8 {HO. + NO2 + O2} + #.2 {HNO3 + O2}
42	2.28e-16	8.50e-13	4.87		NO3 + NO3 = #2 NO2 + O2
43	Phot Set= H2O2				HO2H + HV = #2 HO.
44	1.70e-12	2.90e-12	0.32		HO2H + HO. = HO2. + H2O
45	1.11e-10	4.80e-11	-0.50		HO. + HO2. = H2O + O2
S2OH	9.77e-13	Falloff, F=0.45			HO. + SO2 = HO2. + SULF
	0:	4.00e-31	0.00	-3.3	
	inf:	2.00e-12	0.00	0.0	
H2OH	6.70e-15	7.70e-12	4.17		HO. + H2 = HO2. + H2O
Methyl peroxy and methoxy reactions					
MER1	7.29e-12	2.80e-12	-0.57		C-O2. + NO = NO2 + HCHO + HO2.
MER4	5.21e-12	3.80e-13	-1.55		C-O2. + HO2. = COOH + O2
MEN3	1.30e-12	1.30e-12			C-O2. + NO3 = HCHO + HO2. + NO2
MER5	2.65e-13	2.45e-14	-1.41		C-O2. + C-O2. = MEOH + HCHO + O2
MER6	1.07e-13	5.90e-13	1.01		C-O2. + C-O2. = #2 {HCHO + HO2.}
Peroxy Racical Operators					
RRNO	9.04e-12	2.70e-12	-0.72		RO2-R. + NO = NO2 + HO2.
RRH2	1.49e-11	1.90e-13	-2.58		RO2-R. + HO2. = ROOH + O2 + #-3 XC
RRN3	2.30e-12	2.30e-12			RO2-R. + NO3 = NO2 + O2 + HO2.
RRME	2.00e-13	2.00e-13			RO2-R. + C-O2. = HO2. + #.75 HCHO + #.25 MEOH
RRR2	3.50e-14	3.50e-14			RO2-R. + RO2-R. = HO2.
R2NO	Same k as rxn RRNO				R2O2. + NO = NO2
R2H2	Same k as rxn RRH2				R2O2. + HO2. = HO2.
R2N3	Same k as rxn RRN3				R2O2. + NO3 = NO2
R2ME	Same k as rxn RRME				R2O2. + C-O2. = C-O2.
R2RR	Same k as rxn RRR2				R2O2. + RO2-R. = RO2-R.
R2R3	Same k as rxn RRR2				R2O2. + R2O2. =
RNNO	Same k as rxn RRNO				RO2-N. + NO = RNO3
RNH2	Same k as rxn RRH2				RO2-N. + HO2. = ROOH + #3 XC
RNME	Same k as rxn RRME				RO2-N. + C-O2. = HO2. + #.25 MEOH + #.5 {MEK + PROD2} + #.75 HCHO + XC
RNN3	Same k as rxn RRN3				RO2-N. + NO3 = NO2 + O2 + HO2. + MEK + #2 XC
RNRR	Same k as rxn RRR2				RO2-N. + RO2-R. = HO2. + #.5 {MEK + PROD2} + O2 + XC

Table A-2 (continued)

Label	Rate Parameters [a] k(298)	A	Ea	B	Reaction and Products [b]
RNR2	Same k as rxn RRR2				RO2-N. + R2O2. = RO2-N.
RNRN	Same k as rxn RRR2				RO2-N. + RO2-N. = MEK + HO2. + PROD2 + O2 + #2 XC
APN2	1.05e-11	Falloff, F=0.30			CCO-O2. + NO2 = PAN
	0:	2.70e-28	0.00	-7.1	
	inf:	1.20e-11	0.00	-0.9	
DPAN	5.21e-4	Falloff, F=0.30			PAN = CCO-O2. + NO2
	0:	4.90e-3	24.05	0.0	
	inf:	4.00e+16	27.03	0.0	
APNO	2.13e-11	7.80e-12	-0.60		CCO-O2. + NO = C-O2. + CO2 + NO2
APH2	1.41e-11	4.30e-13	-2.07		CCO-O2. + HO2. = #.75 {CCO-OOH +O2} + #.25 {CCO-OH + O3}
APN3	4.00e-12	4.00e-12			CCO-O2. + NO3 = C-O2. + CO2 + NO2 + O2
APME	9.64e-12	1.80e-12	-0.99		CCO-O2. + C-O2. = CCO-OH + HCHO + O2
APRR	7.50e-12	7.50e-12			CCO-O2. + RO2-R. = CCO-OH
APR2	Same k as rxn APRR				CCO-O2. + R2O2. = CCO-O2.
APRN	Same k as rxn APRR				CCO-O2. + RO2-N. = CCO-OH + PROD2
APAP	1.55e-11	2.90e-12	-0.99		CCO-O2. + CCO-O2. = #2 {C-O2. + CO2} + O2
PPN2	1.21e-11	1.20e-11	0.00	-0.9	RCO-O2. + NO2 = PAN2
PAN2	4.43e-4	2.00e+15	25.44		PAN2 = RCO-O2. + NO2
PPNO	2.80e-11	1.25e-11	-0.48		RCO-O2. + NO = NO2 + CCHO + RO2-R. + CO2
PPH2	Same k as rxn APH2				RCO-O2. + HO2. = #.75 {RCO-OOH + O2} + #.25 {RCO-OH + O3}
PPN3	Same k as rxn APN3				RCO-O2. + NO3 = NO2 + CCHO + RO2-R. + CO2 + O2
PPME	Same k as rxn APME				RCO-O2. + C-O2. = RCO-OH + HCHO + O2
PPRR	Same k as rxn APRR				RCO-O2. + RO2-R. = RCO-OH + O2
PPR2	Same k as rxn APRR				RCO-O2. + R2O2. = RCO-O2.
PPRN	Same k as rxn APRR				RCO-O2. + RO2-N. = RCO-OH + PROD2 + O2
PPAP	Same k as rxn APAP				RCO-O2. + CCO-O2. = #2 CO2 + C-O2. + CCHO + RO2-R. + O2
PPPP	Same k as rxn APAP				RCO-O2. + RCO-O2. = #2 {CCHO + RO2-R. + CO2}
BPN2	1.37e-11	1.37e-11			BZCO-O2. + NO2 = PBZN
BPAN	3.12e-4	7.90e+16	27.82		PBZN = BZCO-O2. + NO2
BPNO	Same k as rxn PPNO				BZCO-O2. + NO = NO2 + CO2 + BZ-O. + R2O2.
BPH2	Same k as rxn APH2				BZCO-O2. + HO2. = #.75 {RCO-OOH + O2} + #.25 {RCO-OH + O3} + #4 XC
BPN3	Same k as rxn APN3				BZCO-O2. + NO3 = NO2 + CO2 + BZ-O. + R2O2. + O2
BPME	Same k as rxn APME				BZCO-O2. + C-O2. = RCO-OH + HCHO + O2 + #4 XC
BPRR	Same k as rxn APRR				BZCO-O2. + RO2-R. = RCO-OH + O2 + #4 XC
BPR2	Same k as rxn APRR				BZCO-O2. + R2O2. = BZCO-O2.
BPRN	Same k as rxn APRR				BZCO-O2. + RO2-N. = RCO-OH + PROD2 + O2 + #4 XC
BPAP	Same k as rxn APAP				BZCO-O2. + CCO-O2. = #2 CO2 + C-O2. + BZ-O. + R2O2.
BPPP	Same k as rxn APAP				BZCO-O2. + RCO-O2. = #2 CO2 + CCHO + RO2-R. + BZ-O. + R2O2.
BPBP	Same k as rxn APAP				BZCO-O2. + BZCO-O2. = #2 {BZ-O. + R2O2. + CO2}
MPN2	Same k as rxn PPN2				MA-RCO3. + NO2 = MA-PAN
MPPN	3.55e-4	1.60e+16	26.80		MA-PAN = MA-RCO3. + NO2
MPNO	Same k as rxn PPNO				MA-RCO3. + NO = NO2 + CO2 + HCHO + CCO-O2.
MPH2	Same k as rxn APH2				MA-RCO3. + HO2. = #.75 {RCO-OOH + O2} + #.25 {RCO-OH + O3} + XC
MPN3	Same k as rxn APN3				MA-RCO3. + NO3 = NO2 + CO2 + HCHO + CCO-O2. + O2

Table A-2 (continued)

Label	Rate Parameters [a] k(298)	A	Ea	B	Reaction and Products [b]
MPME	Same k as rxn APME				MA-RCO3. + C-O2. = RCO-OH + HCHO + XC + O2
MPRR	Same k as rxn APRR				MA-RCO3. + RO2-R. = RCO-OH + XC
MPR2	Same k as rxn APRR				MA-RCO3. + R2O2. = MA-RCO3.
MPRN	Same k as rxn APRR				MA-RCO3. + RO2-N. = #2 RCO-OH + O2 + #4 XC
MPAP	Same k as rxn APAP				MA-RCO3. + CCO-O2. = #2 CO2 + C-O2. + HCHO + CCO-O2. + O2
MPPP	Same k as rxn APAP				MA-RCO3. + RCO-O2. = HCHO + CCO-O2. + CCHO + RO2-R. + #2 CO2
MPBP	Same k as rxn APAP				MA-RCO3. + BZCO-O2. = HCHO + CCO-O2. + BZ-O. + R2O2. + #2 CO2
MPMP	Same k as rxn APAP				MA-RCO3. + MA-RCO3. = #2 {HCHO + CCO-O2. + CO2}
Other Organic Radical Species					
TBON	2.40e-11	2.40e-11			TBU-O. + NO2 = RNO3 + #-2 XC
TBOD	9.87e+2	7.50e+14	16.20		TBU-O. = ACET + C-O2.
BRN2	3.80e-11	2.30e-11	-0.30		BZ-O. + NO2 = NPHE
BRH2	Same k as rxn RRH2				BZ-O. + HO2. = PHEN
BRXX	1.00e-3	1.00e-3			BZ-O. = PHEN
BNN2	Same k as rxn BRN2				BZ(NO2)-O. + NO2 = #2 XN + #6 XC
BNH2	Same k as rxn RRH2				BZ(NO2)-O. + HO2. = NPHE
BNXX	Same k as rxn BRXX				BZ(NO2)-O. = NPHE
Explicit and Lumped Molecule Organic Products					
FAHV	Phot Set= HCHO_R				HCHO + HV = #2 HO2. + CO
FAVS	Phot Set= HCHO_M				HCHO + HV = H2 + CO
FAOH	9.20e-12	8.60e-12	-0.04		HCHO + HO. = HO2. + CO + H2O
FAH2	7.90e-14	9.70e-15	-1.24		HCHO + HO2. = HOCOO.
FAHR	1.51e+2	2.40e+12	13.91		HOCOO. = HO2. + HCHO
FAHN	Same k as rxn MER1				HOCOO. + NO = HCOOH + NO2 + HO2.
FAN3	5.74e-16	2.00e-12	4.83		HCHO + NO3 = HNO3 + HO2. + CO
AAOH	1.58e-11	5.60e-12	-0.62		CCHO + HO. = CCO-O2. + H2O
AAHV	Phot Set= CCHO_R				CCHO + HV = CO + HO2. + C-O2.
AAN3	2.73e-15	1.40e-12	3.70		CCHO + NO3 = HNO3 + CCO-O2.
PAOH	2.00e-11	2.00e-11			RCHO + HO. = #.034 RO2-R. + #.001 RO2-N. + #.965 RCO-O2. + #.034 CO + #.034 CCHO + #-0.003 XC
PAHV	Phot Set= C2CHO				RCHO + HV = CCHO + RO2-R. + CO + HO2.
PAN3	3.67e-15	1.40e-12	3.52		RCHO + NO3 = HNO3 + RCO-O2.
K3OH	1.92e-13	1.10e-12	1.03		ACET + HO. = HCHO + CCO-O2. + R2O2.
K3HV	Phot Set= ACETONE				ACET + HV = CCO-O2. + C-O2.
K4OH	1.18e-12	1.30e-12	0.05	2.0	MEK + HO. = #.37 RO2-R. + #.042 RO2-N. + #.616 R2O2. + #.492 CCO-O2. + #.096 RCO-O2. + #.115 HCHO + #.482 CCHO + #.37 RCHO + #.287 XC
K4HV	Phot Set= KETONE, qy= 1.5e-1				MEK + HV = CCO-O2. + CCHO + RO2-R.
MeOH	9.14e-13	3.10e-12	0.72	2.0	MEOH + HO. = HCHO + HO2.
MER9	5.49e-12	2.90e-12	-0.38		COOH + HO. = H2O + #.35 {HCHO + HO.} + #.65 C-O2.
MERA	Phot Set= COOH				COOH + HV = HCHO + HO2. + HO.
LPR9	1.10e-11	1.10e-11			ROOH + HO. = H2O + RCHO + #.34 RO2-R. + #.66 HO.
LPRA	Phot Set= COOH				ROOH + HV = RCHO + HO2. + HO.

Table A-2 (continued)

Label	Rate Parameters [a] k(298)	A	Ea	B	Reaction and Products [b]
GLHV	Phot Set= GLY_R				GLY + HV = #2 {CO + HO2.}
GLVM	Phot Set= GLY_ABS, qy= 6.0e-3				GLY + HV = HCHO + CO
GLOH	1.10e-11	1.10e-11			GLY + HO. = #.63 HO2. + #1.26 CO + #.37 RCO-O2. + #-.37 XC
GLN3	9.63e-16	2.80e-12	4.72		GLY + NO3 = HNO3 + #.63 HO2. + #1.26 CO + #.37 RCO-O2. + #-.37 XC
MGHV	Phot Set= MGLY_ADJ				MGLY + HV = HO2. + CO + CCO-O2.
MGOH	1.50e-11	1.50e-11			MGLY + HO. = CO + CCO-O2.
MGN3	2.43e-15	1.40e-12	3.77		MGLY + NO3 = HNO3 + CO + CCO-O2.
BAHV	Phot Set= BACL_ADJ				BACL + HV = #2 CCO-O2.
PHOH	2.63e-11	2.63e-11			PHEN + HO. = #.24 BZ-O. + #.76 RO2-R. + #.23 GLY + #4.1 XC
PHN3	3.78e-12	3.78e-12			PHEN + NO3 = HNO3 + BZ-O.
CROH	4.20e-11	4.20e-11			CRES + HO. = #.24 BZ-O. + #.76 RO2-R. + #.23 MGLY + #4.87 XC
CRN3	1.37e-11	1.37e-11			CRES + NO3 = HNO3 + BZ-O. + XC
NPN3	Same k as rxn PHN3				NPHE + NO3 = HNO3 + BZ(NO2)-O.
BZOH	1.29e-11	1.29e-11			BALD + HO. = BZCO-O2.
BZHV	Phot Set= BZCHO, qy= 5.0e-2				BALD + HV = #7 XC
BZNT	2.62e-15	1.40e-12	3.72		BALD + NO3 = HNO3 + BZCO-O2.
MAOH	3.36e-11	1.86e-11	-0.35		METHACRO + HO. = #.5 RO2-R. + #.416 CO + #.084 HCHO + #.416 MEK + #.084 MGLY + #.5 MA-RCO3. + #-0.416 XC
MAO3	1.13e-18	1.36e-15	4.20		METHACRO + O3 = #.008 HO2. + #.1 RO2-R. + #.208 HO. + #.1 RCO-O2. + #.45 CO + #.117 CO2 + #.2 HCHO + #.9 MGLY + #.333 HCOOH + #-0.1 XC
MAN3	4.58e-15	1.50e-12	3.43		METHACRO + NO3 = #.5 {HNO3 + RO2-R. + CO +MA-RCO3.} + #1.5 XC + #.5 XN
MAOP	6.34e-12	6.34e-12			METHACRO + O3P = RCHO + XC
MAHV	Phot Set= ACROLEIN, qy= 4.1e-3				METHACRO + HV = #.34 HO2. + #.33 RO2-R. + #.33 HO. + #.67 CCO-O2. + #.67 CO + #.67 HCHO + #.33 MA-RCO3. + #-0 XC
MVOH	1.89e-11	4.14e-12	-0.90		MVK + HO. = #.3 RO2-R. + #.025 RO2-N. + #.675 R2O2. + #.675 CCO-O2. + #.3 HCHO + #.675 RCHO + #.3 MGLY + #-0.725 XC
MVO3	4.58e-18	7.51e-16	3.02		MVK + O3 = #.064 HO2. + #.05 RO2-R. + #.164 HO. + #.05 RCO-O2. + #.475 CO + #.124 CO2 + #.1 HCHO + #.95 MGLY + #.351 HCOOH + #-0.05 XC
MVN3	(Slow)				MVK + NO3 = #4 XC + XN
MVOP	4.32e-12	4.32e-12			MVK + O3P = #.45 RCHO + #.55 MEK + #.45 XC
MVHV	Phot Set= ACROLEIN, qy= 2.1e-3				MVK + HV = #.3 C-O2. + #.7 CO + #.7 PROD2 + #.3 MA-RCO3. + #-2.4 XC
IPOH	6.19e-11	6.19e-11			ISO-PROD + HO. = #.67 RO2-R. + #.041 RO2-N. + #.289 MA-RCO3. + #.336 CO + #.055 HCHO + #.129 CCHO + #.013 RCHO + #.15 MEK + #.332 PROD2 + #.15 GLY + #.174 MGLY + #-0.504 XC
IPO3	4.18e-18	4.18e-18			ISO-PROD + O3 = #.4 HO2. + #.048 RO2-R. + #.048 RCO-O2. + #.285 HO. + #.498 CO + #.14 CO2 + #.125 HCHO + #.047 CCHO + #.21 MEK + #.023 GLY + #.742 MGLY + #.1 HCOOH + #.372 RCO-OH + #-.33 XC

Table A-2 (continued)

Label	Rate Parameters [a] k(298)	A	Ea	B	Reaction and Products [b]
IPN3	1.00e-13	1.00e-13			ISO-PROD + NO3 = #.799 RO2-R. + #.051 RO2-N. + #.15 MA-RCO3. + #.572 CO + #.15 HNO3 + #.227 HCHO + #.218 RCHO + #.008 MGLY + #.572 RNO3 + #.28 XN + #-.815 XC
IPHV	Phot Set= ACROLEIN, qy= 4.1e-3				ISO-PROD + HV = #1.233 HO2. + #.467 CCO-O2. + #.3 RCO-O2. + #1.233 CO + #.3 HCHO + #.467 CCHO + #.233 MEK + #-.233 XC
Lumped Parameter Organic Products					
K6OH	1.50e-11	1.50e-11			PROD2 + HO. = #.379 HO2. + #.473 RO2-R. + #.07 RO2-N. + #.029 CCO-O2. + #.049 RCO-O2. + #.213 HCHO + #.084 CCHO + #.558 RCHO + #.115 MEK + #.329 PROD2 + #.886 XC
K6HV	Phot Set= KETONE, qy= 2.0e-2				PROD2 + HV = #.96 RO2-R. + #.04 RO2-N. + #.515 R2O2. + #.667 CCO-O2. + #.333 RCO-O2. + #.506 HCHO + #.246 CCHO + #.71 RCHO + #.299 XC
RNOH	7.80e-12	7.80e-12			RNO3 + HO. = #.338 NO2 + #.113 HO2. + #.376 RO2-R. + #.173 RO2-N. + #.596 R2O2. + #.01 HCHO + #.439 CCHO + #.213 RCHO + #.006 ACET + #.177 MEK + #.048 PROD2 + #.31 RNO3 + #.351 XN + #.56 XC
RNHV	Phot Set= IC3ONO2				RNO3 + HV = NO2 + #.341 HO2. + #.564 RO2-R. + #.095 RO2-N. + #.152 R2O2. + #.134 HCHO + #.431 CCHO + #.147 RCHO + #.02 ACET + #.243 MEK + #.435 PROD2 + #.35 XC
Uncharacterized Reactive Aromatic Ring Fragmentation Products					
D1OH	5.00e-11	5.00e-11			DCB1 + HO. = RCHO + RO2-R. + CO
D1HV		(Slow)			DCB1 + HV = HO2. + #2 CO + RO2-R. + GLY + R2O2.
D1O3	2.00e-18	2.00e-18			DCB1 + O3 = #1.5 HO2. + #.5 HO. + #1.5 CO + #.5 CO2 + GLY
D2OH	5.00e-11	5.00e-11			DCB2 + HO. = R2O2. + RCHO + CCO-O2.
D2HV	Phot Set= MGLY_ABS, qy= 3.7e-1				DCB2 + HV = RO2-R. + #.5 {CCO-O2. + HO2.} + CO + R2O2. + #.5 {GLY + MGLY + XC}
D3OH	5.00e-11	5.00e-11			DCB3 + HO. = R2O2. + RCHO + CCO-O2.
D3HV	Phot Set= ACROLEIN, qy= 7.3e+0				DCB3 + HV = RO2-R. + #.5 {CCO-O2. + HO2.} + CO + R2O2. + #.5 {GLY + MGLY + XC}
Base ROG VOCs Used in the Chamber Simulations and Explicit VOCs in the Ambient Simulations					
c1OH	6.37e-15	2.15e-12	3.45		CH4 + HO. = H2O + C-O2.
c2OH	2.54e-13	1.37e-12	0.99	2.0	ETHANE + HO. = RO2-R. + CCHO
c4OH	2.44e-12	1.52e-12	-0.29	2.0	N-C4 + HO. = #.921 RO2-R. + #.079 RO2-N. + #.413 R2O2. + #.632 CCHO + #.12 RCHO + #.485 MEK + #-0.038 XC
c6OH	5.47e-12	1.38e-12	-0.82	2.0	N-C6 + HO. = #.775 RO2-R. + #.225 RO2-N. + #.787 R2O2. + #.011 CCHO + #.113 RCHO + #.688 PROD2 + #.162 XC
c8OH	8.70e-12	2.48e-12	-0.75	2.0	N-C8 + HO. = #.646 RO2-R. + #.354 RO2-N. + #.786 R2O2. + #.024 RCHO + #.622 PROD2 + #2.073 XC
etOH	8.52e-12	1.96e-12	-0.87		ETHENE + HO. = RO2-R. + #1.61 HCHO + #.195 CCHO
etO3	1.59e-18	9.14e-15	5.13		ETHENE + O3 = #.12 HO. + #.12 HO2. + #.5 CO + #.13 CO2 + HCHO + #.37 HCOOH
etN3	2.05e-16	4.39e-13	4.53	2.0	ETHENE + NO3 = RO2-R. + RCHO + #-1 XC + XN
etOA	7.29e-13	1.04e-11	1.57		ETHENE + O3P = #.5 HO2. + #.2 RO2-R. + #.3 C-O2. + #.491 CO + #.191 HCHO + #.25 CCHO + #.009 GLY + #.5 XC
prOH	2.63e-11	4.85e-12	-1.00		PROPENE + HO. = #.984 RO2-R. + #.016 RO2-N. + #.984 HCHO + #.984 CCHO + #-0.048 XC

Table A-2 (continued)

Label	Rate Parameters [a] k(298)	A	Ea	B	Reaction and Products [b]
prO3	1.01e-17	5.51e-15	3.73		PROPENE + O3 = #.32 HO. + #.06 HO2. + #.26 C-O2. + #.51 CO + #.135 CO2 + #.5 HCHO + #.5 CCHO + #.185 HCOOH + #.17 CCO-OH + #.07 INERT + #.07 XC
prN3	9.49e-15	4.59e-13	2.30		PROPENE + NO3 = #.949 RO2-R. + #.051 RO2-N. + #2.693 XC + XN
prOP	3.98e-12	1.18e-11	0.64		PROPENE + O3P = #.45 RCHO + #.55 MEK + #-0.55 XC
t2OH	6.40e-11	1.01e-11	-1.09		T-2-BUTE + HO. = #.965 RO2-R. + #.035 RO2-N. + #1.93 CCHO + #-0.07 XC
t2O3	1.90e-16	6.64e-15	2.10		T-2-BUTE + O3 = #.52 HO. + #.52 C-O2. + #.52 CO + #.14 CO2 + CCHO + #.34 CCO-OH + #.14 INERT + #.14 XC
t2N3	3.91e-13	1.10e-13	-0.76	2.0	T-2-BUTE + NO3 = #.705 NO2 + #.215 RO2-R. + #.08 RO2-N. + #.705 R2O2. + #1.41 CCHO + #.215 RNO3 + #-0.59 XC + #.08 XN
t2OP	2.18e-11	2.18e-11			T-2-BUTE + O3P = MEK
isOH	9.82e-11	2.50e-11	-0.81		ISOPRENE + HO. = #.907 RO2-R. + #.093 RO2-N. + #.079 R2O2. + #.624 HCHO + #.23 METHACRO + #.32 MVK + #.357 ISO-PROD + #-0.167 XC
isO3	1.28e-17	7.86e-15	3.80		ISOPRENE + O3 = #.266 HO. + #.066 RO2-R. + #.008 RO2-N. + #.126 R2O2. + #.192 MA-RCO3. + #.275 CO + #.122 CO2 + #.592 HCHO + #.1 PROD2 + #.39 METHACRO + #.16 MVK + #.204 HCOOH + #.15 RCO-OH + #-0.259 XC
isN3	6.74e-13	3.03e-12	0.89		ISOPRENE + NO3 = #.187 NO2 + #.749 RO2-R. + #.064 RO2-N. + #.187 R2O2. + #.936 ISO-PROD + #-0.064 XC + #.813 XN
isOP	3.60e-11	3.60e-11			ISOPRENE + O3P = #.01 RO2-N. + #.24 R2O2. + #.25 C-O2. + #.24 MA-RCO3. + #.24 HCHO + #.75 PROD2 + #-1.01 XC
tlOH	5.95e-12	1.81e-12	-0.71	0.0	TOLUENE + HO. = #.234 HO2. + #.758 RO2-R. + #.008 RO2-N. + #.116 GLY + #.135 MGLY + #.234 CRES + #.085 BALD + #.46 DCB1 + #.156 DCB2 + #.057 DCB3 + #1.178 XC
mxOH	2.36e-11	2.36e-11	0.00	0.0	M-XYLENE + HO. = #.21 HO2. + #.782 RO2-R. + #.008 RO2-N. + #.107 GLY + #.335 MGLY + #.21 CRES + #.037 BALD + #.347 DCB1 + #.29 DCB2 + #.108 DCB3 + #1.628 XC
<u>Lumped Organic Species used in the Ambient Reactivity Simulations</u>					
t1OH	8.27e-11	1.83e-11	-0.89		TERP + HO. = #.75 RO2-R. + #.25 RO2-N. + #.5 R2O2. + #.276 HCHO + #.474 RCHO + #.276 PROD2 + #5.146 XC
t1O3	6.88e-17	1.08e-15	1.63		TERP + O3 = #.567 HO. + #.033 HO2. + #.031 RO2-R. + #.18 RO2-N. + #.729 R2O2. + #.123 CCO-O2. + #.201 RCO-O2. + #.157 CO + #.037 CO2 + #.235 HCHO + #.205 RCHO + #.13 ACET + #.276 PROD2 + #.001 GLY + #.031 BACL + #.103 HCOOH + #.189 RCO-OH + #4.183 XC
t1N3	6.57e-12	3.66e-12	-0.35		TERP + NO3 = #.474 NO2 + #.276 RO2-R. + #.25 RO2-N. + #.75 R2O2. + #.474 RCHO + #.276 RNO3 + #5.421 XC + #.25 XN
t1OP	3.27e-11	3.27e-11			TERP + O3P = #.147 RCHO + #.853 PROD2 + #4.441 XC
a1OH	2.54e-13	1.37e-12	0.99	2.0	ALK1 + HO. = RO2-R. + CCHO
a2OH	1.04e-12	9.87e-12	1.33		ALK2 + HO. = #.246 HO. + #.121 HO2. + #.612 RO2-R. + #.021 RO2-N. + #.16 CO + #.039 HCHO + #.155 RCHO + #.417 ACET + #.248 GLY + #.121 HCOOH + #0.338 XC
a3OH	2.38e-12	1.02e-11	0.86		ALK3 + HO. = #.695 RO2-R. + #.07 RO2-N. + #.559 R2O2. + #.236 TBU-O. + #.026 HCHO + #.445 CCHO + #.122 RCHO + #.024 ACET + #.332 MEK + #-0.05 XC

Table A-2 (continued)

Label	Rate Parameters [a] k(298)	A	Ea	B	Reaction and Products [b]
a4OH	4.39e-12	5.95e-12	0.18		ALK4 + HO. = #.835 RO2-R. + #.143 RO2-N. + #.936 R2O2. + #.011 C-O2. + #.011 CCO-O2. + #.002 CO + #.024 HCHO + #.455 CCHO + #.244 RCHO + #.452 ACET + #.11 MEK + #.125 PROD2 + #-0.105 XC
a5OH	9.34e-12	1.11e-11	0.10		ALK5 + HO. = #.653 RO2-R. + #.347 RO2-N. + #.948 R2O2. + #.026 HCHO + #.099 CCHO + #.204 RCHO + #.072 ACET + #.089 MEK + #.417 PROD2 + #2.008 XC
b1OH	5.95e-12	1.81e-12	-0.71		ARO1 + HO. = #.224 HO2. + #.765 RO2-R. + #.011 RO2-N. + #.055 PROD2 + #.118 GLY + #.119 MGLY + #.017 PHEN + #.207 CRES + #.059 BALD + #.491 DCB1 + #.108 DCB2 + #.051 DCB3 + #1.288 XC
b2OH	2.64e-11	2.64e-11	0.00		ARO2 + HO. = #.187 HO2. + #.804 RO2-R. + #.009 RO2-N. + #.097 GLY + #.287 MGLY + #.087 BACL + #.187 CRES + #.05 BALD + #.561 DCB1 + #.099 DCB2 + #.093 DCB3 + #1.68 XC
o1OH	3.23e-11	7.10e-12	-0.90		OLE1 + HO. = #.91 RO2-R. + #.09 RO2-N. + #.205 R2O2. + #.732 HCHO + #.294 CCHO + #.497 RCHO + #.005 ACET + #.119 PROD2 + #.92 XC
o1O3	1.06e-17	2.62e-15	3.26		OLE1 + O3 = #.155 HO. + #.056 HO2. + #.022 RO2-R. + #.001 RO2-N. + #.076 C-O2. + #.345 CO + #.086 CO2 + #.5 HCHO + #.154 CCHO + #.363 RCHO + #.001 ACET + #.215 PROD2 + #.185 HCOOH + #.05 CCO-OH + #.119 RCO-OH + #.654 XC
o1N3	1.26e-14	4.45e-14	0.75		OLE1 + NO3 = #.824 RO2-R. + #.176 RO2-N. + #.488 R2O2. + #.009 CCHO + #.037 RCHO + #.024 ACET + #.511 RNO3 + #.677 XC + #.489 XN
o1OP	4.90e-12	1.07e-11	0.47		OLE1 + O3P = #.45 RCHO + #.437 MEK + #.113 PROD2 + #1.224 XC
o2OH	6.33e-11	1.74e-11	-0.76		OLE2 + HO. = #.918 RO2-R. + #.082 RO2-N. + #.001 R2O2. + #.244 HCHO + #.732 CCHO + #.511 RCHO + #.127 ACET + #.072 MEK + #.061 BALD + #.025 METHACRO + #.025 ISO-PROD + #-.054 XC
o2O3	1.07e-16	5.02e-16	0.92		OLE2 + O3 = #.378 HO. + #.003 HO2. + #.033 RO2-R. + #.002 RO2-N. + #.137 R2O2. + #.197 C-O2. + #.137 CCO-O2. + #.006 RCO-O2. + #.265 CO + #.07 CO2 + #.269 HCHO + #.456 CCHO + #.305 RCHO + #.045 ACET + #.026 MEK + #.006 PROD2 + #.042 BALD + #.026 METHACRO + #.073 HCOOH + #.129 CCO-OH + #.303 RCO-OH + #.155 XC
o2N3	7.27e-13	7.27e-13	0.00		OLE2 + NO3 = #.391 NO2 + #.442 RO2-R. + #.136 RO2-N. + #.711 R2O2. + #.03 C-O2. + #.079 HCHO + #.507 CCHO + #.151 RCHO + #.102 ACET + #.001 MEK + #.015 BALD + #.048 MVK + #.321 RNO3 + #.075 XC + #.288 XN
o2OP	2.09e-11	2.09e-11			OLE2 + O3P = #.013 HO2. + #.012 RO2-R. + #.001 RO2-N. + #.012 CO + #.069 RCHO + #.659 MEK + #.259 PROD2 + #.012 METHACRO + #.537 XC
Test Compounds Used in this Study					
	1.28e-11	1.28e-11			2-ME-C9 + HO. = #.551 RO2-R. + #.449 RO2-N. + #.895 R2O2. + #.035 RCHO + #.012 ACET + #.516 PROD2 + #4.066 XC

Table A-2 (continued)

Label	Rate Parameters [a] k(298)	A	Ea	B	Reaction and Products [b]
	1.28e-11	1.28e-11			26DM-C9 + HO. = #.533 RO2-R. + #.467 RO2-N. + #1.036 R2O2. + #.001 CCHO + #.221 RCHO + #.12 ACET + #.006 MEK + #.376 PROD2 + #4.888 XC
	7.40e-12	7.40e-12			34-DE-C6 + HO. = #.619 RO2-R. + #.381 RO2-N. + #1.105 R2O2. + #.007 HCHO + #.337 CCHO + #.319 RCHO + #.709 MEK + #.126 PROD2 + #2.483 XC
Normal Alkane Mineral Spirits Constituents					
	8.70e-12	2.48e-12	-0.75	2.0	N-C8 + HO. = #.646 RO2-R. + #.354 RO2-N. + #.786 R2O2. + #.024 RCHO + #.622 PROD2 + #2.073 XC
	9.99e-12	2.26e-12	-0.89	2.0	N-C9 + HO. = #.602 RO2-R. + #.398 RO2-N. + #.777 R2O2. + #.018 RCHO + #.584 PROD2 + #3.055 XC
	1.12e-11	2.82e-12	-0.83	2.0	N-C10 + HO. = #.572 RO2-R. + #.428 RO2-N. + #.772 R2O2. + #.015 RCHO + #.557 PROD2 + #4.045 XC
	1.29e-11	1.29e-11			N-C11 + HO. = #.553 RO2-R. + #.447 RO2-N. + #.771 R2O2. + #.013 RCHO + #.54 PROD2 + #5.038 XC
	1.39e-11	1.39e-11			N-C12 + HO. = #.542 RO2-R. + #.458 RO2-N. + #.768 R2O2. + #.011 RCHO + #6.034 XC + #.53 PROD2
	1.80e-11	1.80e-11			N-C14 + HO. = #.53 RO2-R. + #.47 RO2-N. + #.765 R2O2. + #.009 RCHO + #8.027 XC + #.521 PROD2
	2.10e-11	2.10e-11			N-C15 + HO. = #.527 RO2-R. + #.473 RO2-N. + #.764 R2O2. + #.008 RCHO + #9.025 XC + #.519 PROD2
Bramched Alkane Mineral Spirits Constituents (other than the test compounds used in this study)					
	8.57e-12	8.57e-12			24-DM-C6 + HO. = #.652 RO2-R. + #.348 RO2-N. + #1.346 R2O2. + #.159 HCHO + #.335 CCHO + #.306 RCHO + #.096 ACET + #.156 MEK + #.293 PROD2 + #1.492 XC
	8.59e-12	8.59e-12			4-ME-C7 + HO. = #.676 RO2-R. + #.324 RO2-N. + #.875 R2O2. + #.002 HCHO + #.004 CCHO + #.377 RCHO + #.115 MEK + #.376 PROD2 + #2.201 XC
	8.31e-12	8.31e-12			2-ME-C7 + HO. = #.659 RO2-R. + #.341 RO2-N. + #.882 R2O2. + #.016 HCHO + #.025 CCHO + #.155 RCHO + #.024 ACET + #.546 PROD2 + #2.077 XC
	9.99e-12	9.99e-12			24-DM-C7 + HO. = #.598 RO2-R. + #.402 RO2-N. + #1.176 R2O2. + #.104 HCHO + #.013 CCHO + #.41 RCHO + #.049 ACET + #.073 MEK + #.381 PROD2 + #2.501 XC
	9.70e-12	9.70e-12			4-ME-C8 + HO. = #.605 RO2-R. + #.395 RO2-N. + #.89 R2O2. + #.001 HCHO + #.034 CCHO + #.127 RCHO + #.006 MEK + #.562 PROD2 + #2.788 XC
	1.01e-11	1.01e-11			2-ME-C8 + HO. = #.587 RO2-R. + #.413 RO2-N. + #.914 R2O2. + #.002 HCHO + #.064 RCHO + #.014 ACET + #.536 PROD2 + #3.072 XC
	1.29e-11	1.29e-11			26DM-C8 + HO. = #.567 RO2-R. + #.433 RO2-N. + #1.096 R2O2. + #.108 CCHO + #.308 RCHO + #.145 ACET + #.071 MEK + #.276 PROD2 + #3.887 XC
	1.14e-11	1.14e-11			4-ME-C9 + HO. = #.572 RO2-R. + #.428 RO2-N. + #.876 R2O2. + #.001 HCHO + #.019 CCHO + #.14 RCHO + #.004 MEK + #.52 PROD2 + #3.831 XC
	1.29e-11	1.29e-11			4-ME-C10 + HO. = #.531 RO2-R. + #.469 RO2-N. + #.907 R2O2. + #.001 CCHO + #.08 RCHO + #.003 MEK + #.5 PROD2 + #4.932 XC

Table A-2 (continued)

Label	Rate Parameters [a] k(298)	A	Ea	B	Reaction and Products [b]
	1.29e-11	1.29e-11			3-ME-C10 + HO. = #.526 RO2-R. + #.474 RO2-N. + #.917 R2O2. + #.029 CCHO + #.038 RCHO + #.012 MEK + #.489 PROD2 + #4.998 XC
	1.45e-11	1.45e-11			36DM-C10 + HO. = #.494 RO2-R. + #.506 RO2-N. + #1.079 R2O2. + #.001 HCHO + #.088 CCHO + #.11 RCHO + #.055 MEK + #.458 PROD2 + #5.488 XC
	1.43e-11	1.43e-11			5-ME-C11 + HO. = #.524 RO2-R. + #.476 RO2-N. + #.867 R2O2. + #.01 CCHO + #.059 RCHO + #.504 PROD2 + #5.923 XC
	1.43e-11	1.43e-11			3-ME-C11 + HO. = #.516 RO2-R. + #.484 RO2-N. + #.896 R2O2. + #.025 CCHO + #.033 RCHO + #.011 MEK + #.484 PROD2 + #5.997 XC
	1.60e-11	1.60e-11			36DM-C11 + HO. = #.488 RO2-R. + #.512 RO2-N. + #1.046 R2O2. + #.001 HCHO + #.07 CCHO + #.124 RCHO + #.046 MEK + #.442 PROD2 + #6.579 XC
	1.57e-11	1.57e-11			5-ME-C12 + HO. = #.514 RO2-R. + #.486 RO2-N. + #.863 R2O2. + #.009 CCHO + #.044 RCHO + #.498 PROD2 + #6.942 XC
	1.57e-11	1.57e-11			3-ME-C12 + HO. = #.51 RO2-R. + #.49 RO2-N. + #.88 R2O2. + #.023 CCHO + #.03 RCHO + #.009 MEK + #.482 PROD2 + #6.997 XC
	1.74e-11	1.74e-11			37DM-C12 + HO. = #.496 RO2-R. + #.504 RO2-N. + #.98 R2O2. + #.055 CCHO + #.11 RCHO + #.03 MEK + #.44 PROD2 + #7.772 XC
	1.71e-11	1.71e-11			6-ME-C13 + HO. = #.512 RO2-R. + #.488 RO2-N. + #.852 R2O2. + #.006 CCHO + #.041 RCHO + #.504 PROD2 + #7.909 XC
	1.71e-11	1.71e-11			3-ME-C13 + HO. = #.506 RO2-R. + #.494 RO2-N. + #.871 R2O2. + #.021 CCHO + #.015 RCHO + #.009 MEK + #.493 PROD2 + #7.958 XC
	1.88e-11	1.88e-11			37DM-C13 + HO. = #.487 RO2-R. + #.513 RO2-N. + #.98 R2O2. + #.045 CCHO + #.087 RCHO + #.028 MEK + #.44 PROD2 + #8.82 XC
	1.85e-11	1.85e-11			6-ME-C14 + HO. = #.51 RO2-R. + #.49 RO2-N. + #.843 R2O2. + #.006 CCHO + #.037 RCHO + #.503 PROD2 + #8.918 XC
	1.85e-11	1.85e-11			3-ME-C14 + HO. = #.505 RO2-R. + #.495 RO2-N. + #.861 R2O2. + #.02 CCHO + #.013 RCHO + #.008 MEK + #.493 PROD2 + #8.961 XC
Cyclic Alkane Mineral Spirits Constituents					
	1.20e-11	1.20e-11			ET-CYCC6 + HO. = #.624 RO2-R. + #.376 RO2-N. + #1.046 R2O2. + #.002 HCHO + #.151 CCHO + #.328 RCHO + #.299 PROD2 + #2.662 XC
	1.34e-11	1.34e-11			C3-CYCC6 + HO. = #.61 RO2-R. + #.389 RO2-N. + #.864 R2O2. + #.001 RCO-O2. + #.001 HCHO + #.363 RCHO + #.388 PROD2 + #3.242 XC
	1.37e-11	1.37e-11			1E4MCYC6 + HO. = #.518 RO2-R. + #.481 RO2-N. + #1.339 R2O2. + #.001 CCO-O2. + #.033 HCHO + #.142 CCHO + #.411 RCHO + #.143 PROD2 + #3.703 XC
	1.49e-11	1.49e-11			C4-CYCC6 + HO. = #.576 RO2-R. + #.423 RO2-N. + #.827 R2O2. + #.024 CCHO + #.179 RCHO + #.467 PROD2 + #4.07 XC

Table A-2 (continued)

Label	Rate Parameters [a]				Reaction and Products [b]
	k(298)	A	Ea	B	
	1.51e-11	1.51e-11			1M3IPCY6 + HO. = #.535 RO2-R. + #.46 RO2-N. + #1.204 R2O2. + #.004 RCO-O2. + #.006 CO + #.008 HCHO + #.005 CCHO + #.263 RCHO + #.339 ACET + #.293 PROD2 + #3.634 XC
	1.55e-11	1.55e-11			14DECYC6 + HO. = #.508 RO2-R. + #.49 RO2-N. + #1.229 R2O2. + #.002 RCO-O2. + #.021 HCHO + #.226 CCHO + #.333 RCHO + #.209 PROD2 + #4.328 XC
	1.63e-11	1.63e-11			C5-CYCC6 + HO. = #.557 RO2-R. + #.443 RO2-N. + #.808 R2O2. + #.016 CCHO + #.147 RCHO + #.456 PROD2 + #5.135 XC
	1.72e-11	1.72e-11			13E5MCC6 + HO. = #.429 RO2-R. + #.566 RO2-N. + #1.371 R2O2. + #.003 CCO-O2. + #.002 RCO-O2. + #.006 CO + #.02 HCHO + #.168 CCHO + #.355 RCHO + #.009 MEK + #.09 PROD2 + #5.587 XC
	1.70e-11	1.70e-11			1E2PCYC6 + HO. = #.461 RO2-R. + #.539 RO2-N. + #1.199 R2O2. + #.001 RCO-O2. + #.007 HCHO + #.031 CCHO + #.186 RCHO + #.349 PROD2 + #5.045 XC
	1.78e-11	1.78e-11			C6-CYCC6 + HO. = #.527 RO2-R. + #.473 RO2-N. + #.849 R2O2. + #.093 RCHO + #.461 PROD2 + #6.118 XC
	1.90e-11	1.90e-11			135ECYC6 + HO. = #.417 RO2-R. + #.58 RO2-N. + #1.353 R2O2. + #.003 RCO-O2. + #.005 CO + #.014 HCHO + #.221 CCHO + #.315 RCHO + #.008 MEK + #.116 PROD2 + #6.373 XC
	1.80e-11	1.80e-11			1M4C5CY6 + HO. = #.482 RO2-R. + #.518 RO2-N. + #1.049 R2O2. + #.001 CCO-O2. + #.001 HCHO + #.015 CCHO + #.21 RCHO + #.326 PROD2 + #6.274 XC
	1.91e-11	1.91e-11			C7-CYCC6 + HO. = #.515 RO2-R. + #.485 RO2-N. + #.855 R2O2. + #.069 RCHO + #.462 PROD2 + #7.108 XC
	2.05e-11	2.05e-11			13E5PCC6 + HO. = #.433 RO2-R. + #.564 RO2-N. + #1.237 R2O2. + #.003 RCO-O2. + #.002 CO + #.01 HCHO + #.132 CCHO + #.342 RCHO + #.002 MEK + #.188 PROD2 + #7.163 XC
	1.94e-11	1.94e-11			1M2C6CC6 + HO. = #.462 RO2-R. + #.537 RO2-N. + #1.08 R2O2. + #.001 RCO-O2. + #.004 HCHO + #.009 CCHO + #.128 RCHO + #.38 PROD2 + #7.092 XC
	2.05e-11	2.05e-11			C8-CYCC6 + HO. = #.511 RO2-R. + #.489 RO2-N. + #.847 R2O2. + #.063 RCHO + #.463 PROD2 + #8.099 XC
	2.19e-11	2.19e-11			13P5ECC6 + HO. = #.445 RO2-R. + #.553 RO2-N. + #1.158 R2O2. + #.002 RCO-O2. + #.001 CO + #.007 HCHO + #.06 CCHO + #.376 RCHO + #.234 PROD2 + #8.017 XC
	2.08e-11	2.08e-11			1M4C7CC6 + HO. = #.455 RO2-R. + #.544 RO2-N. + #1.059 R2O2. + #.001 HCHO + #.131 RCHO + #.349 PROD2 + #8.242 XC
	2.20e-11	2.20e-11			C9-CYCC6 + HO. = #.509 RO2-R. + #.49 RO2-N. + #.838 R2O2. + #.058 RCHO + #.465 PROD2 + #9.091 XC
	2.33e-11	2.33e-11			135PCYC6 + HO. = #.453 RO2-R. + #.545 RO2-N. + #1.106 R2O2. + #.002 RCO-O2. + #.001 CO + #.005 HCHO + #.415 RCHO + #.258 PROD2 + #8.923 XC
	2.22e-11	2.22e-11			1M2C8CC6 + HO. = #.462 RO2-R. + #.538 RO2-N. + #1.035 R2O2. + #.003 HCHO + #.008 CCHO + #.105 RCHO + #.394 PROD2 + #9.08 XC

Table A-2 (continued)

Label	Rate Parameters [a] k(298)	A	Ea	B	Reaction and Products [b]
Lumped Aromatic or Alkene Constituents of Sample "A" [c]					
	3.10e-11	3.10e-11			MS-A-ARO + HO. = 0.189 HO2. + 0.783 RO2-R. + 0.012 RO2-N. + 0.016 RCO-O2. + 0.011 PROD2 + 0.072 GLY + 0.308 MGLY + 0.107 BACL + 0.008 PHEN + 0.181 CRES + 0.042 BALD + 0.565 DCB1 + 0.074 DCB2 + 0.09 DCB3 + 2.318 XC
	3.80e-11	3.80e-11			MS-A-OLE + HO. = 0.681 RO2-R. + 0.319 RO2-N. + 0.324 R2O2. + 0.309 HCHO + 0.656 RCHO + 0.174 PROD2
	3.10e-17	3.10e-17			MS-A-OLE + O3 = 0.054 HO. + 0.048 HO2. + 0.006 RO2-R. + 0.003 R2O2. + 0.206 CO + 0.052 CO2 + 0.4 HCHO + 0.606 RCHO + 0.563 PROD2 + 0.148 HCOOH + 0.031 RCO-OH
	8.49e-14	8.49e-14			MS-A-OLE + NO3 = 0.556 RO2-R. + 0.443 RO2-N. + 0.777 R2O2. + 0.001 RCHO + 0.556 RNO3 + 0.443 XN
	8.58e-12	8.58e-12			MS-A-OLE + O3P = 0.36 RCHO + 0.64 PROD2

[a] Except as indicated, the rate constants are given by $k(T) = A \cdot (T/300)^{B} \cdot e^{-Ea/RT}$, where the units of k and A are cm^3 $molec^{-1}$ s^{-1}, Ea are kcal mol^{-1}, T is ^oK, and R=0.0019872 kcal mol^{-1} deg^{-1}. The following special rate constant expressions are used: Phot Set = *name*: The absorption cross sections and quantum yields for the photolysis reaction are given in Table A-3, where "*name*" indicates the photolysis set used. If a "qy=*number*" notation is given, the number given is the overall quantum yield, which is assumed to be wavelength independent. Falloff: The rate constant as a function of temperature and pressure is calculated using $k(T,M) = \{k0(T)\cdot[M]/[1 + k0(T)\cdot[M]/kinf(T)]\}\cdot F^{Z}$, where $Z = \{1 + [\log_{10}\{k0(T)\cdot[M])/kinf(T)\}]^2\}^{-1}$, [M] is the total pressure in molecules cm^{-3}, F is as indicated on the table, and the temperature dependences of k0 and kinf are as indicated on the table. (Slow): The reaction is assumed to be negligible and is not included in the mechanism. It is shown on the listing for documentation purposes only. k = k0+k3M(1+k3M/k2): The rate constant as a function of temperature and pressure is calculated using $k(T,M) = k0(T) + k3(T)\cdot[M] \cdot(1 + k3(T)\cdot[M]/k2(T))$, where [M] is the total bath gas (air) concentration in molecules cm^{-3}, and the temperature dependences for k0, k2 and k3 are as indicated on the table. k = k1 + k2 [M]: The rate constant as a function of temperature and pressure is calculated using $k(T,M) = k1(T) + k2(T)\cdot[M]$, where [M] is the total bath gas (air) concentration in molecules cm^{-3}, and the temperature dependences for k1, and k2 are as indicated on the table. Same k as Rxn *label*: The rate constant is the same as the reaction with the indicated label.

[b] Format of reaction listing: "=" separates reactants from products; "*#number*" indicates stoichiometric coefficient, "*#coefficient { product list }*" means that the stoichiometric coefficient is applied to all the products listed. See Table A-1 for a listing of the model species used.

[c] Parameters derived from weighed averages of all the aromatic or alkene constituents of Sample "A", as indicated on Table 5.

Table A-3. Listing of the absorption cross-sections and quantum yields for the photolysis reactions.

WL (nm)	Abs (cm^2)	QY	WL (nm)	Abs (cm^2)	QY	WL (nm)	Abs (cm^2)	QY	WL (nm)	Abs (cm^2)	QY	WL (nm)	Abs (cm^2)	QY
							NO2							
205.0	4.31e-19	1.000	210.0	4.72e-19	1.000	215.0	4.95e-19	1.000	220.0	4.56e-19	1.000	225.0	3.79e-19	1.000
230.0	2.74e-19	1.000	235.0	1.67e-19	1.000	240.0	9.31e-20	1.000	245.0	4.74e-20	1.000	250.0	2.48e-20	1.000
255.0	1.95e-20	1.000	260.0	2.24e-20	1.000	265.0	2.73e-20	1.000	270.0	4.11e-20	1.000	275.0	4.90e-20	1.000
280.0	5.92e-20	1.000	285.0	7.39e-20	1.000	290.0	9.00e-20	1.000	295.0	1.09e-19	1.000	300.0	1.31e-19	1.000
305.0	1.57e-19	1.000	310.0	1.86e-19	1.000	315.0	2.15e-19	0.990	320.0	2.48e-19	0.990	325.0	2.81e-19	0.990
330.0	3.13e-19	0.990	335.0	3.43e-19	0.990	340.0	3.80e-19	0.990	345.0	4.07e-19	0.990	350.0	4.31e-19	0.990
355.0	4.72e-19	0.990	360.0	4.83e-19	0.980	365.0	5.17e-19	0.980	370.0	5.32e-19	0.980	375.0	5.51e-19	0.980
380.0	5.64e-19	0.970	385.0	5.76e-19	0.970	390.0	5.93e-19	0.960	395.0	5.85e-19	0.935	400.0	6.02e-19	0.820
405.0	5.78e-19	0.355	410.0	6.00e-19	0.130	411.0	5.93e-19	0.110	412.0	5.86e-19	0.094	413.0	5.79e-19	0.083
414.0	5.72e-19	0.070	415.0	5.65e-19	0.059	416.0	5.68e-19	0.048	417.0	5.71e-19	0.039	418.0	5.75e-19	0.030
419.0	5.78e-19	0.023	420.0	5.81e-19	0.018	421.0	5.72e-19	0.012	422.0	5.64e-19	0.008	423.0	5.55e-19	0.004
424.0	5.47e-19	0.000												
							NO3NO							
585.0	2.89e-18	0.000	586.0	3.32e-18	0.050	587.0	4.16e-18	0.100	588.0	5.04e-18	0.150	589.0	6.13e-18	0.200
590.0	5.96e-18	0.250	591.0	5.44e-18	0.280	592.0	5.11e-18	0.310	593.0	4.58e-18	0.340	594.0	4.19e-18	0.370
595.0	4.29e-18	0.400	596.0	4.62e-18	0.370	597.0	4.36e-18	0.340	598.0	3.67e-18	0.310	599.0	3.10e-18	0.280
600.0	2.76e-18	0.250	601.0	2.86e-18	0.240	602.0	3.32e-18	0.230	603.0	3.80e-18	0.220	604.0	4.37e-18	0.210
605.0	4.36e-18	0.200	606.0	3.32e-18	0.200	607.0	2.40e-18	0.200	608.0	1.85e-18	0.200	609.0	1.71e-18	0.200
610.0	1.77e-18	0.200	611.0	1.91e-18	0.180	612.0	2.23e-18	0.160	613.0	2.63e-18	0.140	614.0	2.55e-18	0.120
615.0	2.26e-18	0.100	616.0	2.09e-18	0.100	617.0	2.11e-18	0.100	618.0	2.39e-18	0.100	619.0	2.56e-18	0.100
620.0	3.27e-18	0.100	621.0	5.24e-18	0.090	622.0	1.02e-17	0.080	623.0	1.47e-17	0.070	624.0	1.21e-17	0.060
625.0	8.38e-18	0.050	626.0	7.30e-18	0.050	627.0	7.53e-18	0.050	628.0	7.37e-18	0.050	629.0	6.98e-18	0.050
630.0	6.76e-18	0.050	631.0	4.84e-18	0.046	632.0	3.27e-18	0.042	633.0	2.17e-18	0.038	634.0	1.64e-18	0.034
635.0	1.44e-18	0.030	636.0	1.69e-18	0.024	637.0	2.07e-18	0.018	638.0	2.03e-18	0.012	639.0	1.58e-18	0.006
640.0	1.23e-18	0.000												
							NO3NO2							
400.0	0.00e+00	1.000	401.0	0.00e+00	1.000	402.0	0.00e+00	1.000	403.0	2.00e-20	1.000	404.0	0.00e+00	1.000
405.0	3.00e-20	1.000	406.0	2.00e-20	1.000	407.0	1.00e-20	1.000	408.0	3.00e-20	1.000	409.0	0.00e+00	1.000
410.0	1.00e-20	1.000	411.0	2.00e-20	1.000	412.0	5.00e-20	1.000	413.0	5.00e-20	1.000	414.0	2.00e-20	1.000
415.0	6.00e-20	1.000	416.0	6.00e-20	1.000	417.0	7.00e-20	1.000	418.0	5.00e-20	1.000	419.0	8.00e-20	1.000
420.0	8.00e-20	1.000	421.0	8.00e-20	1.000	422.0	9.00e-20	1.000	423.0	1.10e-19	1.000	424.0	9.00e-20	1.000
425.0	7.00e-20	1.000	426.0	1.40e-19	1.000	427.0	1.40e-19	1.000	428.0	1.20e-19	1.000	429.0	1.10e-19	1.000
430.0	1.70e-19	1.000	431.0	1.30e-19	1.000	432.0	1.50e-19	1.000	433.0	1.80e-19	1.000	434.0	1.80e-19	1.000
435.0	1.60e-19	1.000	436.0	1.50e-19	1.000	437.0	1.80e-19	1.000	438.0	2.10e-19	1.000	439.0	2.00e-19	1.000
440.0	1.90e-19	1.000	441.0	1.80e-19	1.000	442.0	2.10e-19	1.000	443.0	1.80e-19	1.000	444.0	1.90e-19	1.000
445.0	2.00e-19	1.000	446.0	2.40e-19	1.000	447.0	2.90e-19	1.000	448.0	2.40e-19	1.000	449.0	2.80e-19	1.000
450.0	2.90e-19	1.000	451.0	3.00e-19	1.000	452.0	3.30e-19	1.000	453.0	3.10e-19	1.000	454.0	3.60e-19	1.000
455.0	3.60e-19	1.000	456.0	3.60e-19	1.000	457.0	4.00e-19	1.000	458.0	3.70e-19	1.000	459.0	4.20e-19	1.000
460.0	4.00e-19	1.000	461.0	3.90e-19	1.000	462.0	4.00e-19	1.000	463.0	4.10e-19	1.000	464.0	4.80e-19	1.000
465.0	5.10e-19	1.000	466.0	5.40e-19	1.000	467.0	5.70e-19	1.000	468.0	5.60e-19	1.000	469.0	5.80e-19	1.000
470.0	5.90e-19	1.000	471.0	6.20e-19	1.000	472.0	6.40e-19	1.000	473.0	6.20e-19	1.000	474.0	6.20e-19	1.000
475.0	6.80e-19	1.000	476.0	7.80e-19	1.000	477.0	7.70e-19	1.000	478.0	7.30e-19	1.000	479.0	7.30e-19	1.000
480.0	7.00e-19	1.000	481.0	7.10e-19	1.000	482.0	7.10e-19	1.000	483.0	7.20e-19	1.000	484.0	7.70e-19	1.000
485.0	8.20e-19	1.000	486.0	9.10e-19	1.000	487.0	9.20e-19	1.000	488.0	9.50e-19	1.000	489.0	9.60e-19	1.000
490.0	1.03e-18	1.000	491.0	9.90e-19	1.000	492.0	9.90e-19	1.000	493.0	1.01e-18	1.000	494.0	1.01e-18	1.000
495.0	1.06e-18	1.000	496.0	1.21e-18	1.000	497.0	1.22e-18	1.000	498.0	1.20e-18	1.000	499.0	1.17e-18	1.000
500.0	1.13e-18	1.000	501.0	1.11e-18	1.000	502.0	1.11e-18	1.000	503.0	1.11e-18	1.000	504.0	1.26e-18	1.000
505.0	1.28e-18	1.000	506.0	1.34e-18	1.000	507.0	1.28e-18	1.000	508.0	1.27e-18	1.000	509.0	1.35e-18	1.000
510.0	1.51e-18	1.000	511.0	1.73e-18	1.000	512.0	1.77e-18	1.000	513.0	1.60e-18	1.000	514.0	1.58e-18	1.000
515.0	1.58e-18	1.000	516.0	1.56e-18	1.000	517.0	1.49e-18	1.000	518.0	1.44e-18	1.000	519.0	1.54e-18	1.000
520.0	1.68e-18	1.000	521.0	1.83e-18	1.000	522.0	1.93e-18	1.000	523.0	1.77e-18	1.000	524.0	1.64e-18	1.000
525.0	1.58e-18	1.000	526.0	1.63e-18	1.000	527.0	1.81e-18	1.000	528.0	2.10e-18	1.000	529.0	2.39e-18	1.000
530.0	2.23e-18	1.000	531.0	2.09e-18	1.000	532.0	2.02e-18	1.000	533.0	1.95e-18	1.000	534.0	2.04e-18	1.000
535.0	2.30e-18	1.000	536.0	2.57e-18	1.000	537.0	2.58e-18	1.000	538.0	2.34e-18	1.000	539.0	2.04e-18	1.000
540.0	2.10e-18	1.000	541.0	2.04e-18	1.000	542.0	1.88e-18	1.000	543.0	1.68e-18	1.000	544.0	1.70e-18	1.000
545.0	1.96e-18	1.000	546.0	2.42e-18	1.000	547.0	2.91e-18	1.000	548.0	2.98e-18	1.000	549.0	2.71e-18	1.000
550.0	2.48e-18	1.000	551.0	2.43e-18	1.000	552.0	2.47e-18	1.000	553.0	2.53e-18	1.000	554.0	2.78e-18	1.000
555.0	3.11e-18	1.000	556.0	3.26e-18	1.000	557.0	3.29e-18	1.000	558.0	3.51e-18	1.000	559.0	3.72e-18	1.000
560.0	3.32e-18	1.000	561.0	2.98e-18	1.000	562.0	2.90e-18	1.000	563.0	2.80e-18	1.000	564.0	2.72e-18	1.000
565.0	2.73e-18	1.000	566.0	2.85e-18	1.000	567.0	2.81e-18	1.000	568.0	2.85e-18	1.000	569.0	2.89e-18	1.000
570.0	2.79e-18	1.000	571.0	2.76e-18	1.000	572.0	2.74e-18	1.000	573.0	2.78e-18	1.000	574.0	2.86e-18	1.000
575.0	3.08e-18	1.000	576.0	3.27e-18	1.000	577.0	3.38e-18	1.000	578.0	3.31e-18	1.000	579.0	3.24e-18	1.000
580.0	3.34e-18	1.000	581.0	3.55e-18	1.000	582.0	3.28e-18	1.000	583.0	2.93e-18	1.000	584.0	2.82e-18	1.000
585.0	2.89e-18	1.000	586.0	3.32e-18	0.950	587.0	4.16e-18	0.900	588.0	5.04e-18	0.850	589.0	6.13e-18	0.800
590.0	5.96e-18	0.750	591.0	5.44e-18	0.720	592.0	5.11e-18	0.690	593.0	4.58e-18	0.660	594.0	4.19e-18	0.630
595.0	4.29e-18	0.600	596.0	4.62e-18	0.590	597.0	4.36e-18	0.580	598.0	3.67e-18	0.570	599.0	3.10e-18	0.560
600.0	2.76e-18	0.550	601.0	2.86e-18	0.540	602.0	3.32e-18	0.530	603.0	3.80e-18	0.520	604.0	4.37e-18	0.510
605.0	4.36e-18	0.400	606.0	3.32e-18	0.380	607.0	2.40e-18	0.360	608.0	1.85e-18	0.340	609.0	1.71e-18	0.320

Table A-3 (continued)

WL (nm)	Abs (cm^2)	QY	WL (nm)	Abs (cm^2)	QY	WL (nm)	Abs (cm^2)	QY	WL (nm)	Abs (cm^2)	QY	WL (nm)	Abs (cm^2)	QY
610.0	1.77e-18	0.300	611.0	1.91e-18	0.290	612.0	2.23e-18	0.280	613.0	2.63e-18	0.270	614.0	2.55e-18	0.260
615.0	2.26e-18	0.250	616.0	2.09e-18	0.240	617.0	2.11e-18	0.230	618.0	2.39e-18	0.220	619.0	2.56e-18	0.210
620.0	3.27e-18	0.200	621.0	5.24e-18	0.190	622.0	1.02e-17	0.180	623.0	1.47e-17	0.170	624.0	1.21e-17	0.160
625.0	8.38e-18	0.150	626.0	7.30e-18	0.130	627.0	7.53e-18	0.110	628.0	7.37e-18	0.090	629.0	6.98e-18	0.070
630.0	6.76e-18	0.050	631.0	4.84e-18	0.040	632.0	3.27e-18	0.030	633.0	2.17e-18	0.020	634.0	1.64e-18	0.010
635.0	1.44e-18	0.000												
							O3O3P							
280.0	3.94e-18	0.095	281.0	3.62e-18	0.093	282.0	3.31e-18	0.090	283.0	2.99e-18	0.088	284.0	2.70e-18	0.086
285.0	2.46e-18	0.084	286.0	2.22e-18	0.082	287.0	1.98e-18	0.079	288.0	1.75e-18	0.077	289.0	1.59e-18	0.075
290.0	1.42e-18	0.073	291.0	1.25e-18	0.070	292.0	1.09e-18	0.068	293.0	9.81e-19	0.066	294.0	8.73e-19	0.064
295.0	7.65e-19	0.061	296.0	6.58e-19	0.059	297.0	5.81e-19	0.057	298.0	5.18e-19	0.055	299.0	4.55e-19	0.052
300.0	3.92e-19	0.050	301.0	3.35e-19	0.035	302.0	3.01e-19	0.025	303.0	2.66e-19	0.015	304.0	2.32e-19	0.010
305.0	1.97e-19	0.020	306.0	1.73e-19	0.050	307.0	1.55e-19	0.123	308.0	1.37e-19	0.227	309.0	1.18e-19	0.333
310.0	9.98e-20	0.400	311.0	8.92e-20	0.612	312.0	7.94e-20	0.697	313.0	6.96e-20	0.738	314.0	5.99e-20	0.762
315.0	5.01e-20	0.765	316.0	4.51e-20	0.779	317.0	4.00e-20	0.791	318.0	3.50e-20	0.806	319.0	2.99e-20	0.822
320.0	2.49e-20	0.852	321.0	2.23e-20	0.879	322.0	1.97e-20	0.903	323.0	1.72e-20	0.908	324.0	1.46e-20	0.920
325.0	1.20e-20	0.930	326.0	1.08e-20	0.934	327.0	9.67e-21	0.938	328.0	8.50e-21	0.942	329.0	7.34e-21	0.946
330.0	6.17e-21	0.950	331.0	5.48e-21	0.950	332.0	4.80e-21	0.950	333.0	4.11e-21	0.950	334.0	3.43e-21	0.950
335.0	2.74e-21	0.950	336.0	2.43e-21	0.960	337.0	2.11e-21	0.970	338.0	1.80e-21	0.980	339.0	1.48e-21	0.990
340.0	1.17e-21	1.000	350.0	0.00e+00	1.000	400.0	0.00e+00	1.000	410.0	1.20e-23	1.000	420.0	2.20e-23	1.000
440.0	1.12e-22	1.000	460.0	3.28e-22	1.000	480.0	6.84e-22	1.000	500.0	1.22e-21	1.000	520.0	1.82e-21	1.000
540.0	2.91e-21	1.000	560.0	3.94e-21	1.000	580.0	4.59e-21	1.000	600.0	5.11e-21	1.000	620.0	4.00e-21	1.000
640.0	2.96e-21	1.000	660.0	2.09e-21	1.000	680.0	1.36e-21	1.000	700.0	9.10e-22	1.000	750.0	3.20e-22	1.000
800.0	1.60e-22	1.000	900.0	0.00e+00	1.000									
							O3O1D							
280.0	3.94e-18	0.905	281.0	3.62e-18	0.907	282.0	3.31e-18	0.910	283.0	2.99e-18	0.912	284.0	2.70e-18	0.914
285.0	2.46e-18	0.916	286.0	2.22e-18	0.918	287.0	1.98e-18	0.921	288.0	1.75e-18	0.923	289.0	1.59e-18	0.925
290.0	1.42e-18	0.927	291.0	1.25e-18	0.930	292.0	1.09e-18	0.932	293.0	9.81e-19	0.934	294.0	8.73e-19	0.936
295.0	7.65e-19	0.939	296.0	6.58e-19	0.941	297.0	5.81e-19	0.943	298.0	5.18e-19	0.945	299.0	4.55e-19	0.948
300.0	3.92e-19	0.950	301.0	3.35e-19	0.965	302.0	3.01e-19	0.975	303.0	2.66e-19	0.985	304.0	2.32e-19	0.990
305.0	1.97e-19	0.980	306.0	1.73e-19	0.950	307.0	1.55e-19	0.877	308.0	1.37e-19	0.773	309.0	1.18e-19	0.667
310.0	9.98e-20	0.600	311.0	8.92e-20	0.388	312.0	7.94e-20	0.303	313.0	6.96e-20	0.262	314.0	5.99e-20	0.238
315.0	5.01e-20	0.235	316.0	4.51e-20	0.221	317.0	4.00e-20	0.209	318.0	3.50e-20	0.194	319.0	2.99e-20	0.178
320.0	2.49e-20	0.148	321.0	2.23e-20	0.121	322.0	1.97e-20	0.097	323.0	1.72e-20	0.092	324.0	1.46e-20	0.080
325.0	1.20e-20	0.070	326.0	1.08e-20	0.066	327.0	9.67e-21	0.062	328.0	8.50e-21	0.058	329.0	7.34e-21	0.054
330.0	6.17e-21	0.050	331.0	5.48e-21	0.050	332.0	4.80e-21	0.050	333.0	4.11e-21	0.050	334.0	3.43e-21	0.050
335.0	2.74e-21	0.050	336.0	2.43e-21	0.040	337.0	2.11e-21	0.030	338.0	1.80e-21	0.020	339.0	1.48e-21	0.010
340.0	1.17e-21	0.000												
							HONO-NO							
309.0	0.00e+00	0.410	310.0	1.30e-20	0.410	311.0	1.90e-20	0.411	312.0	2.80e-20	0.421	313.0	2.20e-20	0.432
314.0	3.60e-20	0.443	315.0	3.00e-20	0.454	316.0	1.40e-20	0.464	317.0	3.10e-20	0.475	318.0	5.60e-20	0.486
319.0	3.60e-20	0.496	320.0	4.90e-20	0.507	321.0	7.80e-20	0.518	322.0	4.90e-20	0.529	323.0	5.10e-20	0.539
324.0	7.10e-20	0.550	325.0	5.00e-20	0.561	326.0	2.90e-20	0.571	327.0	6.60e-20	0.582	328.0	1.17e-19	0.593
329.0	6.10e-20	0.604	330.0	1.11e-19	0.614	331.0	1.79e-19	0.625	332.0	8.70e-20	0.636	333.0	7.60e-20	0.646
334.0	9.60e-20	0.657	335.0	9.60e-20	0.668	336.0	7.20e-20	0.679	337.0	5.30e-20	0.689	338.0	1.00e-19	0.700
339.0	1.88e-19	0.711	340.0	1.00e-19	0.721	341.0	1.70e-19	0.732	342.0	3.86e-19	0.743	343.0	1.49e-19	0.754
344.0	9.70e-20	0.764	345.0	1.09e-19	0.775	346.0	1.23e-19	0.786	347.0	1.04e-19	0.796	348.0	9.10e-20	0.807
349.0	7.90e-20	0.818	350.0	1.12e-19	0.829	351.0	2.12e-19	0.839	352.0	1.55e-19	0.850	353.0	1.91e-19	0.861
354.0	5.81e-19	0.871	355.0	3.64e-19	0.882	356.0	1.41e-19	0.893	357.0	1.17e-19	0.904	358.0	1.20e-19	0.914
359.0	1.04e-19	0.925	360.0	9.00e-20	0.936	361.0	8.30e-20	0.946	362.0	8.00e-20	0.957	363.0	9.60e-20	0.968
364.0	1.46e-19	0.979	365.0	1.68e-19	0.989	366.0	1.83e-19	1.000	367.0	3.02e-19	1.000	368.0	5.20e-19	1.000
369.0	3.88e-19	1.000	370.0	1.78e-19	1.000	371.0	1.13e-19	1.000	372.0	1.00e-19	1.000	373.0	7.70e-20	1.000
374.0	6.20e-20	1.000	375.0	5.30e-20	1.000	376.0	5.30e-20	1.000	377.0	5.00e-20	1.000	378.0	5.80e-20	1.000
379.0	8.00e-20	1.000	380.0	9.60e-20	1.000	381.0	1.13e-19	1.000	382.0	1.59e-19	1.000	383.0	2.10e-19	1.000
384.0	2.41e-19	1.000	385.0	2.03e-19	1.000	386.0	1.34e-19	1.000	387.0	9.00e-20	1.000	388.0	5.60e-20	1.000
389.0	3.40e-20	1.000	390.0	2.70e-20	1.000	391.0	2.00e-20	1.000	392.0	1.50e-20	1.000	393.0	1.10e-20	1.000
394.0	6.00e-21	1.000	395.0	1.00e-20	1.000	396.0	4.00e-21	1.000	400.0	0.00e+00	1.000			
							HONO-NO2							
309.0	0.00e+00	0.590	310.0	1.30e-20	0.590	311.0	1.90e-20	0.589	312.0	2.80e-20	0.579	313.0	2.20e-20	0.568
314.0	3.60e-20	0.557	315.0	3.00e-20	0.546	316.0	1.40e-20	0.536	317.0	3.10e-20	0.525	318.0	5.60e-20	0.514
319.0	3.60e-20	0.504	320.0	4.90e-20	0.493	321.0	7.80e-20	0.482	322.0	4.90e-20	0.471	323.0	5.10e-20	0.461
324.0	7.10e-20	0.450	325.0	5.00e-20	0.439	326.0	2.90e-20	0.429	327.0	6.60e-20	0.418	328.0	1.17e-19	0.407
329.0	6.10e-20	0.396	330.0	1.11e-19	0.386	331.0	1.79e-19	0.375	332.0	8.70e-20	0.364	333.0	7.60e-20	0.354
334.0	9.60e-20	0.343	335.0	9.60e-20	0.332	336.0	7.20e-20	0.321	337.0	5.30e-20	0.311	338.0	1.00e-19	0.300
339.0	1.88e-19	0.289	340.0	1.00e-19	0.279	341.0	1.70e-19	0.268	342.0	3.86e-19	0.257	343.0	1.49e-19	0.246
344.0	9.70e-20	0.236	345.0	1.09e-19	0.225	346.0	1.23e-19	0.214	347.0	1.04e-19	0.204	348.0	9.10e-20	0.193
349.0	7.90e-20	0.182	350.0	1.12e-19	0.171	351.0	2.12e-19	0.161	352.0	1.55e-19	0.150	353.0	1.91e-19	0.139
354.0	5.81e-19	0.129	355.0	3.64e-19	0.118	356.0	1.41e-19	0.107	357.0	1.17e-19	0.096	358.0	1.20e-19	0.086
359.0	1.04e-19	0.075	360.0	9.00e-20	0.064	361.0	8.30e-20	0.054	362.0	8.00e-20	0.043	363.0	9.60e-20	0.032

Table A-3 (continued)

WL (nm)	Abs (cm^2)	QY	WL (nm)	Abs (cm^2)	QY	WL (nm)	Abs (cm^2)	QY	WL (nm)	Abs (cm^2)	QY	WL (nm)	Abs (cm^2)	QY
364.0	1.46e-19	0.021	365.0	1.68e-19	0.011	366.0	1.83e-19	0.000						
							HNO3							
190.0	1.36e-17	1.000	195.0	1.02e-17	1.000	200.0	5.88e-18	1.000	205.0	2.80e-18	1.000	210.0	1.04e-18	1.000
215.0	3.65e-19	1.000	220.0	1.49e-19	1.000	225.0	8.81e-20	1.000	230.0	5.75e-20	1.000	235.0	3.75e-20	1.000
240.0	2.58e-20	1.000	245.0	2.11e-20	1.000	250.0	1.97e-20	1.000	255.0	1.95e-20	1.000	260.0	1.91e-20	1.000
265.0	1.80e-20	1.000	270.0	1.62e-20	1.000	275.0	1.38e-20	1.000	280.0	1.12e-20	1.000	285.0	8.58e-21	1.000
290.0	6.15e-21	1.000	295.0	4.12e-21	1.000	300.0	2.63e-21	1.000	305.0	1.50e-21	1.000	310.0	8.10e-22	1.000
315.0	4.10e-22	1.000	320.0	2.00e-22	1.000	325.0	9.50e-23	1.000	330.0	4.30e-23	1.000	335.0	2.20e-23	1.000
340.0	1.00e-23	1.000	345.0	6.00e-24	1.000	350.0	4.00e-24	1.000	355.0	0.00e+00	1.000			
							HO2NO2							
190.0	1.01e-17	1.000	195.0	8.16e-18	1.000	200.0	5.63e-18	1.000	205.0	3.67e-18	1.000	210.0	2.39e-18	1.000
215.0	1.61e-18	1.000	220.0	1.18e-18	1.000	225.0	9.32e-19	1.000	230.0	7.88e-19	1.000	235.0	6.80e-19	1.000
240.0	5.79e-19	1.000	245.0	4.97e-19	1.000	250.0	4.11e-19	1.000	255.0	3.49e-19	1.000	260.0	2.84e-19	1.000
265.0	2.29e-19	1.000	270.0	1.80e-19	1.000	275.0	1.33e-19	1.000	280.0	9.30e-20	1.000	285.0	6.20e-20	1.000
290.0	3.90e-20	1.000	295.0	2.40e-20	1.000	300.0	1.40e-20	1.000	305.0	8.50e-21	1.000	310.0	5.30e-21	1.000
315.0	3.90e-21	1.000	320.0	2.40e-21	1.000	325.0	1.50e-21	1.000	330.0	9.00e-22	1.000	335.0	0.00e+00	1.000
							H2O2							
190.0	6.72e-19	1.000	195.0	5.63e-19	1.000	200.0	4.75e-19	1.000	205.0	4.08e-19	1.000	210.0	3.57e-19	1.000
215.0	3.07e-19	1.000	220.0	2.58e-19	1.000	225.0	2.17e-19	1.000	230.0	1.82e-19	1.000	235.0	1.50e-19	1.000
240.0	1.24e-19	1.000	245.0	1.02e-19	1.000	250.0	8.30e-20	1.000	255.0	6.70e-20	1.000	260.0	5.30e-20	1.000
265.0	4.20e-20	1.000	270.0	3.30e-20	1.000	275.0	2.60e-20	1.000	280.0	2.00e-20	1.000	285.0	1.50e-20	1.000
290.0	1.20e-20	1.000	295.0	9.00e-21	1.000	300.0	6.80e-21	1.000	305.0	5.10e-21	1.000	310.0	3.90e-21	1.000
315.0	2.90e-21	1.000	320.0	2.20e-21	1.000	325.0	1.60e-21	1.000	330.0	1.30e-21	1.000	335.0	1.00e-21	1.000
340.0	7.00e-22	1.000	345.0	5.00e-22	1.000	350.0	4.00e-22	1.000	355.0	0.00e+00	1.000			
							HCHO_R							
240.0	6.40e-22	0.270	241.0	5.60e-22	0.272	242.0	1.05e-21	0.274	243.0	1.15e-21	0.276	244.0	8.20e-22	0.278
245.0	1.03e-21	0.280	246.0	9.80e-22	0.282	247.0	1.35e-21	0.284	248.0	1.91e-21	0.286	249.0	2.82e-21	0.288
250.0	2.05e-21	0.290	251.0	1.70e-21	0.291	252.0	2.88e-21	0.292	253.0	2.55e-21	0.293	254.0	2.55e-21	0.294
255.0	3.60e-21	0.295	256.0	5.09e-21	0.296	257.0	3.39e-21	0.297	258.0	2.26e-21	0.298	259.0	5.04e-21	0.299
260.0	5.05e-21	0.300	261.0	5.49e-21	0.308	262.0	5.20e-21	0.316	263.0	9.33e-21	0.324	264.0	8.23e-21	0.332
265.0	4.30e-21	0.340	266.0	4.95e-21	0.348	267.0	1.24e-20	0.356	268.0	1.11e-20	0.364	269.0	8.78e-21	0.372
270.0	9.36e-21	0.380	271.0	1.79e-20	0.399	272.0	1.23e-20	0.418	273.0	6.45e-21	0.437	274.0	6.56e-21	0.456
275.0	2.23e-20	0.475	276.0	2.42e-20	0.494	277.0	1.40e-20	0.513	278.0	1.05e-20	0.532	279.0	2.55e-20	0.551
280.0	2.08e-20	0.570	281.0	1.48e-20	0.586	282.0	8.81e-21	0.602	283.0	1.07e-20	0.618	284.0	4.49e-20	0.634
285.0	3.59e-20	0.650	286.0	1.96e-20	0.666	287.0	1.30e-20	0.682	288.0	3.36e-20	0.698	289.0	2.84e-20	0.714
290.0	1.30e-20	0.730	291.0	1.75e-20	0.735	292.0	8.32e-21	0.740	293.0	3.73e-20	0.745	294.0	6.54e-20	0.750
295.0	3.95e-20	0.755	296.0	2.33e-20	0.760	297.0	1.51e-20	0.765	298.0	4.04e-20	0.770	299.0	2.87e-20	0.775
300.0	8.71e-21	0.780	301.0	1.72e-20	0.780	302.0	1.06e-20	0.780	303.0	3.20e-20	0.780	304.0	6.90e-20	0.780
305.0	4.91e-20	0.780	306.0	4.63e-20	0.780	307.0	2.10e-20	0.780	308.0	1.49e-20	0.780	309.0	3.41e-20	0.780
310.0	1.95e-20	0.780	311.0	5.21e-21	0.764	312.0	1.12e-20	0.748	313.0	1.12e-20	0.732	314.0	4.75e-20	0.716
315.0	5.25e-20	0.700	316.0	2.90e-20	0.684	317.0	5.37e-20	0.668	318.0	2.98e-20	0.652	319.0	9.18e-21	0.636
320.0	1.26e-20	0.620	321.0	1.53e-20	0.585	322.0	6.69e-21	0.550	323.0	3.45e-21	0.515	324.0	8.16e-21	0.480
325.0	1.85e-20	0.445	326.0	5.95e-20	0.410	327.0	3.49e-20	0.375	328.0	1.09e-20	0.340	329.0	3.35e-20	0.305
330.0	3.32e-20	0.270	331.0	1.07e-20	0.243	332.0	2.89e-21	0.216	333.0	2.15e-21	0.189	334.0	1.71e-21	0.162
335.0	1.43e-21	0.135	336.0	1.94e-21	0.108	337.0	4.17e-21	0.081	338.0	2.36e-20	0.054	339.0	4.71e-20	0.027
340.0	2.48e-20	0.000												
							HCHO_M							
240.0	6.40e-22	0.490	241.0	5.60e-22	0.490	242.0	1.05e-21	0.490	243.0	1.15e-21	0.490	244.0	8.20e-22	0.490
245.0	1.03e-21	0.490	246.0	9.80e-22	0.490	247.0	1.35e-21	0.490	248.0	1.91e-21	0.490	249.0	2.82e-21	0.490
250.0	2.05e-21	0.490	251.0	1.70e-21	0.490	252.0	2.88e-21	0.490	253.0	2.55e-21	0.490	254.0	2.55e-21	0.490
255.0	3.60e-21	0.490	256.0	5.09e-21	0.490	257.0	3.39e-21	0.490	258.0	2.26e-21	0.490	259.0	5.04e-21	0.490
260.0	5.05e-21	0.490	261.0	5.49e-21	0.484	262.0	5.20e-21	0.478	263.0	9.33e-21	0.472	264.0	8.23e-21	0.466
265.0	4.30e-21	0.460	266.0	4.95e-21	0.454	267.0	1.24e-20	0.448	268.0	1.11e-20	0.442	269.0	8.78e-21	0.436
270.0	9.36e-21	0.430	271.0	1.79e-20	0.419	272.0	1.23e-20	0.408	273.0	6.45e-21	0.397	274.0	6.56e-21	0.386
275.0	2.23e-20	0.375	276.0	2.42e-20	0.364	277.0	1.40e-20	0.353	278.0	1.05e-20	0.342	279.0	2.55e-20	0.331
280.0	2.08e-20	0.320	281.0	1.48e-20	0.312	282.0	8.81e-21	0.304	283.0	1.07e-20	0.296	284.0	4.49e-20	0.288
285.0	3.59e-20	0.280	286.0	1.96e-20	0.272	287.0	1.30e-20	0.264	288.0	3.36e-20	0.256	289.0	2.84e-20	0.248
290.0	1.30e-20	0.240	291.0	1.75e-20	0.237	292.0	8.32e-21	0.234	293.0	3.73e-20	0.231	294.0	6.54e-20	0.228
295.0	3.95e-20	0.225	296.0	2.33e-20	0.222	297.0	1.51e-20	0.219	298.0	4.04e-20	0.216	299.0	2.87e-20	0.213
300.0	8.71e-21	0.210	301.0	1.72e-20	0.211	302.0	1.06e-20	0.212	303.0	3.20e-20	0.213	304.0	6.90e-20	0.214
305.0	4.91e-20	0.215	306.0	4.63e-20	0.216	307.0	2.10e-20	0.217	308.0	1.49e-20	0.218	309.0	3.41e-20	0.219
310.0	1.95e-20	0.220	311.0	5.21e-21	0.236	312.0	1.12e-20	0.252	313.0	1.12e-20	0.268	314.0	4.75e-20	0.284
315.0	5.25e-20	0.300	316.0	2.90e-20	0.316	317.0	5.37e-20	0.332	318.0	2.98e-20	0.348	319.0	9.18e-21	0.364
320.0	1.26e-20	0.380	321.0	1.53e-20	0.408	322.0	6.69e-21	0.436	323.0	3.45e-21	0.464	324.0	8.16e-21	0.492
325.0	1.85e-20	0.520	326.0	5.95e-20	0.548	327.0	3.49e-20	0.576	328.0	1.09e-20	0.604	329.0	3.35e-20	0.632
330.0	3.32e-20	0.660	331.0	1.07e-20	0.650	332.0	2.89e-21	0.640	333.0	2.15e-21	0.630	334.0	1.71e-21	0.620
335.0	1.43e-21	0.610	336.0	1.94e-21	0.600	337.0	4.17e-21	0.590	338.0	2.36e-20	0.580	339.0	4.71e-20	0.570
340.0	2.48e-20	0.560	341.0	7.59e-21	0.525	342.0	6.81e-21	0.490	343.0	1.95e-20	0.455	344.0	1.14e-20	0.420
345.0	3.23e-21	0.385	346.0	1.13e-21	0.350	347.0	6.60e-22	0.315	348.0	1.22e-21	0.280	349.0	3.20e-22	0.245

Table A-3 (continued)

WL (nm)	Abs (cm^2)	QY	WL (nm)	Abs (cm^2)	QY	WL (nm)	Abs (cm^2)	QY	WL (nm)	Abs (cm^2)	QY	WL (nm)	Abs (cm^2)	QY
350.0	3.80e-22	0.210	351.0	1.04e-21	0.192	352.0	7.13e-21	0.174	353.0	2.21e-20	0.156	354.0	1.54e-20	0.138
355.0	6.76e-21	0.120	356.0	1.35e-21	0.102	357.0	3.60e-22	0.084	358.0	5.70e-23	0.066	359.0	5.80e-22	0.048
360.0	8.20e-22	0.000												
							CCHO_R							
262.0	2.44e-20	0.326	266.0	3.05e-20	0.358	270.0	3.42e-20	0.390	274.0	4.03e-20	0.466	278.0	4.19e-20	0.542
280.0	4.50e-20	0.580	281.0	4.69e-20	0.575	282.0	4.72e-20	0.570	283.0	4.75e-20	0.565	284.0	4.61e-20	0.560
285.0	4.49e-20	0.555	286.0	4.44e-20	0.550	287.0	4.59e-20	0.545	288.0	4.72e-20	0.540	289.0	4.77e-20	0.535
290.0	4.89e-20	0.530	291.0	4.78e-20	0.520	292.0	4.68e-20	0.510	293.0	4.53e-20	0.500	294.0	4.33e-20	0.490
295.0	4.27e-20	0.480	296.0	4.24e-20	0.470	297.0	4.38e-20	0.460	298.0	4.41e-20	0.450	299.0	4.26e-20	0.440
300.0	4.16e-20	0.430	301.0	3.99e-20	0.418	302.0	3.86e-20	0.406	303.0	3.72e-20	0.394	304.0	3.48e-20	0.382
305.0	3.42e-20	0.370	306.0	3.42e-20	0.354	307.0	3.36e-20	0.338	308.0	3.33e-20	0.322	309.0	3.14e-20	0.306
310.0	2.93e-20	0.290	311.0	2.76e-20	0.266	312.0	2.53e-20	0.242	313.0	2.47e-20	0.218	314.0	2.44e-20	0.194
315.0	2.20e-20	0.170	316.0	2.04e-20	0.156	317.0	2.07e-20	0.142	318.0	1.98e-20	0.128	319.0	1.87e-20	0.114
320.0	1.72e-20	0.100	321.0	1.48e-20	0.088	322.0	1.40e-20	0.076	323.0	1.24e-20	0.064	324.0	1.09e-20	0.052
325.0	1.14e-20	0.040	326.0	1.07e-20	0.032	327.0	8.58e-21	0.024	328.0	7.47e-21	0.016	329.0	7.07e-21	0.008
							C2CHO							
294.0	5.80e-20	0.890	295.0	5.57e-20	0.885	296.0	5.37e-20	0.880	297.0	5.16e-20	0.875	298.0	5.02e-20	0.870
299.0	5.02e-20	0.865	300.0	5.04e-20	0.860	301.0	5.09e-20	0.855	302.0	5.07e-20	0.850	303.0	4.94e-20	0.818
304.0	4.69e-20	0.786	305.0	4.32e-20	0.755	306.0	4.04e-20	0.723	307.0	3.81e-20	0.691	308.0	3.65e-20	0.659
309.0	3.62e-20	0.627	310.0	3.60e-20	0.596	311.0	3.53e-20	0.564	312.0	3.50e-20	0.532	313.0	3.32e-20	0.500
314.0	3.06e-20	0.480	315.0	2.77e-20	0.460	316.0	2.43e-20	0.440	317.0	2.18e-20	0.420	318.0	2.00e-20	0.400
319.0	1.86e-20	0.380	320.0	1.83e-20	0.360	321.0	1.78e-20	0.340	322.0	1.66e-20	0.320	323.0	1.58e-20	0.300
324.0	1.49e-20	0.280	325.0	1.30e-20	0.260	326.0	1.13e-20	0.248	327.0	9.96e-21	0.236	328.0	8.28e-21	0.223
329.0	6.85e-21	0.211	330.0	5.75e-21	0.199	331.0	4.94e-21	0.187	332.0	4.66e-21	0.174	333.0	4.30e-21	0.162
334.0	3.73e-21	0.150	335.0	3.25e-21	0.133	336.0	2.80e-21	0.117	337.0	2.30e-21	0.100	338.0	1.85e-21	0.083
339.0	1.66e-21	0.067	340.0	1.55e-21	0.050	341.0	1.19e-21	0.033	342.0	7.60e-22	0.017	343.0	4.50e-22	0.000
							ACETONE							
250.0	2.47e-20	0.760	254.0	3.04e-20	0.776	258.0	3.61e-20	0.792	262.0	4.15e-20	0.768	266.0	4.58e-20	0.704
270.0	4.91e-20	0.640	274.0	5.06e-20	0.604	278.0	5.07e-20	0.568	280.0	5.05e-20	0.550	281.0	5.01e-20	0.525
282.0	4.94e-20	0.500	283.0	4.86e-20	0.475	284.0	4.76e-20	0.450	285.0	4.68e-20	0.425	286.0	4.58e-20	0.400
287.0	4.50e-20	0.375	288.0	4.41e-20	0.350	289.0	4.29e-20	0.325	290.0	4.19e-20	0.302	291.0	4.08e-20	0.284
292.0	3.94e-20	0.266	293.0	3.81e-20	0.249	294.0	3.67e-20	0.232	295.0	3.52e-20	0.217	296.0	3.35e-20	0.201
297.0	3.20e-20	0.187	298.0	3.07e-20	0.173	299.0	2.91e-20	0.160	300.0	2.77e-20	0.147	301.0	2.66e-20	0.135
302.0	2.53e-20	0.124	303.0	2.37e-20	0.114	304.0	2.24e-20	0.104	305.0	2.11e-20	0.095	306.0	1.95e-20	0.086
307.0	1.80e-20	0.078	308.0	1.66e-20	0.071	309.0	1.54e-20	0.064	310.0	1.41e-20	0.057	311.0	1.28e-20	0.052
312.0	1.17e-20	0.046	313.0	1.08e-20	0.042	314.0	9.67e-21	0.037	315.0	8.58e-21	0.033	316.0	7.77e-21	0.029
317.0	6.99e-21	0.026	318.0	6.08e-21	0.023	319.0	5.30e-21	0.020	320.0	4.67e-21	0.018	321.0	4.07e-21	0.016
322.0	3.44e-21	0.014	323.0	2.87e-21	0.012	324.0	2.43e-21	0.011	325.0	2.05e-21	0.009	326.0	1.68e-21	0.008
327.0	1.35e-21	0.007	328.0	1.08e-21	0.006	329.0	8.60e-22	0.005	330.0	6.70e-22	0.005	331.0	5.10e-22	0.004
332.0	4.00e-22	0.003	333.0	3.10e-22	0.003	334.0	2.60e-22	0.002	335.0	1.70e-22	0.002	336.0	1.40e-22	0.002
337.0	1.10e-22	0.002	338.0	9.00e-23	0.001	339.0	6.00e-23	0.001	340.0	5.00e-23	0.001	341.0	5.00e-23	0.001
342.0	3.00e-23	0.001	343.0	4.00e-23	0.001	344.0	2.00e-23	0.000						
							KETONE							
198.5	3.95e-19	1.000	199.0	1.61e-19	1.000	199.5	7.75e-20	1.000	200.0	3.76e-20	1.000	200.5	2.51e-20	1.000
201.0	1.83e-20	1.000	201.5	1.36e-20	1.000	202.0	1.16e-20	1.000	202.5	8.97e-21	1.000	203.0	4.62e-21	1.000
203.5	3.18e-21	1.000	204.0	2.42e-21	1.000	204.5	2.01e-21	1.000	205.0	1.77e-21	1.000	205.5	1.64e-21	1.000
206.0	1.54e-21	1.000	206.5	1.52e-21	1.000	207.0	1.54e-21	1.000	207.5	1.62e-21	1.000	208.0	1.64e-21	1.000
208.5	1.60e-21	1.000	209.0	1.57e-21	1.000	209.5	1.49e-21	1.000	210.0	1.47e-21	1.000	210.5	1.52e-21	1.000
211.0	1.50e-21	1.000	211.5	1.62e-21	1.000	212.0	1.81e-21	1.000	212.5	2.10e-21	1.000	213.0	2.23e-21	1.000
213.5	2.06e-21	1.000	214.0	1.69e-21	1.000	214.5	1.49e-21	1.000	215.0	1.42e-21	1.000	215.5	1.42e-21	1.000
216.0	1.42e-21	1.000	216.5	1.48e-21	1.000	217.0	1.48e-21	1.000	217.5	1.53e-21	1.000	218.0	1.56e-21	1.000
218.5	1.67e-21	1.000	219.0	1.68e-21	1.000	219.5	1.78e-21	1.000	220.0	1.85e-21	1.000	220.5	1.92e-21	1.000
221.0	2.01e-21	1.000	221.5	2.11e-21	1.000	222.0	2.23e-21	1.000	222.5	2.33e-21	1.000	223.0	2.48e-21	1.000
223.5	2.60e-21	1.000	224.0	2.74e-21	1.000	224.5	2.85e-21	1.000	225.0	3.04e-21	1.000	225.5	3.15e-21	1.000
226.0	3.33e-21	1.000	226.5	3.55e-21	1.000	227.0	3.73e-21	1.000	227.5	3.93e-21	1.000	228.0	4.11e-21	1.000
228.5	4.34e-21	1.000	229.0	4.56e-21	1.000	229.5	4.75e-21	1.000	230.0	5.01e-21	1.000	230.5	5.27e-21	1.000
231.0	5.53e-21	1.000	231.5	5.83e-21	1.000	232.0	6.15e-21	1.000	232.5	6.45e-21	1.000	233.0	6.73e-21	1.000
233.5	7.02e-21	1.000	234.0	7.42e-21	1.000	234.5	7.83e-21	1.000	235.0	8.11e-21	1.000	235.5	8.45e-21	1.000
236.0	8.82e-21	1.000	236.5	9.21e-21	1.000	237.0	9.65e-21	1.000	237.5	1.00e-20	1.000	238.0	1.05e-20	1.000
238.5	1.10e-20	1.000	239.0	1.15e-20	1.000	239.5	1.20e-20	1.000	240.0	1.23e-20	1.000	240.5	1.28e-20	1.000
241.0	1.32e-20	1.000	241.5	1.38e-20	1.000	242.0	1.44e-20	1.000	242.5	1.50e-20	1.000	243.0	1.57e-20	1.000
243.5	1.63e-20	1.000	244.0	1.68e-20	1.000	244.5	1.75e-20	1.000	245.0	1.81e-20	1.000	245.5	1.88e-20	1.000
246.0	1.96e-20	1.000	246.5	2.03e-20	1.000	247.0	2.11e-20	1.000	247.5	2.19e-20	1.000	248.0	2.25e-20	1.000
248.5	2.33e-20	1.000	249.0	2.40e-20	1.000	249.5	2.48e-20	1.000	250.0	2.56e-20	1.000	250.5	2.64e-20	1.000
251.0	2.73e-20	1.000	251.5	2.81e-20	1.000	252.0	2.88e-20	1.000	252.5	2.98e-20	1.000	253.0	3.07e-20	1.000
253.5	3.16e-20	1.000	254.0	3.25e-20	1.000	254.5	3.34e-20	1.000	255.0	3.43e-20	1.000	255.5	3.51e-20	1.000
256.0	3.59e-20	1.000	256.5	3.67e-20	1.000	257.0	3.75e-20	1.000	257.5	3.84e-20	1.000	258.0	3.94e-20	1.000
258.5	4.03e-20	1.000	259.0	4.13e-20	1.000	259.5	4.22e-20	1.000	260.0	4.28e-20	1.000	260.5	4.33e-20	1.000
261.0	4.41e-20	1.000	261.5	4.49e-20	1.000	262.0	4.57e-20	1.000	262.5	4.65e-20	1.000	263.0	4.72e-20	1.000
263.5	4.78e-20	1.000	264.0	4.85e-20	1.000	264.5	4.92e-20	1.000	265.0	4.99e-20	1.000	265.5	5.04e-20	1.000
266.0	5.12e-20	1.000	266.5	5.22e-20	1.000	267.0	5.28e-20	1.000	267.5	5.34e-20	1.000	268.0	5.41e-20	1.000

Table A-3 (continued)

WL (nm)	Abs (cm^2)	QY	WL (nm)	Abs (cm^2)	QY	WL (nm)	Abs (cm^2)	QY	WL (nm)	Abs (cm^2)	QY	WL (nm)	Abs (cm^2)	QY
268.5	5.46e-20	1.000	269.0	5.51e-20	1.000	269.5	5.55e-20	1.000	270.0	5.59e-20	1.000	270.5	5.63e-20	1.000
271.0	5.66e-20	1.000	271.5	5.70e-20	1.000	272.0	5.74e-20	1.000	272.5	5.78e-20	1.000	273.0	5.81e-20	1.000
273.5	5.86e-20	1.000	274.0	5.90e-20	1.000	274.5	5.93e-20	1.000	275.0	5.96e-20	1.000	275.5	5.97e-20	1.000
276.0	5.98e-20	1.000	276.5	5.98e-20	1.000	277.0	5.99e-20	1.000	277.5	5.99e-20	1.000	278.0	5.98e-20	1.000
278.5	5.96e-20	1.000	279.0	5.96e-20	1.000	279.5	5.95e-20	1.000	280.0	5.94e-20	1.000	280.5	5.92e-20	1.000
281.0	5.90e-20	1.000	281.5	5.88e-20	1.000	282.0	5.86e-20	1.000	282.5	5.83e-20	1.000	283.0	5.79e-20	1.000
283.5	5.75e-20	1.000	284.0	5.71e-20	1.000	284.5	5.67e-20	1.000	285.0	5.61e-20	1.000	285.5	5.56e-20	1.000
286.0	5.51e-20	1.000	286.5	5.45e-20	1.000	287.0	5.41e-20	1.000	287.5	5.37e-20	1.000	288.0	5.33e-20	1.000
288.5	5.27e-20	1.000	289.0	5.21e-20	1.000	289.5	5.15e-20	1.000	290.0	5.08e-20	1.000	290.5	4.99e-20	1.000
291.0	4.89e-20	1.000	291.5	4.82e-20	1.000	292.0	4.73e-20	1.000	292.5	4.62e-20	1.000	293.0	4.53e-20	1.000
293.5	4.41e-20	1.000	294.0	4.32e-20	1.000	294.5	4.23e-20	1.000	295.0	4.15e-20	1.000	295.5	4.11e-20	1.000
296.0	4.01e-20	1.000	296.5	3.94e-20	1.000	297.0	3.88e-20	1.000	297.5	3.77e-20	1.000	298.0	3.69e-20	1.000
298.5	3.63e-20	1.000	299.0	3.54e-20	1.000	299.5	3.46e-20	1.000	300.0	3.36e-20	1.000	300.5	3.24e-20	1.000
301.0	3.16e-20	1.000	301.5	3.06e-20	1.000	302.0	2.95e-20	1.000	302.5	2.82e-20	1.000	303.0	2.70e-20	1.000
303.5	2.59e-20	1.000	304.0	2.49e-20	1.000	304.5	2.42e-20	1.000	305.0	2.34e-20	1.000	305.5	2.28e-20	1.000
306.0	2.19e-20	1.000	306.5	2.11e-20	1.000	307.0	2.04e-20	1.000	307.5	1.93e-20	1.000	308.0	1.88e-20	1.000
308.5	1.80e-20	1.000	309.0	1.73e-20	1.000	309.5	1.66e-20	1.000	310.0	1.58e-20	1.000	310.5	1.48e-20	1.000
311.0	1.42e-20	1.000	311.5	1.34e-20	1.000	312.0	1.26e-20	1.000	312.5	1.17e-20	1.000	313.0	1.13e-20	1.000
313.5	1.08e-20	1.000	314.0	1.04e-20	1.000	314.5	9.69e-21	1.000	315.0	8.91e-21	1.000	315.5	8.61e-21	1.000
316.0	7.88e-21	1.000	316.5	7.25e-21	1.000	317.0	6.92e-21	1.000	317.5	6.43e-21	1.000	318.0	6.07e-21	1.000
318.5	5.64e-21	1.000	319.0	5.19e-21	1.000	319.5	4.66e-21	1.000	320.0	4.36e-21	1.000	320.5	3.95e-21	1.000
321.0	3.64e-21	1.000	321.5	3.38e-21	1.000	322.0	3.17e-21	1.000	322.5	2.80e-21	1.000	323.0	2.62e-21	1.000
323.5	2.29e-21	1.000	324.0	2.13e-21	1.000	324.5	1.93e-21	1.000	325.0	1.70e-21	1.000	325.5	1.58e-21	1.000
326.0	1.48e-21	1.000	326.5	1.24e-21	1.000	327.0	1.20e-21	1.000	327.5	1.04e-21	1.000	328.0	9.51e-22	1.000
328.5	8.44e-22	1.000	329.0	7.26e-22	1.000	329.5	6.70e-22	1.000	330.0	6.08e-22	1.000	330.5	5.15e-22	1.000
331.0	4.56e-22	1.000	331.5	4.13e-22	1.000	332.0	3.56e-22	1.000	332.5	3.30e-22	1.000	333.0	2.97e-22	1.000
333.5	2.67e-22	1.000	334.0	2.46e-22	1.000	334.5	2.21e-22	1.000	335.0	1.93e-22	1.000	335.5	1.56e-22	1.000
336.0	1.47e-22	1.000	336.5	1.37e-22	1.000	337.0	1.27e-22	1.000	337.5	1.19e-22	1.000	338.0	1.09e-22	1.000
338.5	1.01e-22	1.000	339.0	9.09e-23	1.000	339.5	8.22e-23	1.000	340.0	7.66e-23	1.000	340.5	7.43e-23	1.000
341.0	6.83e-23	1.000	341.5	6.72e-23	1.000	342.0	6.04e-23	1.000	342.5	4.78e-23	1.000	343.0	0.00e+00	1.000
COOH														
210.0	3.12e-19	1.000	215.0	2.09e-19	1.000	220.0	1.54e-19	1.000	225.0	1.22e-19	1.000	230.0	9.62e-20	1.000
235.0	7.61e-20	1.000	240.0	6.05e-20	1.000	245.0	4.88e-20	1.000	250.0	3.98e-20	1.000	255.0	3.23e-20	1.000
260.0	2.56e-20	1.000	265.0	2.11e-20	1.000	270.0	1.70e-20	1.000	275.0	1.39e-20	1.000	280.0	1.09e-20	1.000
285.0	8.63e-21	1.000	290.0	6.91e-21	1.000	295.0	5.51e-21	1.000	300.0	4.13e-21	1.000	305.0	3.13e-21	1.000
310.0	2.39e-21	1.000	315.0	1.82e-21	1.000	320.0	1.37e-21	1.000	325.0	1.05e-21	1.000	330.0	7.90e-22	1.000
335.0	6.10e-22	1.000	340.0	4.70e-22	1.000	345.0	3.50e-22	1.000	350.0	2.70e-22	1.000	355.0	2.10e-22	1.000
360.0	1.60e-22	1.000	365.0	1.20e-22	1.000	370.0	0.00e+00	1.000						
GLY_R														
230.0	2.87e-21	1.000	235.0	2.87e-21	1.000	240.0	4.30e-21	1.000	245.0	5.73e-21	1.000	250.0	8.60e-21	1.000
255.0	1.15e-20	1.000	260.0	1.43e-20	1.000	265.0	1.86e-20	1.000	270.0	2.29e-20	1.000	275.0	2.58e-20	1.000
280.0	2.87e-20	1.000	285.0	3.30e-20	1.000	290.0	3.15e-20	1.000	295.0	3.30e-20	1.000	300.0	3.58e-20	1.000
305.0	2.72e-20	1.000	310.0	2.72e-20	1.000	312.5	2.87e-20	1.000	315.0	2.29e-20	1.000	320.0	1.43e-20	1.000
325.0	1.15e-20	1.000	327.5	1.43e-20	1.000	330.0	1.15e-20	1.000	335.0	2.87e-21	1.000	340.0	0.00e+00	1.000
345.0	0.00e+00	1.000	350.0	0.00e+00	1.000	355.0	0.00e+00	1.000	360.0	2.29e-21	1.000	365.0	2.87e-21	1.000
370.0	8.03e-21	1.000	375.0	1.00e-20	1.000	380.0	1.72e-20	0.972	382.0	1.58e-20	0.855	384.0	1.49e-20	0.737
386.0	1.49e-20	0.619	388.0	2.87e-20	0.502	390.0	3.15e-20	0.384	391.0	3.24e-20	0.326	392.0	3.04e-20	0.267
393.0	2.23e-20	0.208	394.0	2.63e-20	0.149	395.0	3.04e-20	0.090	396.0	2.63e-20	0.032	397.0	2.43e-20	0.000
398.0	3.24e-20	0.000	399.0	3.04e-20	0.000	400.0	2.84e-20	0.000	401.0	3.24e-20	0.000	402.0	4.46e-20	0.000
403.0	5.27e-20	0.000	404.0	4.26e-20	0.000	405.0	3.04e-20	0.000	406.0	3.04e-20	0.000	407.0	2.84e-20	0.000
408.0	2.43e-20	0.000	409.0	2.84e-20	0.000	410.0	6.08e-20	0.000	411.0	5.07e-20	0.000	411.5	6.08e-20	0.000
412.0	4.86e-20	0.000	413.0	8.31e-20	0.000	413.5	6.48e-20	0.000	414.0	7.50e-20	0.000	414.5	8.11e-20	0.000
415.0	8.11e-20	0.000	415.5	6.89e-20	0.000	416.0	4.26e-20	0.000	417.0	4.86e-20	0.000	418.0	5.88e-20	0.000
GLY_ABS														
230.0	2.87e-21	1.000	235.0	2.87e-21	1.000	240.0	4.30e-21	1.000	245.0	5.73e-21	1.000	250.0	8.60e-21	1.000
255.0	1.15e-20	1.000	260.0	1.43e-20	1.000	265.0	1.86e-20	1.000	270.0	2.29e-20	1.000	275.0	2.58e-20	1.000
280.0	2.87e-20	1.000	285.0	3.30e-20	1.000	290.0	3.15e-20	1.000	295.0	3.30e-20	1.000	300.0	3.58e-20	1.000
305.0	2.72e-20	1.000	310.0	2.72e-20	1.000	312.5	2.87e-20	1.000	315.0	2.29e-20	1.000	320.0	1.43e-20	1.000
325.0	1.15e-20	1.000	327.5	1.43e-20	1.000	330.0	1.15e-20	1.000	335.0	2.87e-21	1.000	340.0	0.00e+00	1.000
355.0	0.00e+00	1.000	360.0	2.29e-21	1.000	365.0	2.87e-21	1.000	370.0	8.03e-21	1.000	375.0	1.00e-20	1.000
380.0	1.72e-20	1.000	382.0	1.58e-20	1.000	384.0	1.49e-20	1.000	386.0	1.49e-20	1.000	388.0	2.87e-20	1.000
390.0	3.15e-20	1.000	391.0	3.24e-20	1.000	392.0	3.04e-20	1.000	393.0	2.23e-20	1.000	394.0	2.63e-20	1.000
395.0	3.04e-20	1.000	396.0	2.63e-20	1.000	397.0	2.43e-20	1.000	398.0	3.24e-20	1.000	399.0	3.04e-20	1.000
400.0	2.84e-20	1.000	401.0	3.24e-20	1.000	402.0	4.46e-20	1.000	403.0	5.27e-20	1.000	404.0	4.26e-20	1.000
405.0	3.04e-20	1.000	406.0	3.04e-20	1.000	407.0	2.84e-20	1.000	408.0	2.43e-20	1.000	409.0	2.84e-20	1.000
410.0	6.08e-20	1.000	411.0	5.07e-20	1.000	411.5	6.08e-20	1.000	412.0	4.86e-20	1.000	413.0	8.31e-20	1.000
413.5	6.48e-20	1.000	414.0	7.50e-20	1.000	414.5	8.11e-20	1.000	415.0	8.11e-20	1.000	415.5	6.89e-20	1.000
416.0	4.26e-20	1.000	417.0	4.86e-20	1.000	418.0	5.88e-20	1.000	419.0	6.69e-20	1.000	420.0	3.85e-20	1.000
421.0	5.67e-20	1.000	421.5	4.46e-20	1.000	422.0	5.27e-20	1.000	422.5	1.05e-19	1.000	423.0	8.51e-20	1.000
424.0	6.08e-20	1.000	425.0	7.29e-20	1.000	426.0	1.18e-19	1.000	426.5	1.30e-19	1.000	427.0	1.07e-19	1.000
428.0	1.66e-19	1.000	429.0	4.05e-20	1.000	430.0	5.07e-20	1.000	431.0	4.86e-20	1.000	432.0	4.05e-20	1.000

Table A-3 (continued)

WL (nm)	Abs (cm^2)	QY	WL (nm)	Abs (cm^2)	QY	WL (nm)	Abs (cm^2)	QY	WL (nm)	Abs (cm^2)	QY	WL (nm)	Abs (cm^2)	QY
433.0	3.65e-20	1.000	434.0	4.05e-20	1.000	434.5	6.08e-20	1.000	435.0	5.07e-20	1.000	436.0	8.11e-20	1.000
436.5	1.13e-19	1.000	437.0	5.27e-20	1.000	438.0	1.01e-19	1.000	438.5	1.38e-19	1.000	439.0	7.70e-20	1.000
440.0	2.47e-19	1.000	441.0	8.11e-20	1.000	442.0	6.08e-20	1.000	443.0	7.50e-20	1.000	444.0	9.32e-20	1.000
445.0	1.13e-19	1.000	446.0	5.27e-20	1.000	447.0	2.43e-20	1.000	448.0	2.84e-20	1.000	449.0	3.85e-20	1.000
450.0	6.08e-20	1.000	451.0	1.09e-19	1.000	451.5	9.32e-20	1.000	452.0	1.22e-19	1.000	453.0	2.39e-19	1.000
454.0	1.70e-19	1.000	455.0	3.40e-19	1.000	455.5	4.05e-19	1.000	456.0	1.01e-19	1.000	457.0	1.62e-20	1.000
458.0	1.22e-20	1.000	458.5	1.42e-20	1.000	459.0	4.05e-21	1.000	460.0	4.05e-21	1.000	460.5	6.08e-21	1.000
461.0	2.03e-21	1.000	462.0	0.00e+00	1.000									
						MGLY_ADJ								
219.0	9.84e-21	1.000	219.5	1.04e-20	1.000	220.0	1.06e-20	1.000	220.5	1.11e-20	1.000	221.0	1.15e-20	1.000
221.5	1.18e-20	1.000	222.0	1.22e-20	1.000	222.5	1.24e-20	1.000	223.0	1.26e-20	1.000	223.5	1.26e-20	1.000
224.0	1.25e-20	1.000	224.5	1.24e-20	1.000	225.0	1.25e-20	1.000	225.5	1.27e-20	1.000	226.0	1.27e-20	1.000
226.5	1.29e-20	1.000	227.0	1.31e-20	1.000	227.5	1.32e-20	1.000	228.0	1.35e-20	1.000	228.5	1.37e-20	1.000
229.0	1.40e-20	1.000	229.5	1.42e-20	1.000	230.0	1.48e-20	1.000	230.5	1.53e-20	1.000	231.0	1.57e-20	1.000
231.5	1.59e-20	1.000	232.0	1.61e-20	1.000	232.5	1.62e-20	1.000	233.0	1.61e-20	1.000	233.5	1.68e-20	1.000
234.0	1.74e-20	1.000	234.5	1.80e-20	1.000	235.0	1.84e-20	1.000	235.5	1.87e-20	1.000	236.0	1.89e-20	1.000
236.5	1.91e-20	1.000	237.0	1.93e-20	1.000	237.5	1.94e-20	1.000	238.0	1.96e-20	1.000	238.5	1.96e-20	1.000
239.0	2.01e-20	1.000	239.5	2.04e-20	1.000	240.0	2.08e-20	1.000	240.5	2.10e-20	1.000	241.0	2.14e-20	1.000
241.5	2.16e-20	1.000	242.0	2.19e-20	1.000	242.5	2.20e-20	1.000	243.0	2.23e-20	1.000	243.5	2.26e-20	1.000
244.0	2.28e-20	1.000	244.5	2.29e-20	1.000	245.0	2.30e-20	1.000	245.5	2.32e-20	1.000	246.0	2.33e-20	1.000
246.5	2.35e-20	1.000	247.0	2.38e-20	1.000	247.5	2.41e-20	1.000	248.0	2.46e-20	1.000	248.5	2.51e-20	1.000
249.0	2.57e-20	1.000	249.5	2.61e-20	1.000	250.0	2.65e-20	1.000	250.5	2.67e-20	1.000	251.0	2.69e-20	1.000
251.5	2.69e-20	1.000	252.0	2.71e-20	1.000	252.5	2.72e-20	1.000	253.0	2.73e-20	1.000	253.5	2.74e-20	1.000
254.0	2.76e-20	1.000	254.5	2.78e-20	1.000	255.0	2.82e-20	1.000	255.5	2.87e-20	1.000	256.0	2.93e-20	1.000
256.5	2.98e-20	1.000	257.0	3.07e-20	1.000	257.5	3.12e-20	1.000	258.0	3.17e-20	1.000	258.5	3.21e-20	1.000
259.0	3.26e-20	1.000	259.5	3.28e-20	1.000	260.0	3.29e-20	1.000	260.5	3.31e-20	1.000	261.0	3.33e-20	1.000
261.5	3.34e-20	1.000	262.0	3.36e-20	1.000	262.5	3.38e-20	1.000	263.0	3.42e-20	1.000	263.5	3.44e-20	1.000
264.0	3.48e-20	1.000	264.5	3.54e-20	1.000	265.0	3.59e-20	1.000	265.5	3.65e-20	1.000	266.0	3.73e-20	1.000
266.5	3.80e-20	1.000	267.0	3.87e-20	1.000	267.5	3.95e-20	1.000	268.0	4.02e-20	1.000	268.5	4.08e-20	1.000
269.0	4.13e-20	1.000	269.5	4.17e-20	1.000	270.0	4.20e-20	1.000	270.5	4.22e-20	1.000	271.0	4.22e-20	1.000
271.5	4.22e-20	1.000	272.0	4.23e-20	1.000	272.5	4.24e-20	1.000	273.0	4.27e-20	1.000	273.5	4.29e-20	1.000
274.0	4.31e-20	1.000	274.5	4.33e-20	1.000	275.0	4.37e-20	1.000	275.5	4.42e-20	1.000	276.0	4.48e-20	1.000
276.5	4.56e-20	1.000	277.0	4.64e-20	1.000	277.5	4.71e-20	1.000	278.0	4.78e-20	1.000	278.5	4.83e-20	1.000
279.0	4.87e-20	1.000	279.5	4.90e-20	1.000	280.0	4.92e-20	1.000	280.5	4.93e-20	1.000	281.0	4.94e-20	1.000
281.5	4.92e-20	1.000	282.0	4.90e-20	1.000	282.5	4.86e-20	1.000	283.0	4.83e-20	1.000	283.5	4.79e-20	1.000
284.0	4.76e-20	1.000	284.5	4.72e-20	1.000	285.0	4.70e-20	1.000	285.5	4.68e-20	1.000	286.0	4.66e-20	1.000
286.5	4.65e-20	1.000	287.0	4.65e-20	1.000	287.5	4.68e-20	1.000	288.0	4.73e-20	1.000	288.5	4.78e-20	1.000
289.0	4.84e-20	1.000	289.5	4.89e-20	1.000	290.0	4.92e-20	1.000	290.5	4.92e-20	1.000	291.0	4.90e-20	1.000
291.5	4.86e-20	1.000	292.0	4.81e-20	1.000	292.5	4.75e-20	1.000	293.0	4.70e-20	1.000	293.5	4.65e-20	1.000
294.0	4.58e-20	1.000	294.5	4.48e-20	1.000	295.0	4.38e-20	1.000	295.5	4.27e-20	1.000	296.0	4.17e-20	1.000
296.5	4.07e-20	1.000	297.0	3.99e-20	1.000	297.5	3.94e-20	1.000	298.0	3.88e-20	1.000	298.5	3.82e-20	1.000
299.0	3.76e-20	1.000	299.5	3.72e-20	1.000	300.0	3.69e-20	1.000	300.5	3.68e-20	1.000	301.0	3.70e-20	1.000
301.5	3.72e-20	1.000	302.0	3.74e-20	1.000	302.5	3.74e-20	1.000	303.0	3.75e-20	1.000	303.5	3.71e-20	1.000
304.0	3.62e-20	1.000	304.5	3.51e-20	1.000	305.0	3.38e-20	1.000	305.5	3.25e-20	1.000	306.0	3.15e-20	1.000
306.5	3.04e-20	1.000	307.0	2.92e-20	1.000	307.5	2.80e-20	1.000	308.0	2.71e-20	1.000	308.5	2.63e-20	1.000
309.0	2.52e-20	1.000	309.5	2.43e-20	1.000	310.0	2.34e-20	1.000	310.5	2.25e-20	1.000	311.0	2.19e-20	1.000
311.5	2.12e-20	1.000	312.0	2.06e-20	1.000	312.5	2.02e-20	1.000	313.0	1.96e-20	1.000	313.5	1.92e-20	1.000
314.0	1.91e-20	1.000	314.5	1.88e-20	1.000	315.0	1.86e-20	1.000	315.5	1.85e-20	1.000	316.0	1.86e-20	1.000
316.5	1.87e-20	1.000	317.0	1.87e-20	1.000	317.5	1.87e-20	1.000	318.0	1.83e-20	1.000	318.5	1.75e-20	1.000
319.0	1.69e-20	1.000	319.5	1.60e-20	1.000	320.0	1.50e-20	1.000	320.5	1.41e-20	1.000	321.0	1.34e-20	1.000
321.5	1.27e-20	1.000	322.0	1.21e-20	1.000	322.5	1.18e-20	1.000	323.0	1.14e-20	1.000	323.5	1.08e-20	1.000
324.0	1.01e-20	1.000	324.5	9.62e-21	1.000	325.0	9.28e-21	1.000	325.5	8.75e-21	1.000	326.0	8.49e-21	1.000
326.5	8.21e-21	1.000	327.0	7.71e-21	1.000	327.5	7.38e-21	1.000	328.0	7.18e-21	1.000	328.5	6.86e-21	1.000
329.0	6.71e-21	1.000	329.5	6.63e-21	1.000	330.0	6.46e-21	1.000	330.5	6.29e-21	1.000	331.0	6.21e-21	1.000
331.5	6.18e-21	1.000	332.0	6.20e-21	1.000	332.5	5.49e-21	1.000	333.0	5.21e-21	1.000	333.5	5.38e-21	1.000
334.0	5.35e-21	1.000	334.5	5.04e-21	1.000	335.0	4.94e-21	1.000	335.5	4.90e-21	1.000	336.0	4.52e-21	1.000
336.5	4.26e-21	1.000	337.0	4.11e-21	1.000	337.5	3.76e-21	1.000	338.0	3.61e-21	1.000	338.5	3.58e-21	1.000
339.0	3.47e-21	1.000	339.5	3.32e-21	1.000	340.0	3.22e-21	1.000	340.5	3.10e-21	1.000	341.0	3.00e-21	1.000
341.5	2.94e-21	1.000	342.0	2.89e-21	1.000	342.5	2.86e-21	1.000	343.0	2.88e-21	1.000	343.5	2.88e-21	1.000
344.0	2.89e-21	0.992	344.5	2.91e-21	0.984	345.0	2.95e-21	0.976	345.5	3.00e-21	0.968	346.0	3.08e-21	0.960
346.5	3.18e-21	0.953	347.0	3.25e-21	0.945	347.5	3.30e-21	0.937	348.0	3.39e-21	0.929	348.5	3.51e-21	0.921
349.0	3.63e-21	0.913	349.5	3.73e-21	0.905	350.0	3.85e-21	0.897	350.5	3.99e-21	0.889	351.0	4.27e-21	0.881
351.5	4.47e-21	0.873	352.0	4.63e-21	0.865	352.5	4.78e-21	0.858	353.0	4.92e-21	0.850	353.5	5.07e-21	0.842
354.0	5.23e-21	0.834	354.5	5.39e-21	0.826	355.0	5.56e-21	0.818	355.5	5.77e-21	0.810	356.0	5.97e-21	0.802
356.5	6.15e-21	0.794	357.0	6.35e-21	0.786	357.5	6.56e-21	0.778	358.0	6.76e-21	0.770	358.5	6.95e-21	0.763
359.0	7.20e-21	0.755	359.5	7.44e-21	0.747	360.0	7.64e-21	0.739	360.5	7.89e-21	0.731	361.0	8.15e-21	0.723
361.5	8.43e-21	0.715	362.0	8.71e-21	0.707	362.5	9.02e-21	0.699	363.0	9.33e-21	0.691	363.5	9.65e-21	0.683
364.0	1.00e-20	0.675	364.5	1.04e-20	0.668	365.0	1.08e-20	0.660	365.5	1.11e-20	0.652	366.0	1.15e-20	0.644
366.5	1.19e-20	0.636	367.0	1.23e-20	0.628	367.5	1.27e-20	0.620	368.0	1.31e-20	0.612	368.5	1.35e-20	0.604
369.0	1.40e-20	0.596	369.5	1.44e-20	0.588	370.0	1.47e-20	0.580	370.5	1.51e-20	0.573	371.0	1.55e-20	0.565
371.5	1.59e-20	0.557	372.0	1.64e-20	0.549	372.5	1.70e-20	0.541	373.0	1.73e-20	0.533	373.5	1.77e-20	0.525
374.0	1.81e-20	0.517	374.5	1.86e-20	0.509	375.0	1.90e-20	0.501	375.5	1.96e-20	0.493	376.0	2.02e-20	0.486

Table A-3 (continued)

WL (nm)	Abs (cm^2)	QY	WL (nm)	Abs (cm^2)	QY	WL (nm)	Abs (cm^2)	QY	WL (nm)	Abs (cm^2)	QY	WL (nm)	Abs (cm^2)	QY
376.5	2.06e-20	0.478	377.0	2.10e-20	0.470	377.5	2.14e-20	0.462	378.0	2.18e-20	0.454	378.5	2.24e-20	0.446
379.0	2.30e-20	0.438	379.5	2.37e-20	0.430	380.0	2.42e-20	0.422	380.5	2.47e-20	0.414	381.0	2.54e-20	0.406
381.5	2.62e-20	0.398	382.0	2.69e-20	0.391	382.5	2.79e-20	0.383	383.0	2.88e-20	0.375	383.5	2.96e-20	0.367
384.0	3.02e-20	0.359	384.5	3.10e-20	0.351	385.0	3.20e-20	0.343	385.5	3.29e-20	0.335	386.0	3.39e-20	0.327
386.5	3.51e-20	0.319	387.0	3.62e-20	0.311	387.5	3.69e-20	0.303	388.0	3.70e-20	0.296	388.5	3.77e-20	0.288
389.0	3.88e-20	0.280	389.5	3.97e-20	0.272	390.0	4.03e-20	0.264	390.5	4.12e-20	0.256	391.0	4.22e-20	0.248
391.5	4.29e-20	0.240	392.0	4.30e-20	0.232	392.5	4.38e-20	0.224	393.0	4.47e-20	0.216	393.5	4.55e-20	0.208
394.0	4.56e-20	0.201	394.5	4.59e-20	0.193	395.0	4.67e-20	0.185	395.5	4.80e-20	0.177	396.0	4.87e-20	0.169
396.5	4.96e-20	0.161	397.0	5.08e-20	0.153	397.5	5.19e-20	0.145	398.0	5.23e-20	0.137	398.5	5.39e-20	0.129
399.0	5.46e-20	0.121	399.5	5.54e-20	0.113	400.0	5.59e-20	0.106	400.5	5.77e-20	0.098	401.0	5.91e-20	0.090
401.5	5.99e-20	0.082	402.0	6.06e-20	0.074	402.5	6.20e-20	0.066	403.0	6.35e-20	0.058	403.5	6.52e-20	0.050
404.0	6.54e-20	0.042	404.5	6.64e-20	0.034	405.0	6.93e-20	0.026	405.5	7.15e-20	0.018	406.0	7.19e-20	0.011
406.5	7.32e-20	0.003	407.0	7.58e-20	0.000	407.5	7.88e-20	0.000	408.0	7.97e-20	0.000	408.5	7.91e-20	0.000
409.0	8.11e-20	0.000	409.5	8.41e-20	0.000	410.0	8.53e-20	0.000	410.5	8.59e-20	0.000	411.0	8.60e-20	0.000
411.5	8.80e-20	0.000	412.0	9.04e-20	0.000	412.5	9.45e-20	0.000	413.0	9.34e-20	0.000	413.5	9.37e-20	0.000
414.0	9.63e-20	0.000	414.5	9.71e-20	0.000	415.0	9.70e-20	0.000	415.5	9.65e-20	0.000	416.0	9.69e-20	0.000
416.5	9.89e-20	0.000	417.0	1.00e-19	0.000	417.5	1.02e-19	0.000	418.0	1.00e-19	0.000	418.5	1.02e-19	0.000
419.0	1.01e-19	0.000	419.5	1.01e-19	0.000	420.0	1.03e-19	0.000	420.5	1.01e-19	0.000	421.0	1.04e-19	0.000
							BACL_ADJ							
230.0	1.30e-20	1.000	232.5	1.46e-20	1.000	235.0	1.68e-20	1.000	237.5	1.84e-20	1.000	240.0	2.16e-20	1.000
242.5	2.49e-20	1.000	245.0	2.65e-20	1.000	247.5	2.71e-20	1.000	250.0	3.03e-20	1.000	252.5	3.46e-20	1.000
255.0	3.46e-20	1.000	257.5	3.57e-20	1.000	260.0	3.95e-20	1.000	262.5	4.17e-20	1.000	265.0	4.17e-20	1.000
267.5	4.22e-20	1.000	270.0	4.60e-20	1.000	272.5	4.54e-20	1.000	275.0	4.33e-20	1.000	277.5	4.22e-20	1.000
280.0	4.44e-20	1.000	282.5	4.33e-20	1.000	285.0	3.90e-20	1.000	287.5	3.57e-20	1.000	290.0	3.25e-20	1.000
292.5	2.92e-20	1.000	295.0	2.60e-20	1.000	297.5	2.16e-20	1.000	300.0	1.79e-20	1.000	302.5	1.73e-20	1.000
305.0	1.46e-20	1.000	307.5	1.08e-20	1.000	310.0	9.20e-21	1.000	312.5	7.03e-21	1.000	315.0	6.49e-21	1.000
317.5	5.41e-21	1.000	320.0	5.41e-21	1.000	322.5	5.41e-21	1.000	325.0	4.33e-21	1.000	327.5	3.25e-21	1.000
330.0	3.79e-21	1.000	332.5	3.79e-21	1.000	335.0	4.33e-21	1.000	337.5	4.87e-21	1.000	340.0	5.41e-21	1.000
342.5	5.95e-21	1.000	345.0	6.49e-21	1.000	347.5	7.03e-21	1.000	350.0	8.12e-21	0.995	352.5	7.57e-21	0.960
355.0	9.20e-21	0.925	357.5	9.74e-21	0.890	360.0	1.08e-20	0.855	362.5	1.19e-20	0.820	365.0	1.41e-20	0.785
367.5	1.51e-20	0.750	370.0	1.79e-20	0.715	372.5	2.00e-20	0.680	375.0	2.11e-20	0.645	377.5	2.33e-20	0.610
380.0	2.60e-20	0.575	382.5	2.81e-20	0.540	385.0	3.14e-20	0.505	387.5	3.46e-20	0.470	390.0	3.90e-20	0.435
392.5	4.11e-20	0.399	395.0	4.33e-20	0.364	397.5	4.38e-20	0.329	400.0	4.65e-20	0.294	402.5	4.81e-20	0.259
405.0	5.19e-20	0.224	407.5	5.84e-20	0.189	410.0	6.06e-20	0.154	412.5	6.49e-20	0.119	415.0	6.92e-20	0.084
417.5	6.87e-20	0.049	420.0	6.82e-20	0.014	422.5	6.71e-20	0.000	425.0	6.49e-20	0.000	427.5	5.95e-20	0.000
430.0	5.73e-20	0.000	432.5	6.28e-20	0.000	435.0	6.01e-20	0.000	437.5	5.84e-20	0.000	440.0	5.95e-20	0.000
442.5	6.49e-20	0.000	445.0	5.95e-20	0.000	447.5	4.98e-20	0.000	450.0	3.79e-20	0.000	452.5	2.81e-20	0.000
455.0	1.73e-20	0.000	457.5	1.08e-20	0.000	460.0	5.41e-21	0.000	462.5	3.79e-21	0.000	465.0	2.16e-21	0.000
467.5	1.08e-21	0.000	470.0	1.08e-21	0.000	472.5	0.00e+00	0.000						
							BZCHO							
299.0	1.78e-19	1.000	304.0	7.40e-20	1.000	306.0	6.91e-20	1.000	309.0	6.41e-20	1.000	313.0	6.91e-20	1.000
314.0	6.91e-20	1.000	318.0	6.41e-20	1.000	325.0	8.39e-20	1.000	332.0	7.65e-20	1.000	338.0	8.88e-20	1.000
342.0	8.88e-20	1.000	346.0	7.89e-20	1.000	349.0	7.89e-20	1.000	354.0	9.13e-20	1.000	355.0	8.14e-20	1.000
364.0	5.67e-20	1.000	368.0	6.66e-20	1.000	369.0	8.39e-20	1.000	370.0	8.39e-20	1.000	372.0	3.45e-20	1.000
374.0	3.21e-20	1.000	376.0	2.47e-20	1.000	377.0	2.47e-20	1.000	380.0	3.58e-20	1.000	382.0	9.90e-21	1.000
386.0	0.00e+00	1.000												
							ACROLEIN							
250.0	1.80e-21	1.000	252.0	2.05e-21	1.000	253.0	2.20e-21	1.000	254.0	2.32e-21	1.000	255.0	2.45e-21	1.000
256.0	2.56e-21	1.000	257.0	2.65e-21	1.000	258.0	2.74e-21	1.000	259.0	2.83e-21	1.000	260.0	2.98e-21	1.000
261.0	3.24e-21	1.000	262.0	3.47e-21	1.000	263.0	3.58e-21	1.000	264.0	3.93e-21	1.000	265.0	4.67e-21	1.000
266.0	5.10e-21	1.000	267.0	5.38e-21	1.000	268.0	5.73e-21	1.000	269.0	6.13e-21	1.000	270.0	6.64e-21	1.000
271.0	7.20e-21	1.000	272.0	7.77e-21	1.000	273.0	8.37e-21	1.000	274.0	8.94e-21	1.000	275.0	9.55e-21	1.000
276.0	1.04e-20	1.000	277.0	1.12e-20	1.000	278.0	1.19e-20	1.000	279.0	1.27e-20	1.000	280.0	1.27e-20	1.000
281.0	1.26e-20	1.000	282.0	1.26e-20	1.000	283.0	1.28e-20	1.000	284.0	1.33e-20	1.000	285.0	1.38e-20	1.000
286.0	1.44e-20	1.000	287.0	1.50e-20	1.000	288.0	1.57e-20	1.000	289.0	1.63e-20	1.000	290.0	1.71e-20	1.000
291.0	1.78e-20	1.000	292.0	1.86e-20	1.000	293.0	1.95e-20	1.000	294.0	2.05e-20	1.000	295.0	2.15e-20	1.000
296.0	2.26e-20	1.000	297.0	2.37e-20	1.000	298.0	2.48e-20	1.000	299.0	2.60e-20	1.000	300.0	2.73e-20	1.000
301.0	2.85e-20	1.000	302.0	2.99e-20	1.000	303.0	3.13e-20	1.000	304.0	3.27e-20	1.000	305.0	3.39e-20	1.000
306.0	3.51e-20	1.000	307.0	3.63e-20	1.000	308.0	3.77e-20	1.000	309.0	3.91e-20	1.000	310.0	4.07e-20	1.000
311.0	4.25e-20	1.000	312.0	4.39e-20	1.000	313.0	4.44e-20	1.000	314.0	4.50e-20	1.000	315.0	4.59e-20	1.000
316.0	4.75e-20	1.000	317.0	4.90e-20	1.000	318.0	5.05e-20	1.000	319.0	5.19e-20	1.000	320.0	5.31e-20	1.000
321.0	5.43e-20	1.000	322.0	5.52e-20	1.000	323.0	5.60e-20	1.000	324.0	5.67e-20	1.000	325.0	5.67e-20	1.000
326.0	5.62e-20	1.000	327.0	5.63e-20	1.000	328.0	5.71e-20	1.000	329.0	5.76e-20	1.000	330.0	5.80e-20	1.000
331.0	5.95e-20	1.000	332.0	6.23e-20	1.000	333.0	6.39e-20	1.000	334.0	6.38e-20	1.000	335.0	6.24e-20	1.000
336.0	6.01e-20	1.000	337.0	5.79e-20	1.000	338.0	5.63e-20	1.000	339.0	5.56e-20	1.000	340.0	5.52e-20	1.000
341.0	5.54e-20	1.000	342.0	5.53e-20	1.000	343.0	5.47e-20	1.000	344.0	5.41e-20	1.000	345.0	5.40e-20	1.000
346.0	5.48e-20	1.000	347.0	5.90e-20	1.000	348.0	6.08e-20	1.000	349.0	6.00e-20	1.000	350.0	5.53e-20	1.000
351.0	5.03e-20	1.000	352.0	4.50e-20	1.000	353.0	4.03e-20	1.000	354.0	3.75e-20	1.000	355.0	3.55e-20	1.000
356.0	3.45e-20	1.000	357.0	3.46e-20	1.000	358.0	3.49e-20	1.000	359.0	3.41e-20	1.000	360.0	3.23e-20	1.000
361.0	2.95e-20	1.000	362.0	2.81e-20	1.000	363.0	2.91e-20	1.000	364.0	3.25e-20	1.000	365.0	3.54e-20	1.000
366.0	3.30e-20	1.000	367.0	2.78e-20	1.000	368.0	2.15e-20	1.000	369.0	1.59e-20	1.000	370.0	1.19e-20	1.000

Table A-3 (continued)

WL (nm)	Abs (cm^2)	QY	WL (nm)	Abs (cm^2)	QY	WL (nm)	Abs (cm^2)	QY	WL (nm)	Abs (cm^2)	QY	WL (nm)	Abs (cm^2)	QY
371.0	8.99e-21	1.000	372.0	7.22e-21	1.000	373.0	5.86e-21	1.000	374.0	4.69e-21	1.000	375.0	3.72e-21	1.000
376.0	3.57e-21	1.000	377.0	3.55e-21	1.000	378.0	2.83e-21	1.000	379.0	1.69e-21	1.000	380.0	8.29e-24	1.000
381.0	0.00e+00	1.000												
							IC3ONO2							
185.0	1.79e-17	1.000	188.0	1.81e-17	1.000	190.0	1.79e-17	1.000	195.0	1.61e-17	1.000	200.0	1.26e-17	1.000
205.0	8.67e-18	1.000	210.0	4.98e-18	1.000	215.0	2.47e-18	1.000	220.0	1.17e-18	1.000	225.0	5.80e-19	1.000
230.0	3.10e-19	1.000	235.0	1.80e-19	1.000	240.0	1.10e-19	1.000	245.0	7.00e-20	1.000	250.0	5.70e-20	1.000
255.0	5.20e-20	1.000	260.0	4.90e-20	1.000	265.0	4.60e-20	1.000	270.0	4.10e-20	1.000	275.0	3.60e-20	1.000
280.0	2.90e-20	1.000	285.0	2.30e-20	1.000	290.0	1.70e-20	1.000	295.0	1.20e-20	1.000	300.0	8.10e-21	1.000
305.0	5.20e-21	1.000	310.0	3.20e-21	1.000	315.0	1.90e-21	1.000	320.0	1.10e-21	1.000	325.0	6.10e-22	1.000
330.0	3.70e-22	1.000	335.0	0.00e+00	1.000									
							MGLY_ABS							
219.0	9.84e-21	1.000	219.5	1.04e-20	1.000	220.0	1.06e-20	1.000	220.5	1.11e-20	1.000	221.0	1.15e-20	1.000
221.5	1.18e-20	1.000	222.0	1.22e-20	1.000	222.5	1.24e-20	1.000	223.0	1.26e-20	1.000	223.5	1.26e-20	1.000
224.0	1.25e-20	1.000	224.5	1.24e-20	1.000	225.0	1.25e-20	1.000	225.5	1.27e-20	1.000	226.0	1.27e-20	1.000
226.5	1.29e-20	1.000	227.0	1.31e-20	1.000	227.5	1.32e-20	1.000	228.0	1.35e-20	1.000	228.5	1.37e-20	1.000
229.0	1.40e-20	1.000	229.5	1.42e-20	1.000	230.0	1.48e-20	1.000	230.5	1.53e-20	1.000	231.0	1.57e-20	1.000
231.5	1.59e-20	1.000	232.0	1.61e-20	1.000	232.5	1.62e-20	1.000	233.0	1.61e-20	1.000	233.5	1.68e-20	1.000
234.0	1.74e-20	1.000	234.5	1.80e-20	1.000	235.0	1.84e-20	1.000	235.5	1.87e-20	1.000	236.0	1.89e-20	1.000
236.5	1.91e-20	1.000	237.0	1.93e-20	1.000	237.5	1.94e-20	1.000	238.0	1.96e-20	1.000	238.5	1.96e-20	1.000
239.0	2.01e-20	1.000	239.5	2.04e-20	1.000	240.0	2.08e-20	1.000	240.5	2.10e-20	1.000	241.0	2.14e-20	1.000
241.5	2.16e-20	1.000	242.0	2.19e-20	1.000	242.5	2.20e-20	1.000	243.0	2.23e-20	1.000	243.5	2.26e-20	1.000
244.0	2.28e-20	1.000	244.5	2.29e-20	1.000	245.0	2.30e-20	1.000	245.5	2.32e-20	1.000	246.0	2.33e-20	1.000
246.5	2.35e-20	1.000	247.0	2.38e-20	1.000	247.5	2.41e-20	1.000	248.0	2.46e-20	1.000	248.5	2.51e-20	1.000
249.0	2.57e-20	1.000	249.5	2.61e-20	1.000	250.0	2.65e-20	1.000	250.5	2.67e-20	1.000	251.0	2.69e-20	1.000
251.5	2.69e-20	1.000	252.0	2.71e-20	1.000	252.5	2.72e-20	1.000	253.0	2.73e-20	1.000	253.5	2.74e-20	1.000
254.0	2.76e-20	1.000	254.5	2.78e-20	1.000	255.0	2.82e-20	1.000	255.5	2.87e-20	1.000	256.0	2.93e-20	1.000
256.5	2.98e-20	1.000	257.0	3.07e-20	1.000	257.5	3.12e-20	1.000	258.0	3.17e-20	1.000	258.5	3.21e-20	1.000
259.0	3.26e-20	1.000	259.5	3.28e-20	1.000	260.0	3.29e-20	1.000	260.5	3.31e-20	1.000	261.0	3.33e-20	1.000
261.5	3.34e-20	1.000	262.0	3.36e-20	1.000	262.5	3.38e-20	1.000	263.0	3.42e-20	1.000	263.5	3.44e-20	1.000
264.0	3.48e-20	1.000	264.5	3.54e-20	1.000	265.0	3.59e-20	1.000	265.5	3.65e-20	1.000	266.0	3.73e-20	1.000
266.5	3.80e-20	1.000	267.0	3.87e-20	1.000	267.5	3.95e-20	1.000	268.0	4.02e-20	1.000	268.5	4.08e-20	1.000
269.0	4.13e-20	1.000	269.5	4.17e-20	1.000	270.0	4.20e-20	1.000	270.5	4.22e-20	1.000	271.0	4.22e-20	1.000
271.5	4.22e-20	1.000	272.0	4.23e-20	1.000	272.5	4.24e-20	1.000	273.0	4.27e-20	1.000	273.5	4.29e-20	1.000
274.0	4.31e-20	1.000	274.5	4.33e-20	1.000	275.0	4.37e-20	1.000	275.5	4.42e-20	1.000	276.0	4.48e-20	1.000
276.5	4.56e-20	1.000	277.0	4.64e-20	1.000	277.5	4.71e-20	1.000	278.0	4.78e-20	1.000	278.5	4.83e-20	1.000
279.0	4.87e-20	1.000	279.5	4.90e-20	1.000	280.0	4.92e-20	1.000	280.5	4.93e-20	1.000	281.0	4.94e-20	1.000
281.5	4.92e-20	1.000	282.0	4.90e-20	1.000	282.5	4.86e-20	1.000	283.0	4.83e-20	1.000	283.5	4.79e-20	1.000
284.0	4.76e-20	1.000	284.5	4.72e-20	1.000	285.0	4.70e-20	1.000	285.5	4.68e-20	1.000	286.0	4.66e-20	1.000
286.5	4.65e-20	1.000	287.0	4.65e-20	1.000	287.5	4.68e-20	1.000	288.0	4.73e-20	1.000	288.5	4.78e-20	1.000
289.0	4.84e-20	1.000	289.5	4.89e-20	1.000	290.0	4.92e-20	1.000	290.5	4.92e-20	1.000	291.0	4.90e-20	1.000
291.5	4.86e-20	1.000	292.0	4.81e-20	1.000	292.5	4.75e-20	1.000	293.0	4.70e-20	1.000	293.5	4.65e-20	1.000
294.0	4.58e-20	1.000	294.5	4.48e-20	1.000	295.0	4.38e-20	1.000	295.5	4.27e-20	1.000	296.0	4.17e-20	1.000
296.5	4.07e-20	1.000	297.0	3.99e-20	1.000	297.5	3.94e-20	1.000	298.0	3.88e-20	1.000	298.5	3.82e-20	1.000
299.0	3.76e-20	1.000	299.5	3.72e-20	1.000	300.0	3.69e-20	1.000	300.5	3.68e-20	1.000	301.0	3.70e-20	1.000
301.5	3.72e-20	1.000	302.0	3.74e-20	1.000	302.5	3.74e-20	1.000	303.0	3.75e-20	1.000	303.5	3.71e-20	1.000
304.0	3.62e-20	1.000	304.5	3.51e-20	1.000	305.0	3.38e-20	1.000	305.5	3.25e-20	1.000	306.0	3.15e-20	1.000
306.5	3.04e-20	1.000	307.0	2.92e-20	1.000	307.5	2.80e-20	1.000	308.0	2.71e-20	1.000	308.5	2.63e-20	1.000
309.0	2.52e-20	1.000	309.5	2.43e-20	1.000	310.0	2.34e-20	1.000	310.5	2.25e-20	1.000	311.0	2.19e-20	1.000
311.5	2.12e-20	1.000	312.0	2.06e-20	1.000	312.5	2.02e-20	1.000	313.0	1.96e-20	1.000	313.5	1.92e-20	1.000
314.0	1.91e-20	1.000	314.5	1.88e-20	1.000	315.0	1.86e-20	1.000	315.5	1.85e-20	1.000	316.0	1.86e-20	1.000
316.5	1.87e-20	1.000	317.0	1.87e-20	1.000	317.5	1.87e-20	1.000	318.0	1.83e-20	1.000	318.5	1.75e-20	1.000
319.0	1.69e-20	1.000	319.5	1.60e-20	1.000	320.0	1.50e-20	1.000	320.5	1.41e-20	1.000	321.0	1.34e-20	1.000
321.5	1.27e-20	1.000	322.0	1.21e-20	1.000	322.5	1.18e-20	1.000	323.0	1.14e-20	1.000	323.5	1.08e-20	1.000
324.0	1.01e-20	1.000	324.5	9.62e-21	1.000	325.0	9.28e-21	1.000	325.5	8.75e-21	1.000	326.0	8.49e-21	1.000
326.5	8.21e-21	1.000	327.0	7.71e-21	1.000	327.5	7.38e-21	1.000	328.0	7.18e-21	1.000	328.5	6.86e-21	1.000
329.0	6.71e-21	1.000	329.5	6.63e-21	1.000	330.0	6.46e-21	1.000	330.5	6.29e-21	1.000	331.0	6.21e-21	1.000
331.5	6.18e-21	1.000	332.0	6.20e-21	1.000	332.5	5.49e-21	1.000	333.0	5.21e-21	1.000	333.5	5.38e-21	1.000
334.0	5.35e-21	1.000	334.5	5.04e-21	1.000	335.0	4.94e-21	1.000	335.5	4.90e-21	1.000	336.0	4.52e-21	1.000
336.5	4.26e-21	1.000	337.0	4.11e-21	1.000	337.5	3.76e-21	1.000	338.0	3.61e-21	1.000	338.5	3.58e-21	1.000
339.0	3.47e-21	1.000	339.5	3.32e-21	1.000	340.0	3.22e-21	1.000	340.5	3.10e-21	1.000	341.0	3.00e-21	1.000
341.5	2.94e-21	1.000	342.0	2.89e-21	1.000	342.5	2.86e-21	1.000	343.0	2.88e-21	1.000	343.5	2.88e-21	1.000
344.0	2.89e-21	1.000	344.5	2.91e-21	1.000	345.0	2.95e-21	1.000	345.5	3.00e-21	1.000	346.0	3.08e-21	1.000
346.5	3.18e-21	1.000	347.0	3.25e-21	1.000	347.5	3.30e-21	1.000	348.0	3.39e-21	1.000	348.5	3.51e-21	1.000
349.0	3.63e-21	1.000	349.5	3.73e-21	1.000	350.0	3.85e-21	1.000	350.5	3.99e-21	1.000	351.0	4.27e-21	1.000
351.5	4.47e-21	1.000	352.0	4.63e-21	1.000	352.5	4.78e-21	1.000	353.0	4.92e-21	1.000	353.5	5.07e-21	1.000
354.0	5.23e-21	1.000	354.5	5.39e-21	1.000	355.0	5.56e-21	1.000	355.5	5.77e-21	1.000	356.0	5.97e-21	1.000
356.5	6.15e-21	1.000	357.0	6.35e-21	1.000	357.5	6.56e-21	1.000	358.0	6.76e-21	1.000	358.5	6.95e-21	1.000
359.0	7.20e-21	1.000	359.5	7.44e-21	1.000	360.0	7.64e-21	1.000	360.5	7.89e-21	1.000	361.0	8.15e-21	1.000
361.5	8.43e-21	1.000	362.0	8.71e-21	1.000	362.5	9.02e-21	1.000	363.0	9.33e-21	1.000	363.5	9.65e-21	1.000
364.0	1.00e-20	1.000	364.5	1.04e-20	1.000	365.0	1.08e-20	1.000	365.5	1.11e-20	1.000	366.0	1.15e-20	1.000

Table A-3 (continued)

WL (nm)	Abs (cm^2)	QY	WL (nm)	Abs (cm^2)	QY	WL (nm)	Abs (cm^2)	QY	WL (nm)	Abs (cm^2)	QY	WL (nm)	Abs (cm^2)	QY
366.5	1.19e-20	1.000	367.0	1.23e-20	1.000	367.5	1.27e-20	1.000	368.0	1.31e-20	1.000	368.5	1.35e-20	1.000
369.0	1.40e-20	1.000	369.5	1.44e-20	1.000	370.0	1.47e-20	1.000	370.5	1.51e-20	1.000	371.0	1.55e-20	1.000
371.5	1.59e-20	1.000	372.0	1.64e-20	1.000	372.5	1.70e-20	1.000	373.0	1.73e-20	1.000	373.5	1.77e-20	1.000
374.0	1.81e-20	1.000	374.5	1.86e-20	1.000	375.0	1.90e-20	1.000	375.5	1.96e-20	1.000	376.0	2.02e-20	1.000
376.5	2.06e-20	1.000	377.0	2.10e-20	1.000	377.5	2.14e-20	1.000	378.0	2.18e-20	1.000	378.5	2.24e-20	1.000
379.0	2.30e-20	1.000	379.5	2.37e-20	1.000	380.0	2.42e-20	1.000	380.5	2.47e-20	1.000	381.0	2.54e-20	1.000
381.5	2.62e-20	1.000	382.0	2.69e-20	1.000	382.5	2.79e-20	1.000	383.0	2.88e-20	1.000	383.5	2.96e-20	1.000
384.0	3.02e-20	1.000	384.5	3.10e-20	1.000	385.0	3.20e-20	1.000	385.5	3.29e-20	1.000	386.0	3.39e-20	1.000
386.5	3.51e-20	1.000	387.0	3.62e-20	1.000	387.5	3.69e-20	1.000	388.0	3.70e-20	1.000	388.5	3.77e-20	1.000
389.0	3.88e-20	1.000	389.5	3.97e-20	1.000	390.0	4.03e-20	1.000	390.5	4.12e-20	1.000	391.0	4.22e-20	1.000
391.5	4.29e-20	1.000	392.0	4.30e-20	1.000	392.5	4.38e-20	1.000	393.0	4.47e-20	1.000	393.5	4.55e-20	1.000
394.0	4.56e-20	1.000	394.5	4.59e-20	1.000	395.0	4.67e-20	1.000	395.5	4.80e-20	1.000	396.0	4.87e-20	1.000
396.5	4.96e-20	1.000	397.0	5.08e-20	1.000	397.5	5.19e-20	1.000	398.0	5.23e-20	1.000	398.5	5.39e-20	1.000
399.0	5.46e-20	1.000	399.5	5.54e-20	1.000	400.0	5.59e-20	1.000	400.5	5.77e-20	1.000	401.0	5.91e-20	1.000
401.5	5.99e-20	1.000	402.0	6.06e-20	1.000	402.5	6.20e-20	1.000	403.0	6.35e-20	1.000	403.5	6.52e-20	1.000
404.0	6.54e-20	1.000	404.5	6.64e-20	1.000	405.0	6.93e-20	1.000	405.5	7.15e-20	1.000	406.0	7.19e-20	1.000
406.5	7.32e-20	1.000	407.0	7.58e-20	1.000	407.5	7.88e-20	1.000	408.0	7.97e-20	1.000	408.5	7.91e-20	1.000
409.0	8.11e-20	1.000	409.5	8.41e-20	1.000	410.0	8.53e-20	1.000	410.5	8.59e-20	1.000	411.0	8.60e-20	1.000
411.5	8.80e-20	1.000	412.0	9.04e-20	1.000	412.5	9.45e-20	1.000	413.0	9.34e-20	1.000	413.5	9.37e-20	1.000
414.0	9.63e-20	1.000	414.5	9.71e-20	1.000	415.0	9.70e-20	1.000	415.5	9.65e-20	1.000	416.0	9.69e-20	1.000
416.5	9.89e-20	1.000	417.0	1.00e-19	1.000	417.5	1.02e-19	1.000	418.0	1.00e-19	1.000	418.5	1.02e-19	1.000
419.0	1.01e-19	1.000	419.5	1.01e-19	1.000	420.0	1.03e-19	1.000	420.5	1.01e-19	1.000	421.0	1.04e-19	1.000
421.5	1.05e-19	1.000	422.0	1.06e-19	1.000	422.5	1.04e-19	1.000	423.0	1.05e-19	1.000	423.5	1.05e-19	1.000
424.0	1.01e-19	1.000	424.5	1.01e-19	1.000	425.0	1.05e-19	1.000	425.5	1.03e-19	1.000	426.0	1.02e-19	1.000
426.5	1.01e-19	1.000	427.0	9.77e-20	1.000	427.5	9.81e-20	1.000	428.0	1.00e-19	1.000	428.5	1.02e-19	1.000
429.0	9.89e-20	1.000	429.5	9.85e-20	1.000	430.0	1.04e-19	1.000	430.5	1.08e-19	1.000	431.0	1.05e-19	1.000
431.5	1.02e-19	1.000	432.0	9.64e-20	1.000	432.5	1.01e-19	1.000	433.0	1.06e-19	1.000	433.5	1.09e-19	1.000
434.0	1.04e-19	1.000	434.5	1.03e-19	1.000	435.0	1.07e-19	1.000	435.5	1.16e-19	1.000	436.0	1.09e-19	1.000
436.5	1.11e-19	1.000	437.0	9.81e-20	1.000	437.5	9.71e-20	1.000	438.0	1.06e-19	1.000	438.5	1.16e-19	1.000
439.0	1.08e-19	1.000	439.5	1.05e-19	1.000	440.0	9.70e-20	1.000	440.5	1.01e-19	1.000	441.0	1.04e-19	1.000
441.5	1.07e-19	1.000	442.0	1.02e-19	1.000	442.5	9.68e-20	1.000	443.0	1.00e-19	1.000	443.5	1.14e-19	1.000
444.0	1.13e-19	1.000	444.5	1.03e-19	1.000	445.0	9.74e-20	1.000	445.5	8.46e-20	1.000	446.0	8.70e-20	1.000
446.5	9.97e-20	1.000	447.0	1.01e-19	1.000	447.5	9.15e-20	1.000	448.0	9.41e-20	1.000	448.5	8.99e-20	1.000
449.0	1.10e-19	1.000	449.5	9.12e-20	1.000	450.0	8.56e-20	1.000	450.5	8.28e-20	1.000	451.0	6.15e-20	1.000
451.5	5.56e-20	1.000	452.0	6.47e-20	1.000	452.5	7.27e-20	1.000	453.0	5.75e-20	1.000	453.5	5.08e-20	1.000
454.0	4.38e-20	1.000	454.5	3.81e-20	1.000	455.0	3.61e-20	1.000	455.5	3.61e-20	1.000	456.0	3.13e-20	1.000
456.5	2.72e-20	1.000	457.0	2.44e-20	1.000	457.5	2.22e-20	1.000	458.0	1.82e-20	1.000	458.5	1.43e-20	1.000
459.0	1.32e-20	1.000	459.5	1.05e-20	1.000	460.0	8.95e-21	1.000	460.5	8.90e-21	1.000	461.0	7.94e-21	1.000
461.5	7.04e-21	1.000	462.0	6.46e-21	1.000	462.5	5.63e-21	1.000	463.0	4.78e-21	1.000	463.5	3.94e-21	1.000
464.0	3.26e-21	1.000	464.5	2.97e-21	1.000	465.0	2.65e-21	1.000	465.5	2.46e-21	1.000	466.0	2.27e-21	1.000
466.5	2.08e-21	1.000	467.0	1.86e-21	1.000	467.5	1.76e-21	1.000	468.0	1.60e-21	1.000	468.5	1.44e-21	1.000
469.0	1.34e-21	1.000	469.5	1.20e-21	1.000	470.0	1.07e-21	1.000	470.5	1.02e-21	1.000	471.0	9.92e-22	1.000
471.5	9.97e-22	1.000	472.0	8.87e-22	1.000	472.5	8.27e-22	1.000	473.0	7.76e-22	1.000	473.5	7.15e-22	1.000
474.0	6.71e-22	1.000	474.5	6.67e-22	1.000	475.0	6.10e-22	1.000	475.5	6.17e-22	1.000	476.0	5.54e-22	1.000
476.5	5.22e-22	1.000	477.0	5.10e-22	1.000	477.5	5.17e-22	1.000	478.0	4.80e-22	1.000	478.5	4.71e-22	1.000
479.0	4.60e-22	1.000	479.5	4.35e-22	1.000	480.0	3.90e-22	1.000	480.5	3.71e-22	1.000	481.0	3.62e-22	1.000
481.5	3.52e-22	1.000	482.0	3.05e-22	1.000	482.5	3.05e-22	1.000	483.0	2.86e-22	1.000	483.5	2.53e-22	1.000
484.0	2.75e-22	1.000	484.5	2.59e-22	1.000	485.0	2.47e-22	1.000	485.5	2.36e-22	1.000	486.0	2.12e-22	1.000
486.5	1.89e-22	1.000	487.0	1.93e-22	1.000	487.5	1.86e-22	1.000	488.0	1.82e-22	1.000	488.5	1.75e-22	1.000
489.0	1.74e-22	1.000	489.5	1.72e-22	1.000	490.0	1.66e-22	1.000	490.5	1.75e-22	1.000	491.0	1.54e-22	1.000
491.5	1.74e-22	1.000	492.0	1.63e-22	1.000	492.5	1.53e-22	1.000	493.0	1.52e-22	1.000	493.5	5.85e-23	1.000
494.0	0.00e+00	1.000												

Table A-4. Chamber effect and background characterization parameters used in the environmental chamber model simulations for mechanism evaluation.

Cham.	Set [a]	Value	Discussion
NO_2 photolysis rate			Light intensity as measured by the NO_2 photolysis rate. The rate constants for the other photolysis reactions are calculated using the NO_2 photolysis rate assigned to the experiment and the photolysis rate constant ratios calculated using the relative spectral distribution for the light source.
DTC439-442		0.176 → 0.174	NO_2 photolysis rate assigned for experiment declined linearly with run number, based on linear fits of plots of results of actinometry experiments against run number. Note that the lights were changed between DTC442 and DTC476, resulting in an increase in the light intensity. The light intensity was relatively constant for DTC725 through DTC749.
DTC476-487		0.224 → 0.221	
DTC725-749		0.161	
RN-I (ppb)			Ratio of the rate of wall + hν -> HONO to the NO_2 photolysis rate.
DTC	11	0.080	Average of value of RS-I that gave best fits to n-butane - NOx chamber experiments carried out in this chamber. The initial HONO was optimized at the same time. If a temperature dependence is shown, it was derived from the temperature dependence of the RN-I values that best fit characterization data in outdoor chamber experiments, with the same activation energy used in all cases. If a temperature dependence is not shown, then the temperature variation for experiments in this set is small compared to the run-to-run variability in the best fit RN-I values. Note that the radical source in Sets 3, 12, 13, and 16 runs was anomalously high. Any dependence of apparent radical source on initial NOx levels in Teflon bag chambers was found to be much less than the run-to-run variability.
	14	0.081	
	15	0.057	
	18	0.066	
HONO-F (unitless)			Ratio of the initial HONO concentration to the measured initial NO_2. [The initial NO_2 in the experiment is reduced by a factor of 1 - (HONO-F)]. Unless the characterization data indicate otherwise, it is assumed that the initial HONO is introduced with the NO2 injection, so is it is assumed to be proportional to the initial NO2 concentration.
DTC	11	0.6%	Average of value of initial HONO to initial NO2 that gave best fits to n-butane - NO_x chamber experiments carried out in this chamber. The RN-I parameter was optimized at the same time.
	14	0.6%	
	15	0.7%	
	18	0.8%	
E-NO2/K1 (ppb)			Ratio of rate of NO2 offgasing from the walls to the NO2 photolysis rate.
All Teflon Bag Chambers		0	The NOx offgasing caused by representing the radical source by HONO offgasing appears to be sufficient for accounting for NOx offgasing effects in most cases. RN-I parameters adjusted to fit experiments sensitive to the radical source are consistent with NOx offgasing rates adjusted to fit pure air or aldehyde - air runs, to within the uncertainty and variability.
K(NO2W) (min^{-1})			Rate of unimolecular loss (or hydrolysis) of NO2 to the walls.
All Teflon Bag Chambers		1.6e-4	Based on dark NO_2 decay and HONO formation measured in the ETC by Pitts et al. (1984). Assumed to be the same in all Teflon bag chambers, regardless of volume.
YHONO			Yield of HONO in the unimolecular reaction (hydrolysis) of NO2 on the walls.
All Teflon Bag Chambers		0.2	Based on dark NO_2 decay and HONO formation measured in the ETC by Pitts et al. (1984). Assumed to be the same in all Teflon bag chambers, regardless of volume.

Table A-4 (continued)

Cham.	Set [a]	Value	Discussion
K(O3W) (min^{-1})			Unimolecular loss rate of O_3 to the walls.
DTC	All	1.5e-4	Based on results of O_3 decay in Teflon bag chambers experiments as discussed by Carter et al (1995c).
CTC	All	8.5e-5	Based on results of O_3 decay experiments in this chamber
k(N26I) (min^{-1})			Rate constant for N_2O_5 -> 2 Wall-NO_x. This represents the humidity-independent portion of the wall loss of N_2O_5, or the intercept of plots of rates of N_2O_5 loss against humidity.
All Teflon Bag Chambers		2.8e-3	Based on N_2O_5 decay rate measurements made by Tuazon et al (1983) for the ETC. Assumed to be independent of chamber size (Carter et al, 1995c).
k(N26S) (ppm^{-1} min^{-1})			Rate constant for N_2O_5 + H_2O -> 2 Wall-NO_x. This represents the humidity dependent portion of the wall loss of N_2O_5, or the slope of plots of rates of N_2O_5 loss against humidity.
All Teflon Bag Chambers		1.1e-6	Based on N_2O_5 decay rate measurements made by Tuazon et al (1983) for the ETC. Assumed to be independent of chamber size (Carter et al, 1995c).
k(XSHC) (min^{-1})			Rate constant for OH -> HO_2. This represents the effects of reaction of OH with reactive VOCs in the background air or offgased from the chamber walls. This parameter does not significantly affect model simulations of experiments other than pure air runs.
All Teflon Bag Chambers		250	Estimated from modeling several pure air in the ITC (Carter et al, 1996d), and also consistent with simulations of pure air runs in the ETC (Carter et al, 1997b).
H2O (ppm)			Default water vapor concentration for runs where no humidity data are available.
DTC	all	1.0e+3	Experiments in this chamber were carried out using dried purified air. The limited humidity data for such runs indicate that the humidity was less than 5%, probably no more than ~2.5%, and possibly much less than that. The default value corresponds to ~2.5 - 3% RH for the conditions of most experiments.

[a] Set refers to the characterization set, which refers to the group of experiments assumed to have the same run conditions and represented using the same chamber-dependent parameters. See Carter et al (1995) for more discussion. Mineral spirits runs DTC439 through DTC442 are assigned characterization set 11. For mineral spirits runs DTC476 through DTC487, the characterization runs indicated the chamber radical source was somewhat higher on Side A, so the Side A runs during this period are assigned characterization set 14, and the Side B runs are assigned set 15. The branched alkane experiments carried out for this project, DTC725 through DTC749, are assigned characterization set 18.